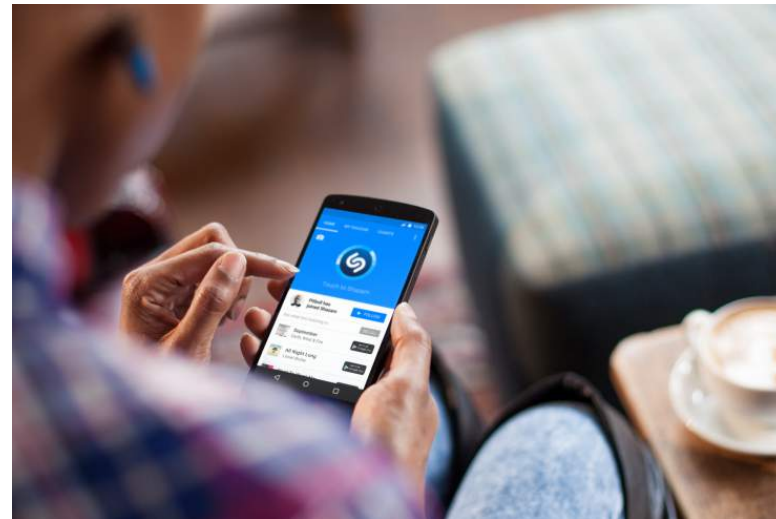
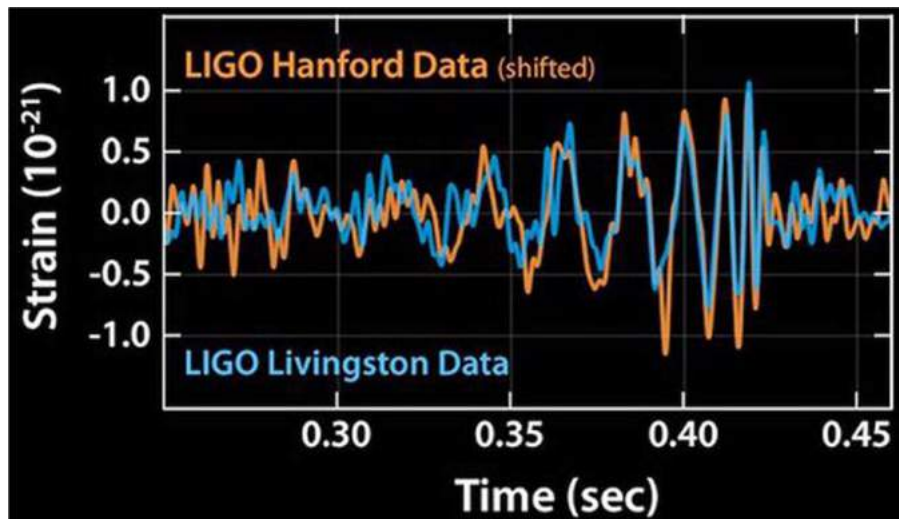
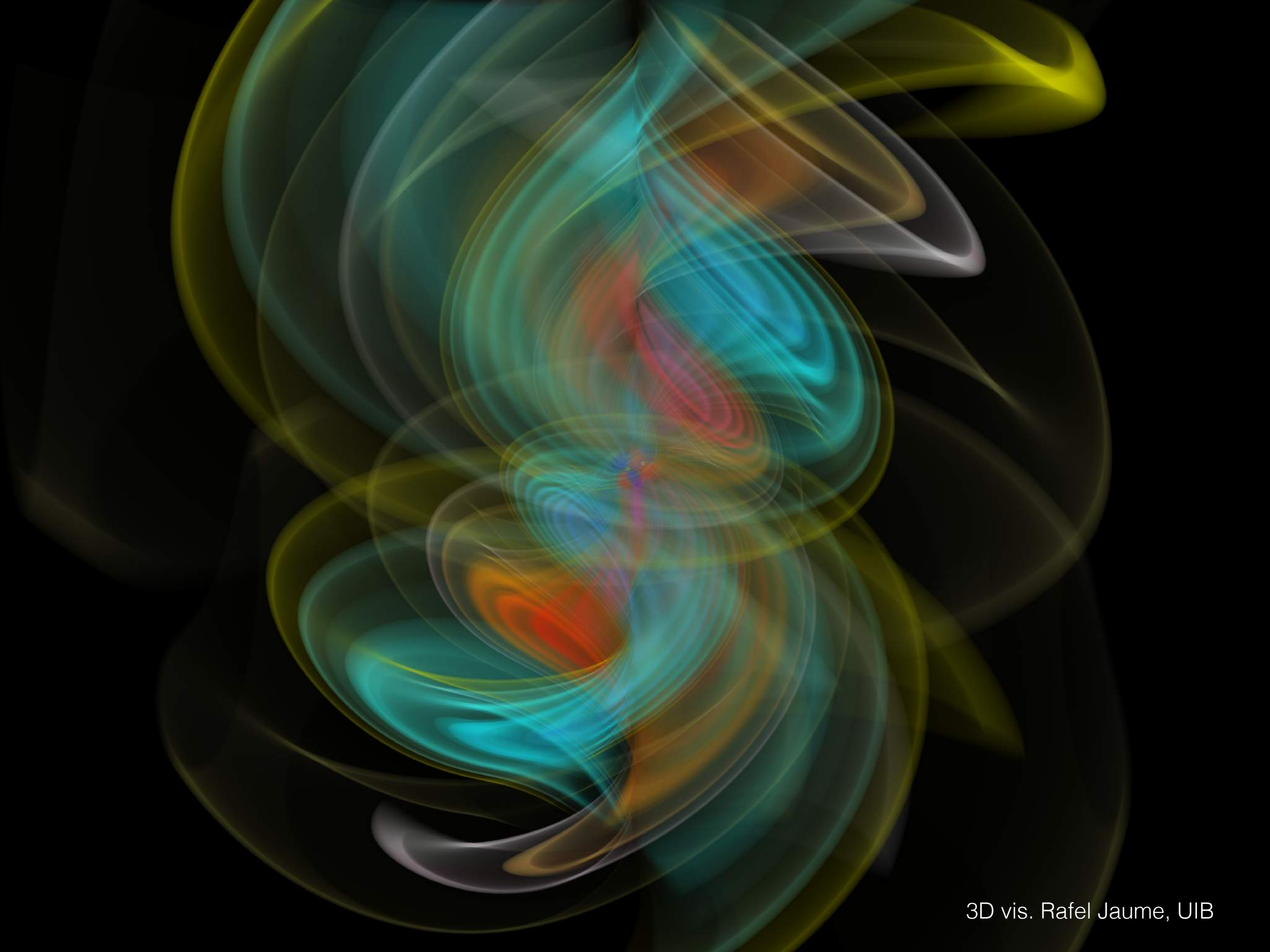


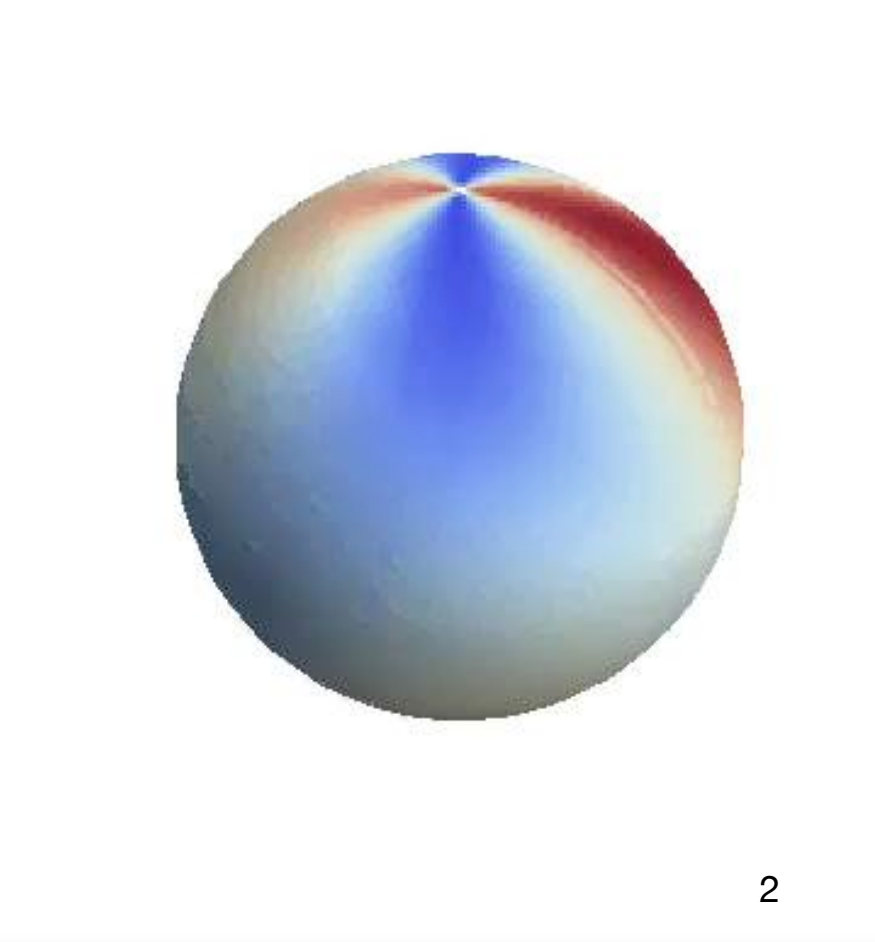
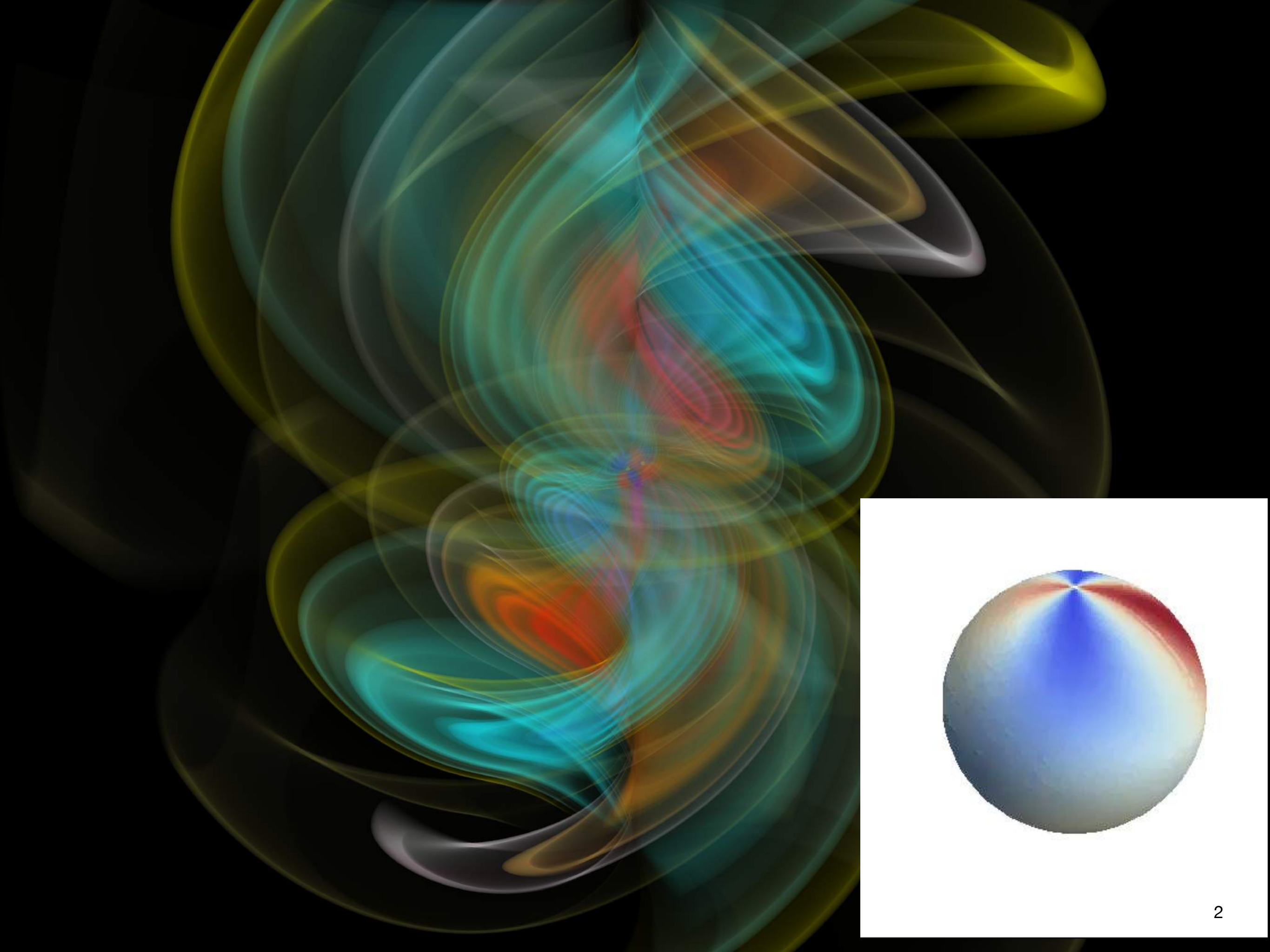
Modelling the gravitational wave signal from compact binary coalescence



Sascha Husa, UIB

Sao Paulo 5/12/2018





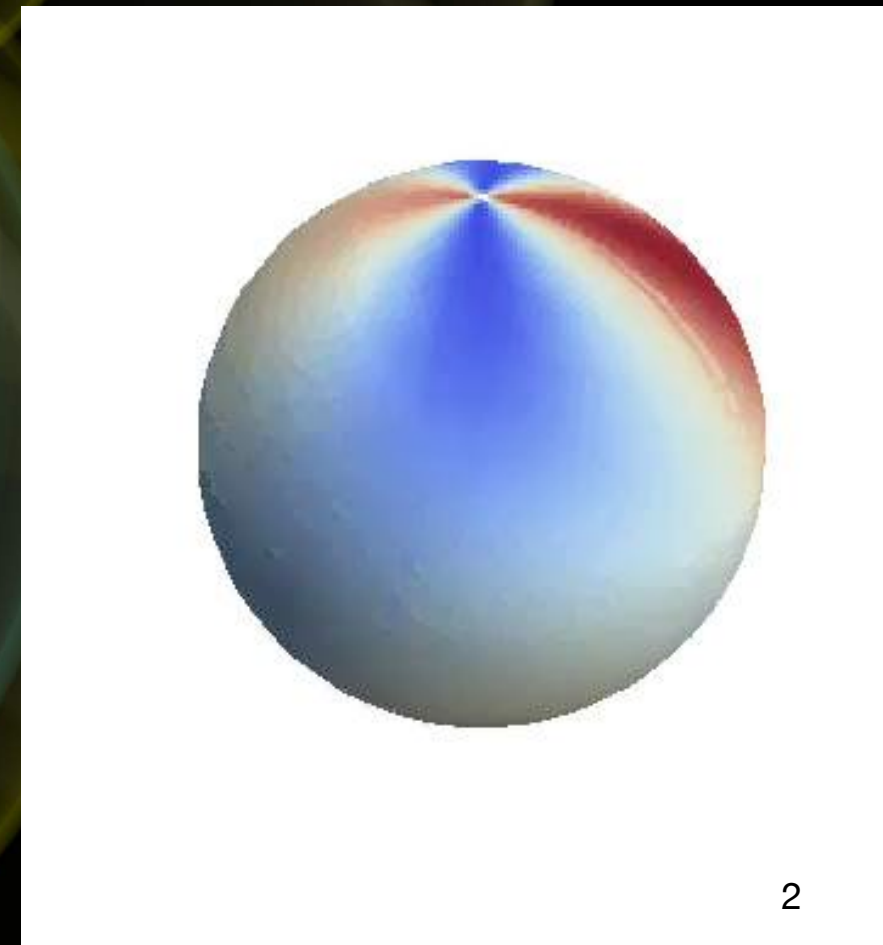
The Challenge

Model the GW signal for astrophysical plausible parameter space of coalescing BH, NS, ? - in general relativity + for alternative theories.

No hair theorem: black holes are simple (masses, spin vectors):

binary described by 9 dimensionless parameters:

mass ratio (1), spins (6), eccentricity (2) + scaled by total mass.



The Challenge

Model the GW signal for astrophysical plausible parameter space of coalescing BH, NS, ? - in general relativity + for alternative theories.

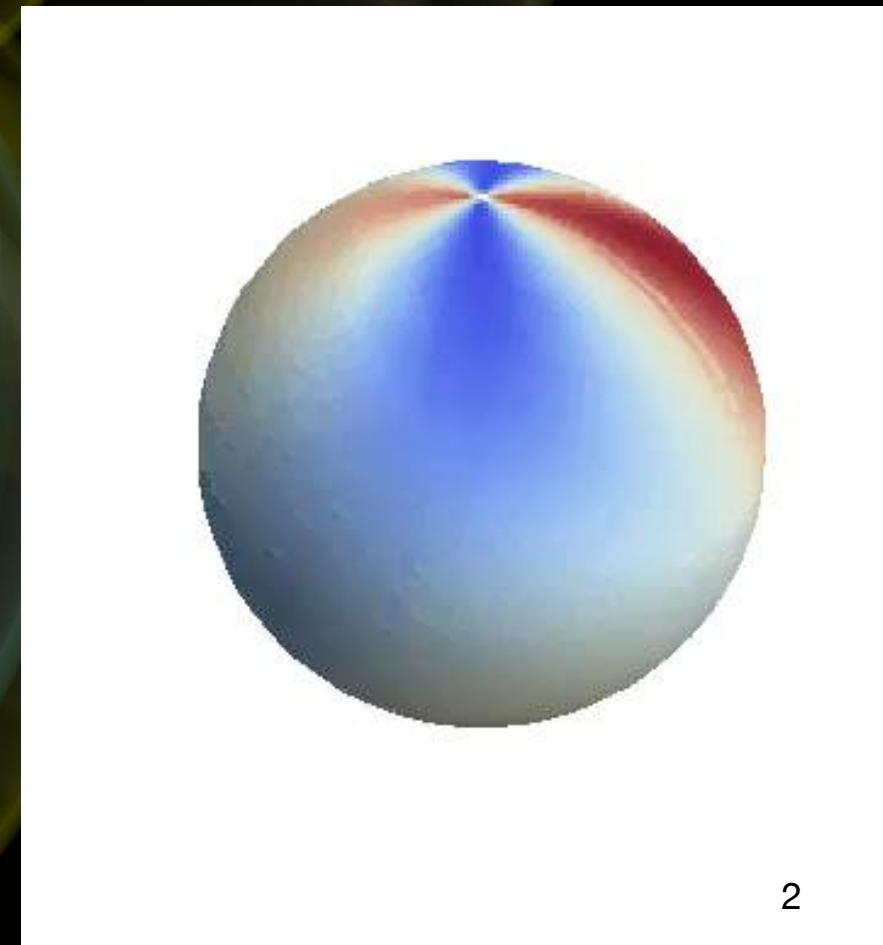
No hair theorem: black holes are simple (masses, spin vectors):

binary described by 9 dimensionless parameters:

mass ratio (1), spins (6), eccentricity (2) + scaled by total mass.

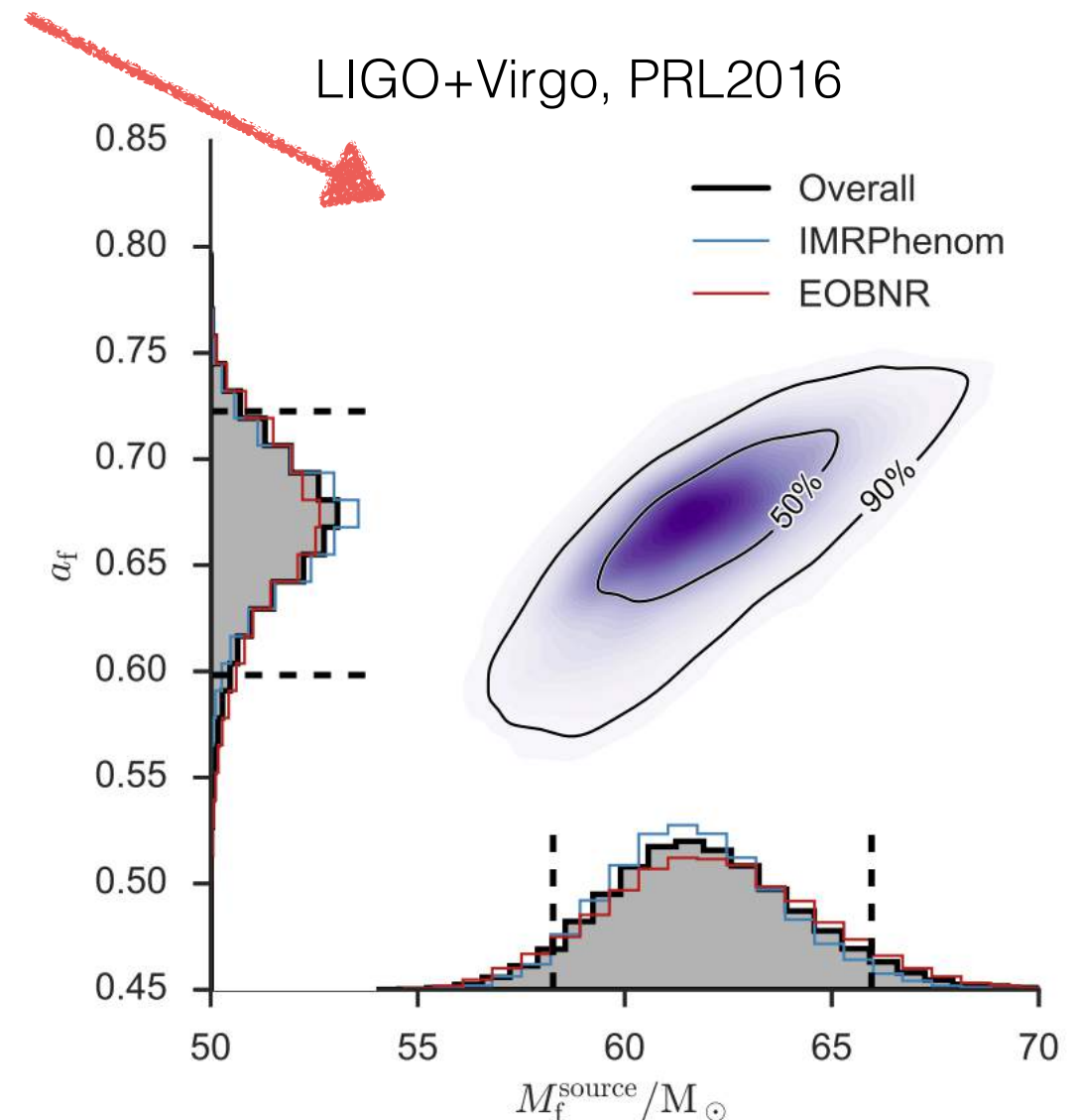
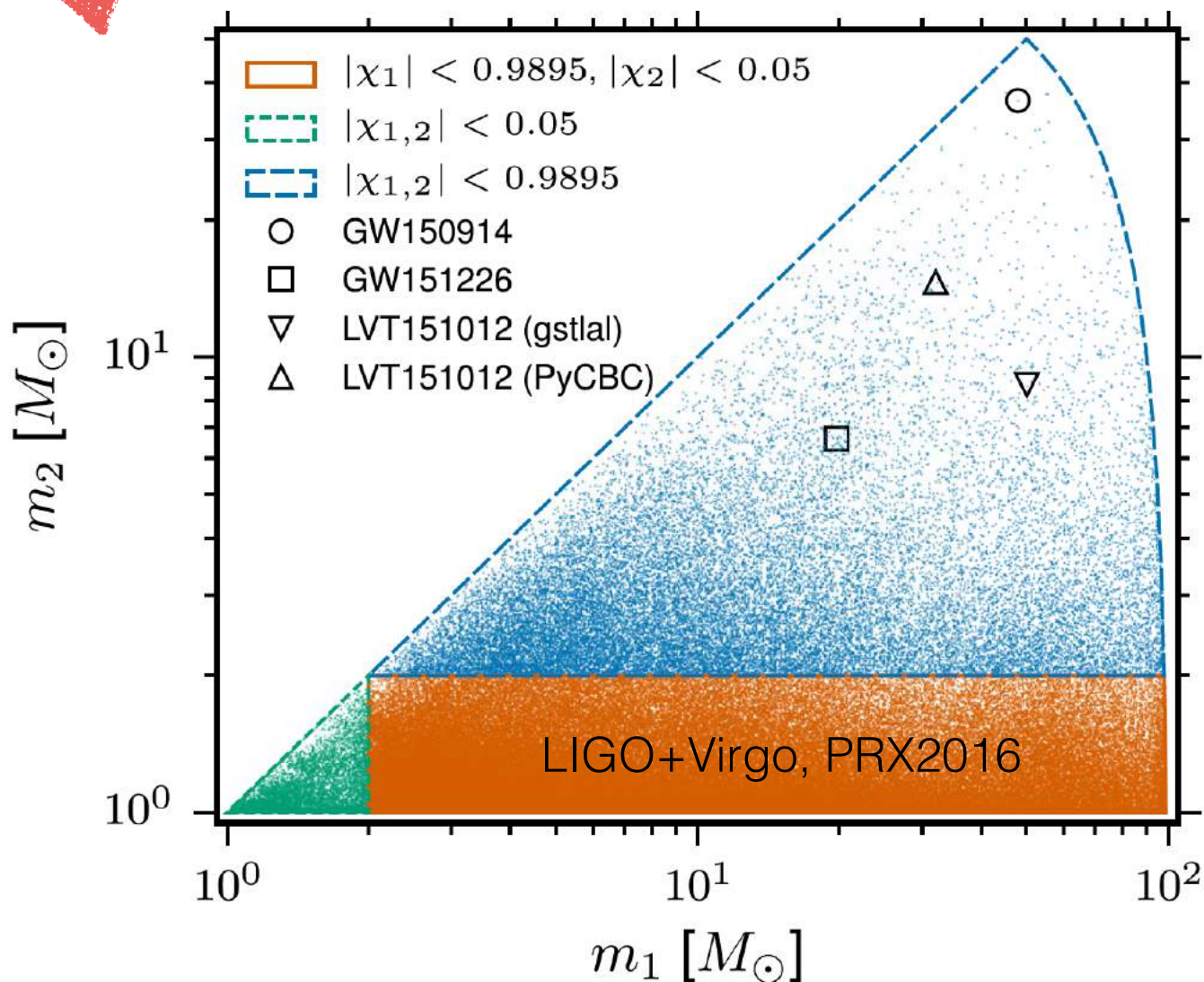
Requirements:

- Accuracy: Keep up with detector sensitivity!
- Fast evaluation for Bayesian inference
need $\sim 10^7$ evaluations
- How accurately can we measure different quantities?



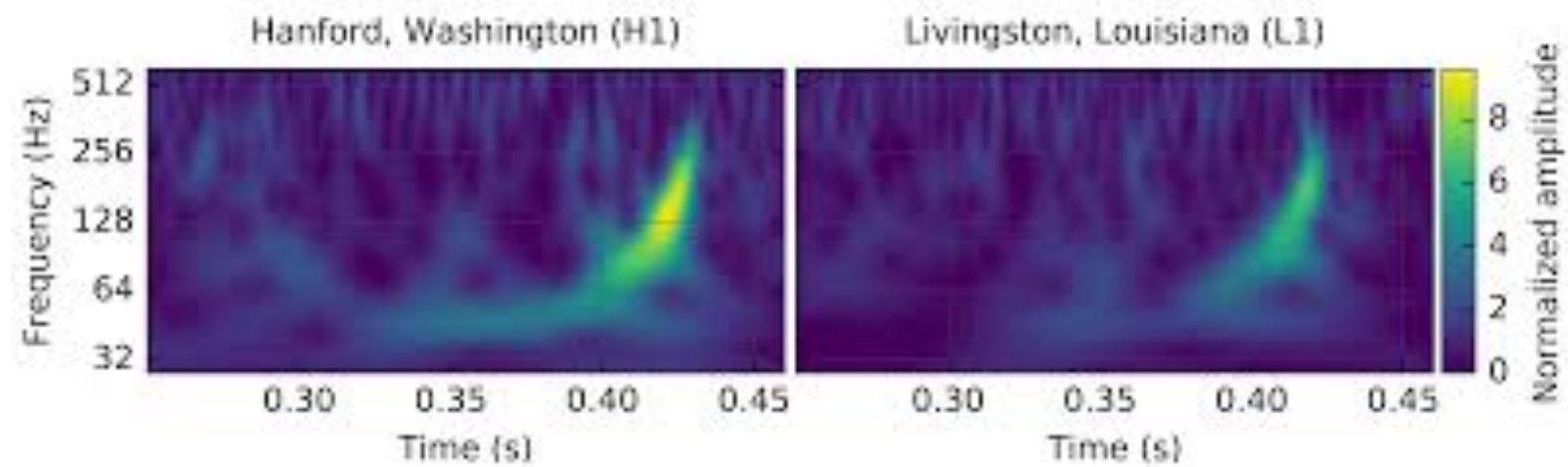
2-Step LIGO/Virgo Compact binary workflow

- **Searches -> detection:** what is the statistical evidence of seeing a signal above background, fixed template bank.
 - Search pipelines: matched filter [PyCBC, GstLAL], time-frequency excess power [cWB].
- **Bayesian parameter estimation:** vary templates with random walks in parameter space, using MCMC etc.



Data Analysis methods for transients

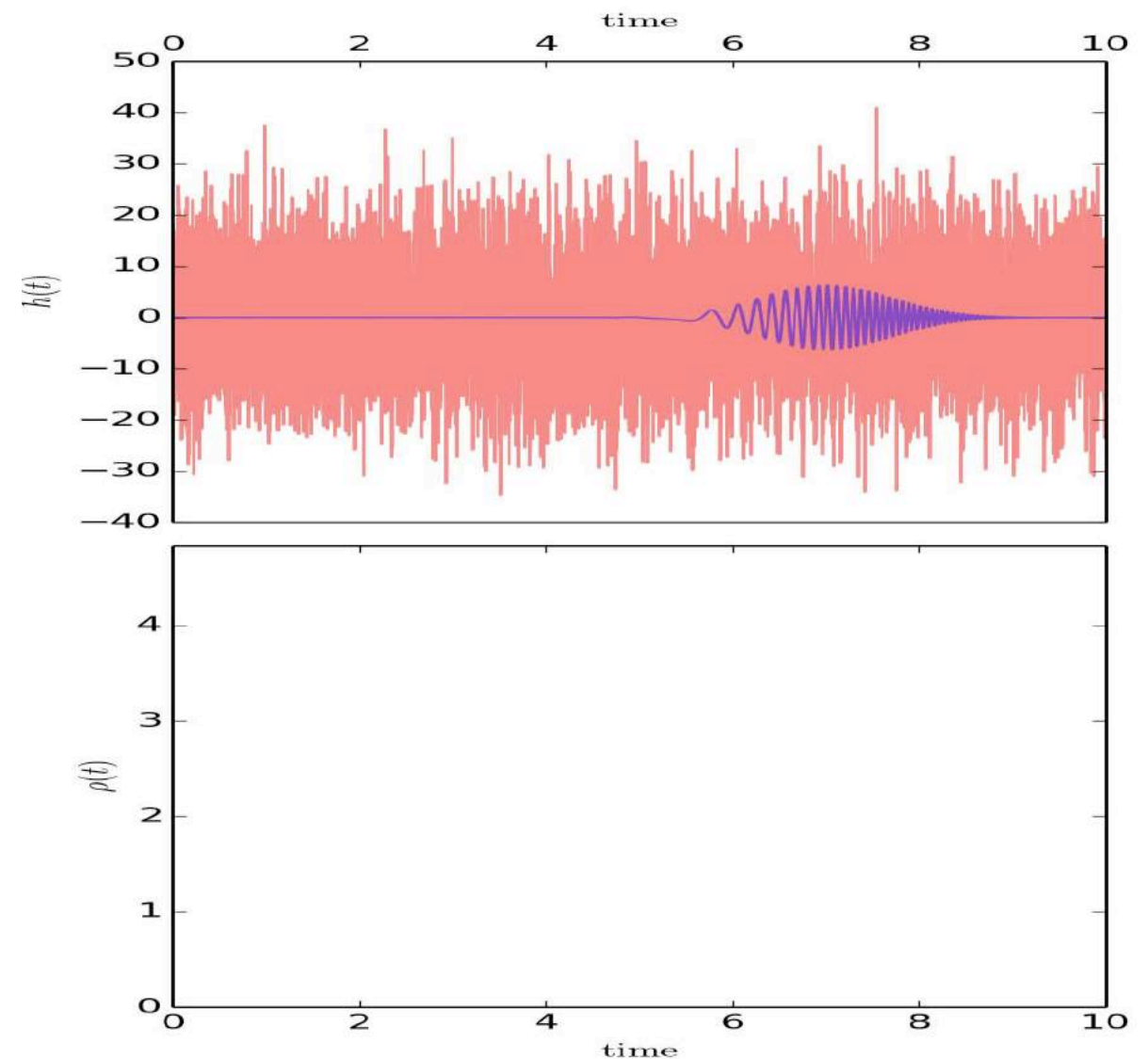
- **time frequency pattern recognition** for un-modeled searches
(tuned to waveform models)



- **matched filter:** optimal analysis using accurate waveform models as signal templates

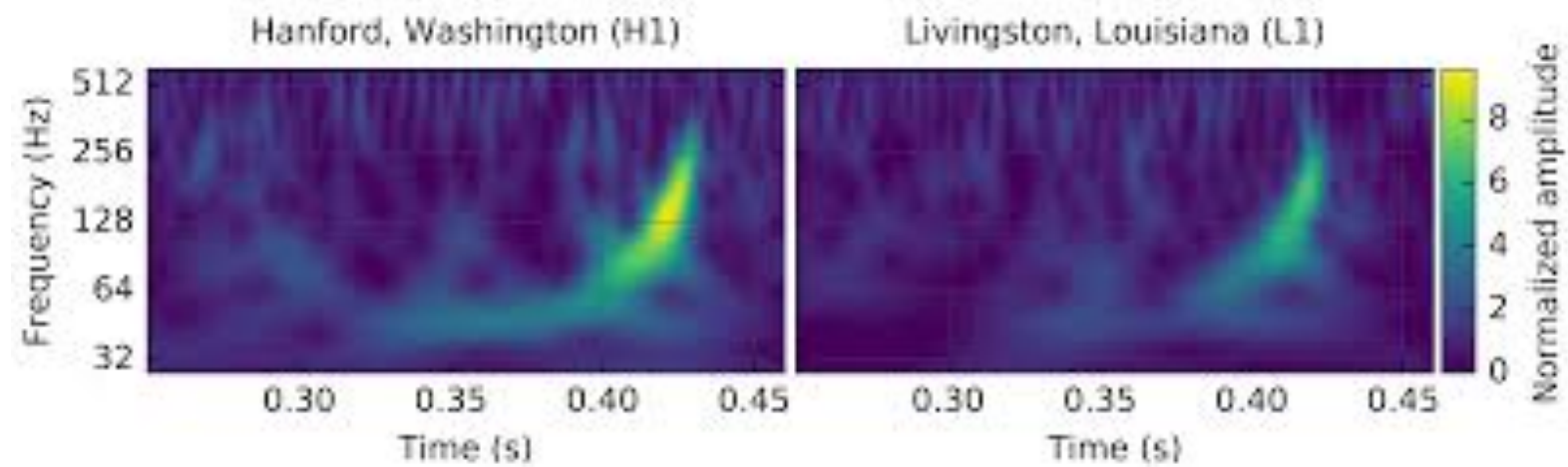
method of choice to identify the sources

Identification of sources is limited by detector sensitivity + accuracy of waveform models.



Data Analysis methods for transients

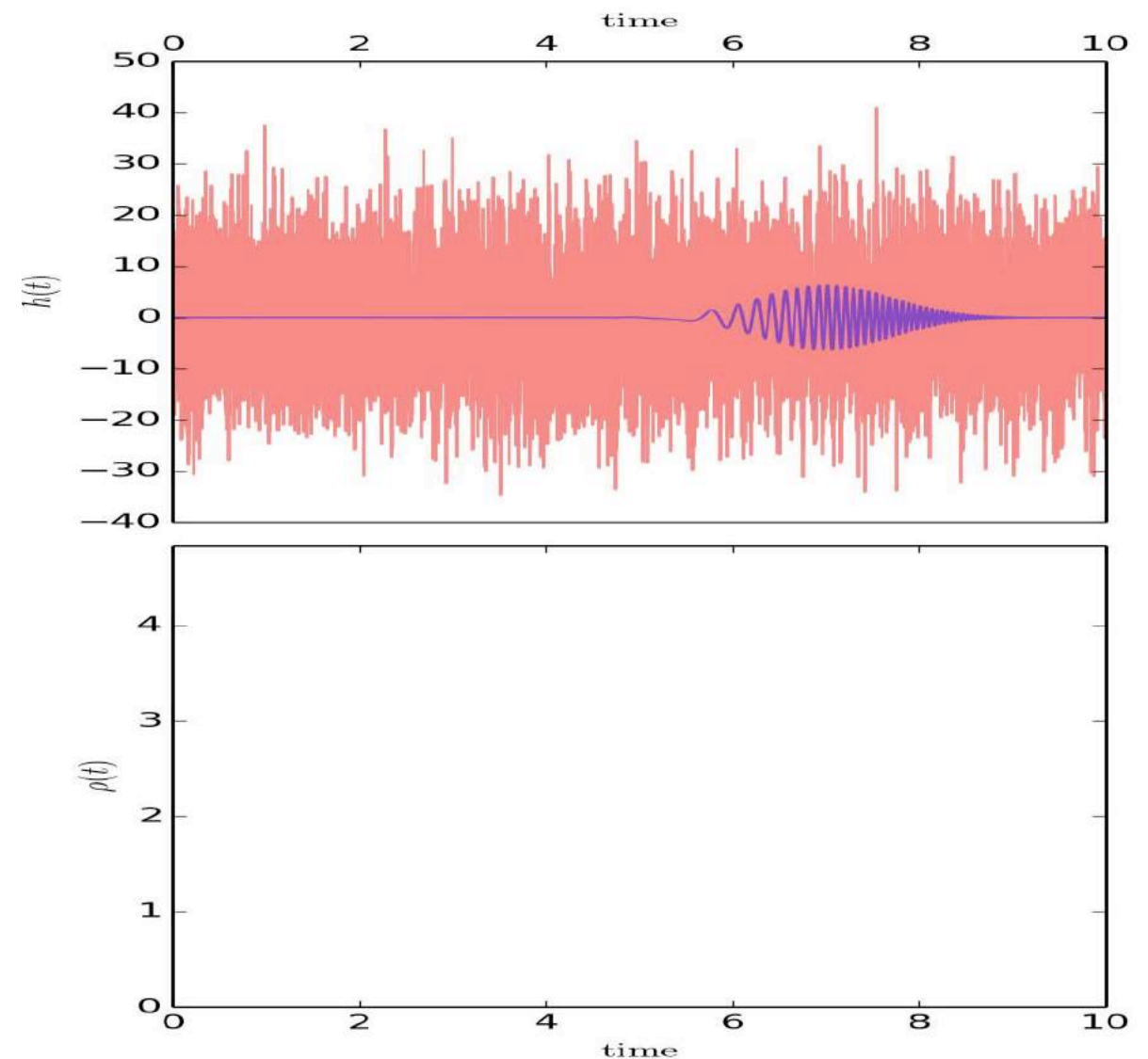
- **time frequency pattern recognition** for un-modeled searches
(tuned to waveform models)



- **matched filter:** optimal analysis using accurate waveform models as signal templates

method of choice to identify the sources

Identification of sources is limited by detector sensitivity + accuracy of waveform models.



The Chirp - first step beyond Newton

Simplest approximation of the signal:

Newtonian point particles + energy loss from quadrupole formula:

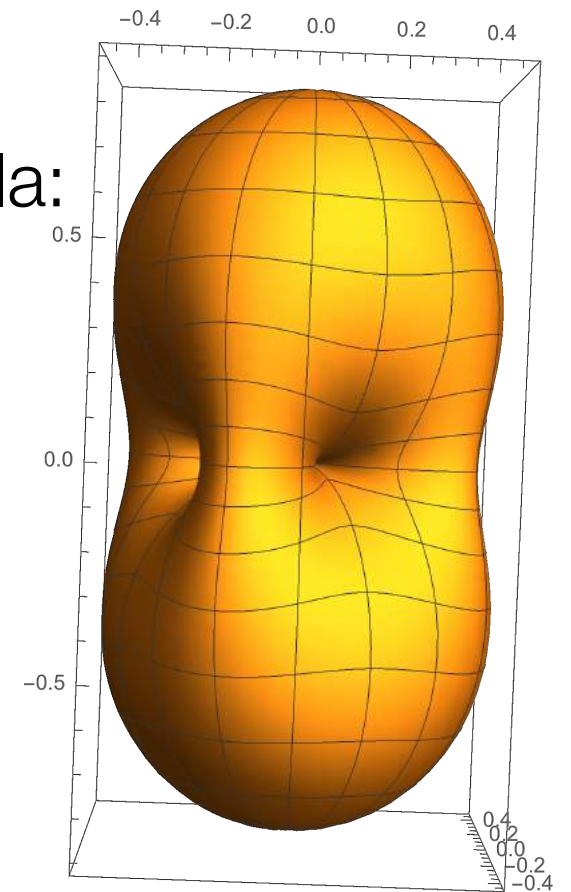
The Chirp - first step beyond Newton

Simplest approximation of the signal:

Newtonian point particles + energy loss from quadrupole formula:

$$h_+(t) = \frac{4}{r} \left(\frac{GM_c}{c^2} \right)^{5/3} \left(\frac{\pi f_{\text{gw}}}{c} \right)^{2/3} \frac{1 + \cos^2 \theta}{2} \cos(2\pi f_{\text{gw}} t_{\text{ret}} + 2\phi),$$

$$h_\times(t) = \frac{4}{r} \left(\frac{GM_c}{c^2} \right)^{5/3} \left(\frac{\pi f_{\text{gw}}}{c} \right)^{2/3} \cos \theta \sin(2\pi f_{\text{gw}} t_{\text{ret}} + 2\phi),$$



Quadrupole wave pattern

The Chirp - first step beyond Newton

Simplest approximation of the signal:

Newtonian point particles + energy loss from quadrupole formula:

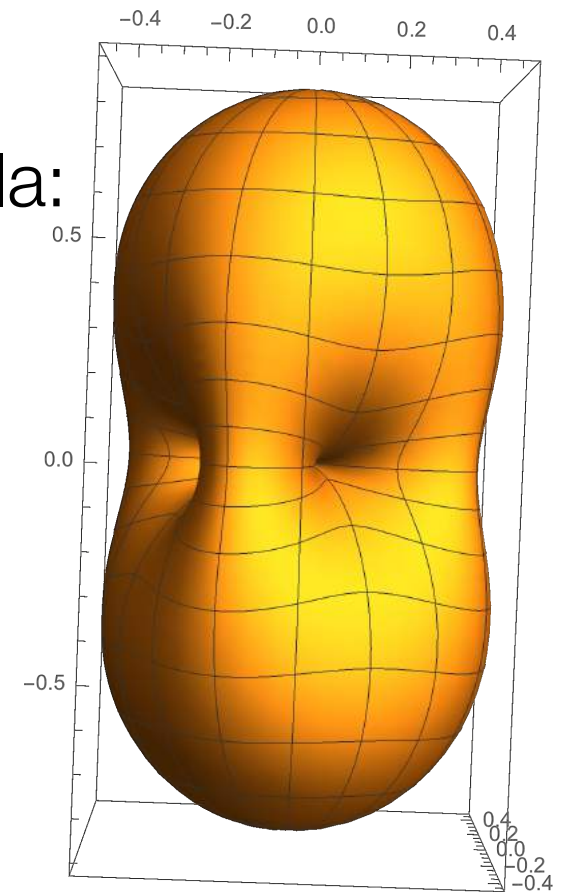
$$h_+(t) = \frac{4}{r} \left(\frac{GM_c}{c^2} \right)^{5/3} \left(\frac{\pi f_{\text{gw}}}{c} \right)^{2/3} \frac{1 + \cos^2 \theta}{2} \cos(2\pi f_{\text{gw}} t_{\text{ret}} + 2\phi),$$

$$h_\times(t) = \frac{4}{r} \left(\frac{GM_c}{c^2} \right)^{5/3} \left(\frac{\pi f_{\text{gw}}}{c} \right)^{2/3} \cos \theta \sin(2\pi f_{\text{gw}} t_{\text{ret}} + 2\phi),$$

$$P = \dot{E} = \frac{32}{5} \frac{c^5}{G} \left(\frac{\pi GM_c f_{\text{GW}}}{c^3} \right)^{10/3}$$

**Only intrinsic source parameter:
chirp mass M_c .**

$$M_c = \frac{(m_1 m_2)^{3/5}}{(m_1 + m_2)^{1/5}}$$



Quadrupole wave pattern

The Chirp - first step beyond Newton

Simplest approximation of the signal:

Newtonian point particles + energy loss from quadrupole formula:

$$h_+(t) = \frac{4}{r} \left(\frac{GM_c}{c^2} \right)^{5/3} \left(\frac{\pi f_{\text{gw}}}{c} \right)^{2/3} \frac{1 + \cos^2 \theta}{2} \cos(2\pi f_{\text{gw}} t_{\text{ret}} + 2\phi),$$

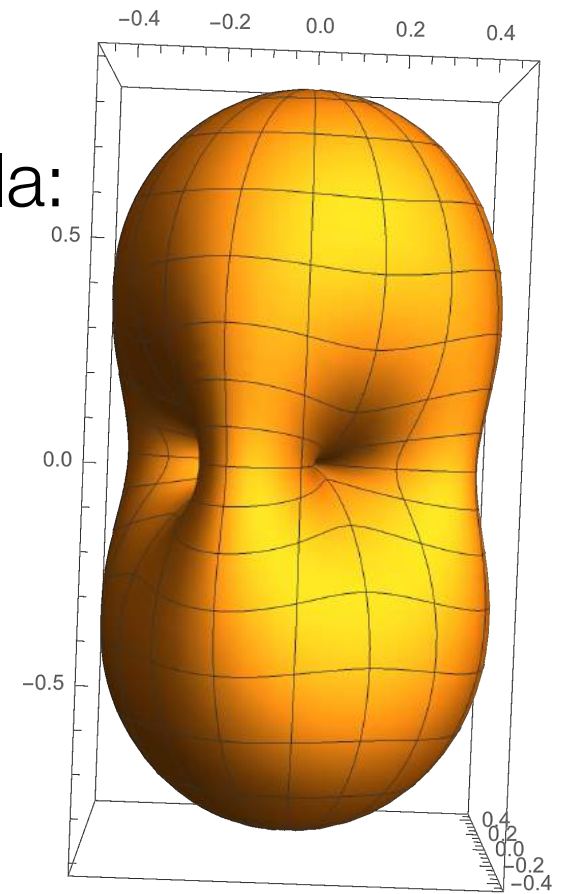
$$h_\times(t) = \frac{4}{r} \left(\frac{GM_c}{c^2} \right)^{5/3} \left(\frac{\pi f_{\text{gw}}}{c} \right)^{2/3} \cos \theta \sin(2\pi f_{\text{gw}} t_{\text{ret}} + 2\phi),$$

$$P = \dot{E} = \frac{32}{5} \frac{c^5}{G} \left(\frac{\pi GM_c f_{\text{GW}}}{c^3} \right)^{10/3}$$

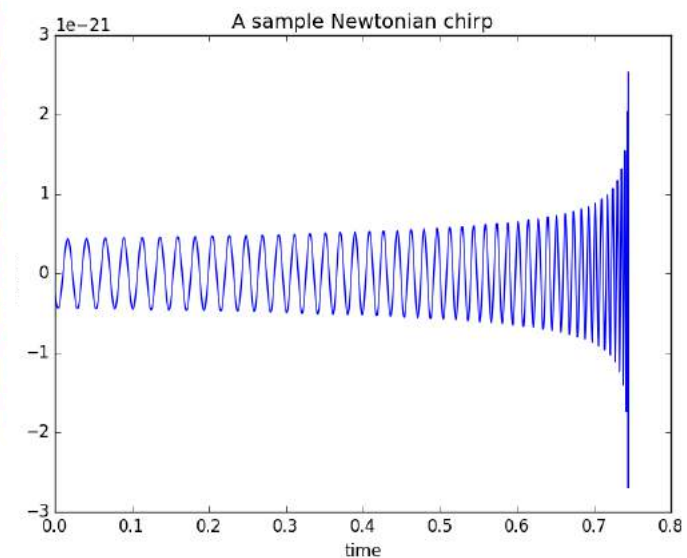
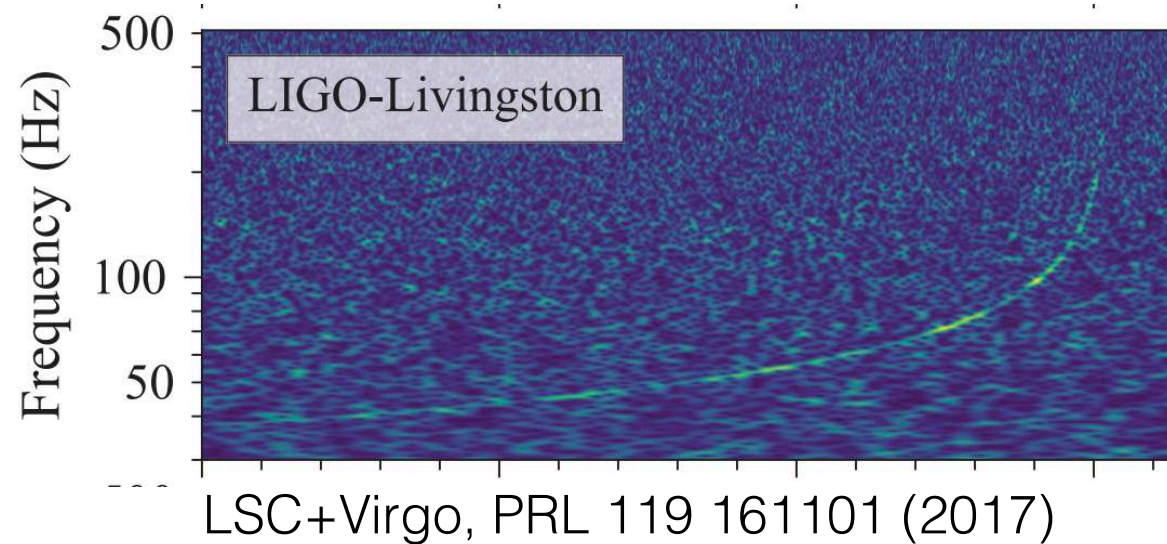
**Only intrinsic source parameter:
chirp mass M_c .**

$$M_c = \frac{(m_1 m_2)^{3/5}}{(m_1 + m_2)^{1/5}}$$

$$\frac{df}{dt} = \frac{dE}{dt} \frac{df}{dE} = \frac{P(f)}{\frac{dE}{df}}$$



Quadrupole wave pattern



The Chirp - first step beyond Newton

Simplest approximation of the signal:

Newtonian point particles + energy loss from quadrupole formula:

$$h_+(t) = \frac{4}{r} \left(\frac{GM_c}{c^2} \right)^{5/3} \left(\frac{\pi f_{\text{gw}}}{c} \right)^{2/3} \frac{1 + \cos^2 \theta}{2} \cos(2\pi f_{\text{gw}} t_{\text{ret}} + 2\phi),$$

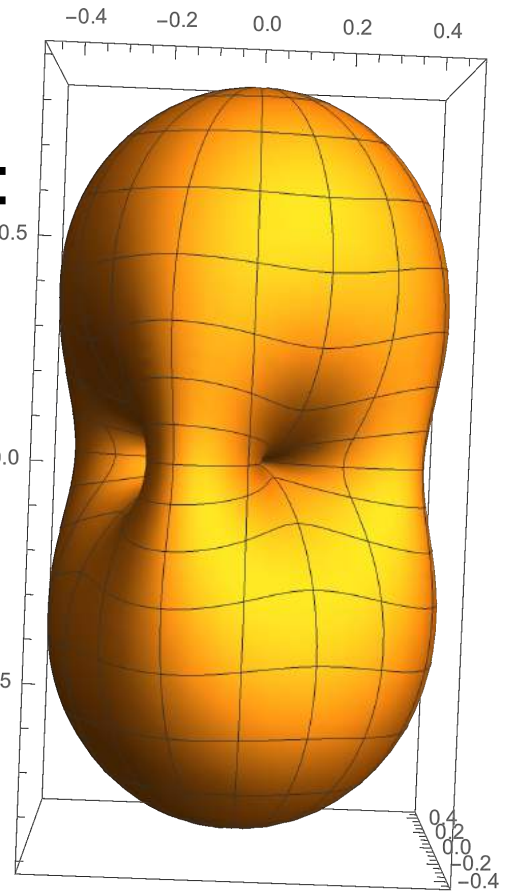
$$h_\times(t) = \frac{4}{r} \left(\frac{GM_c}{c^2} \right)^{5/3} \left(\frac{\pi f_{\text{gw}}}{c} \right)^{2/3} \cos \theta \sin(2\pi f_{\text{gw}} t_{\text{ret}} + 2\phi),$$

$$P = \dot{E} = \frac{32}{5} \frac{c^5}{G} \left(\frac{\pi GM_c f_{\text{GW}}}{c^3} \right)^{10/3}$$

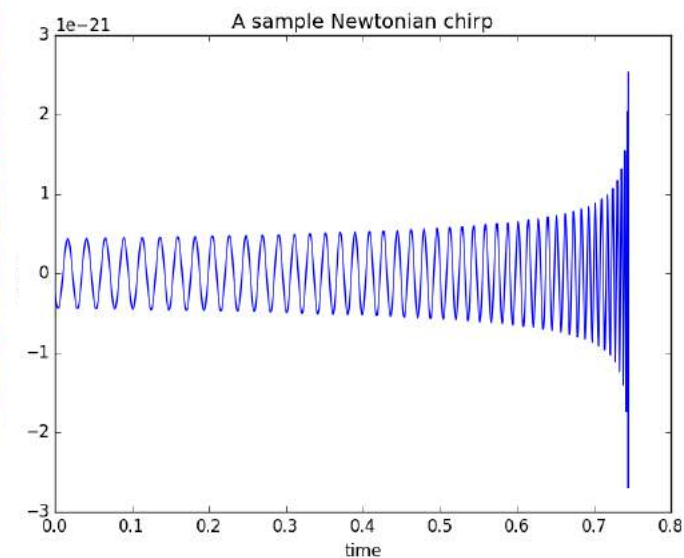
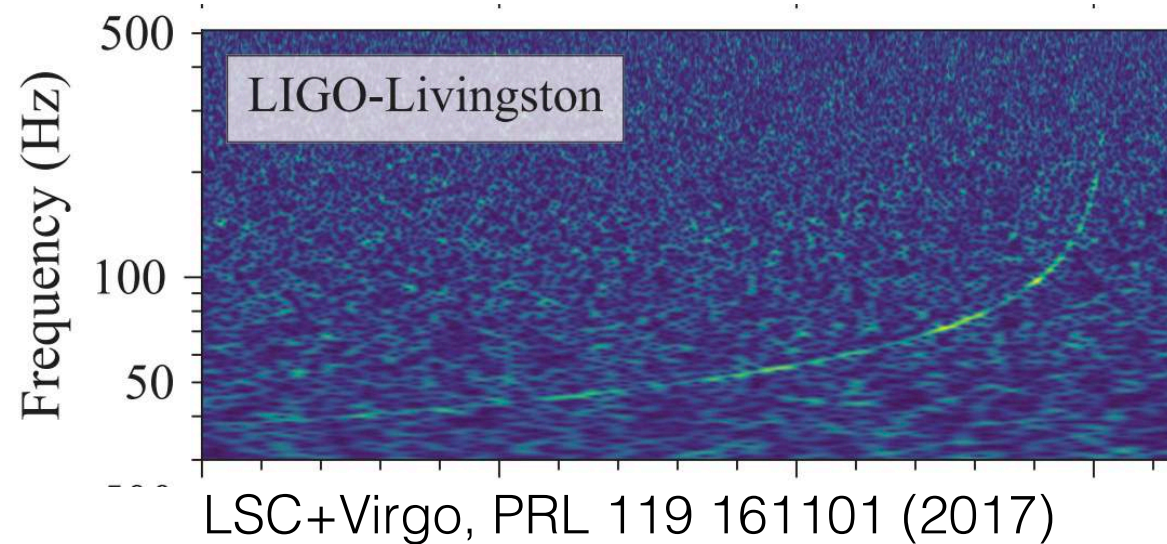
**Only intrinsic source parameter:
chirp mass M_c .**

$$M_c = \frac{(m_1 m_2)^{3/5}}{(m_1 + m_2)^{1/5}}$$

$$\frac{df}{dt} = \frac{dE}{dt} \frac{df}{dE} = \frac{P(f)}{\frac{dE}{df}}$$



Quadrupole wave pattern



Degeneracy:

only measure M_c , not both component masses.

Good for searches - bad for parameter estimation!

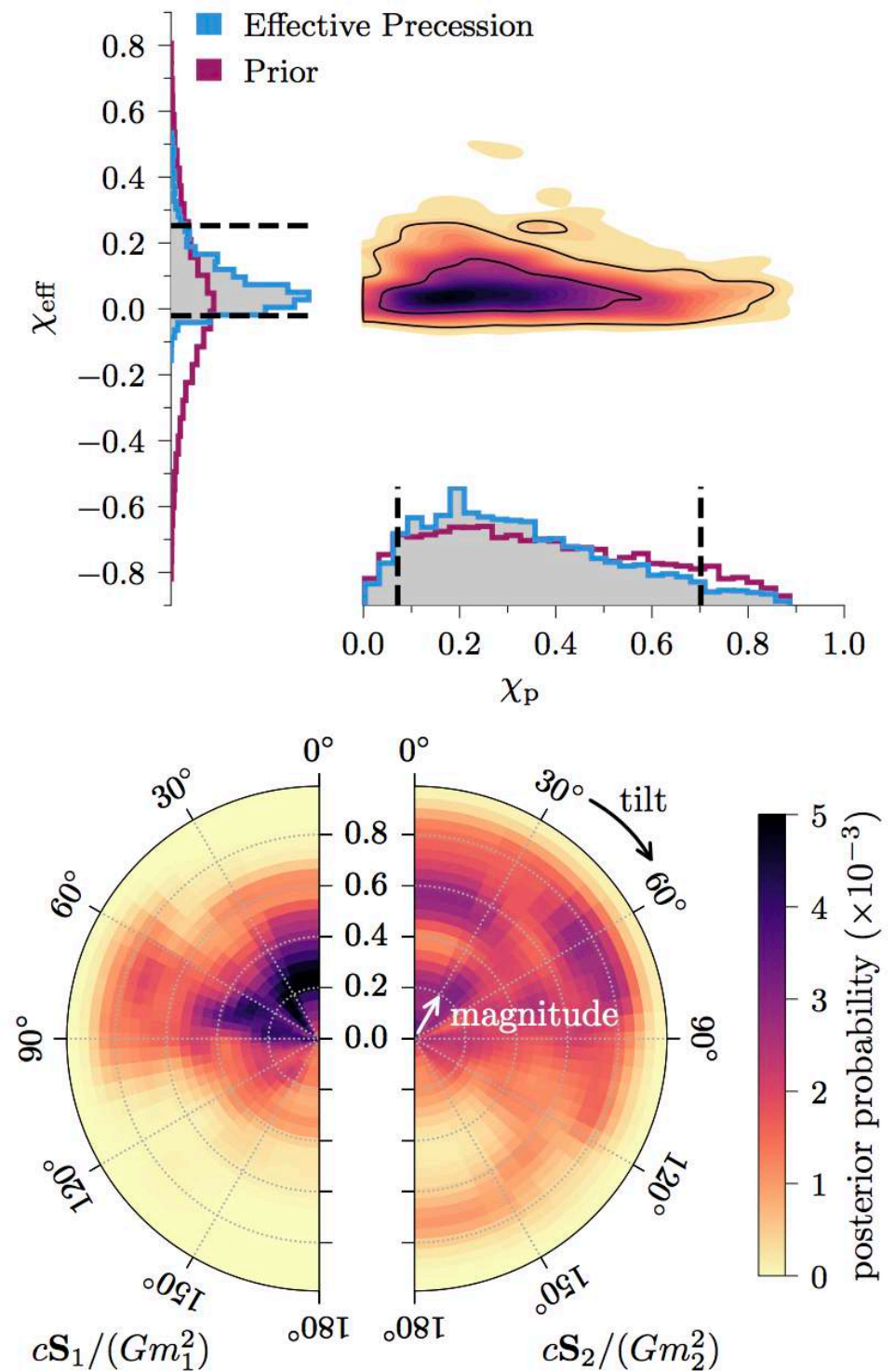
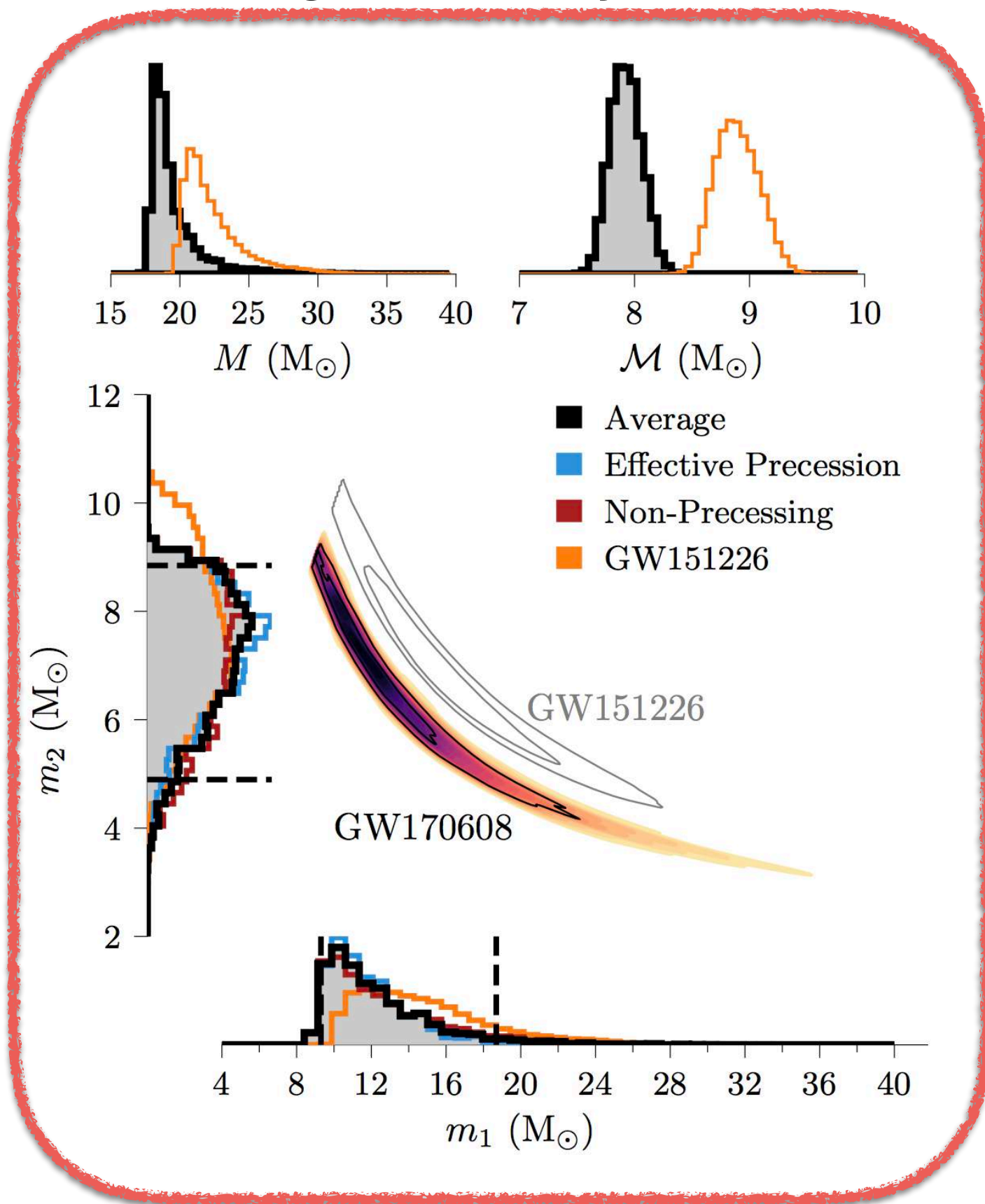
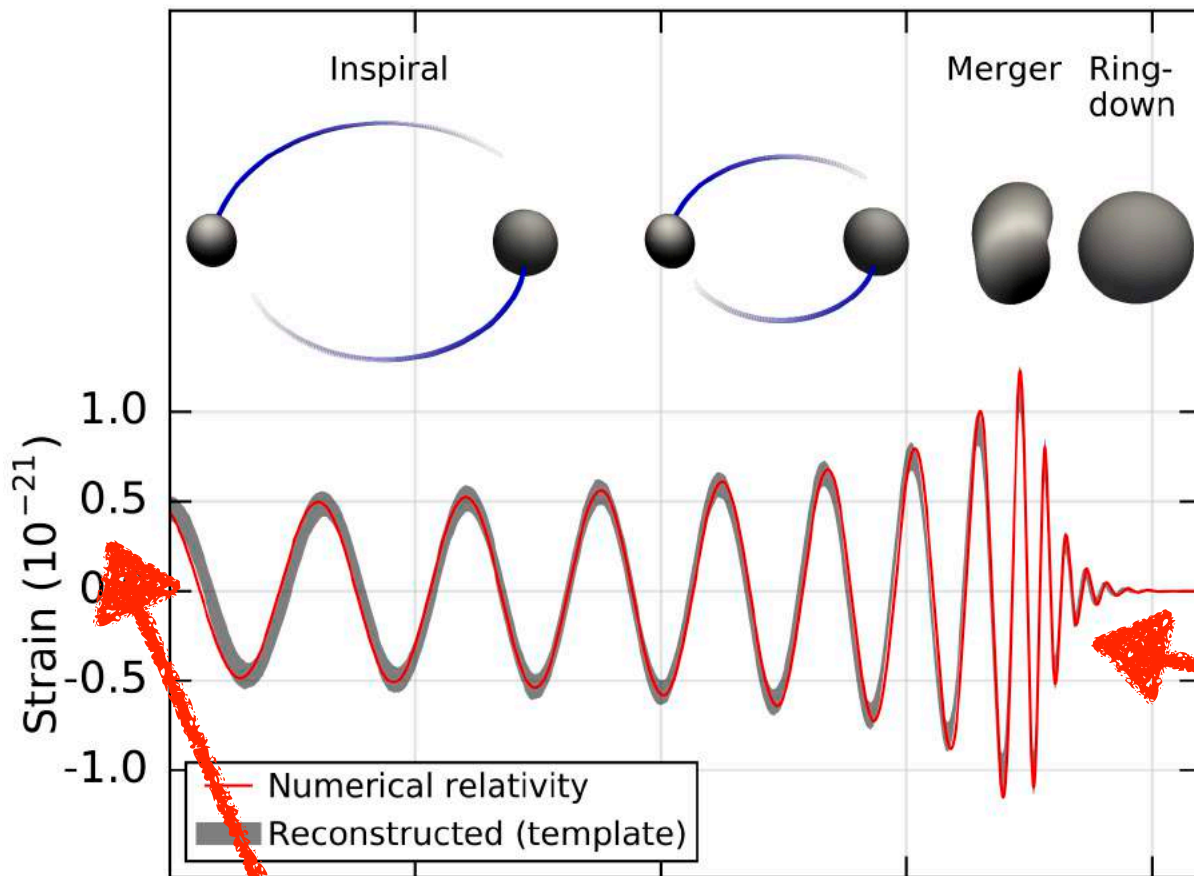


Figure 2. Posterior probability densities for binary component masses (m_1 , m_2), total mass (M), and chirp mass

GW anatomy & the need for numerical relativity



Detector signal for non-precessing binaries seen \sim face-on/off or $l=2, m=2$ -spherical harmonic.

$M \geq 12M_{\odot}$ requires NR for construction of detection templates.

(linear) black hole perturbation theory

“QNM” ringdown:

Describe signal in terms of damped sinusoids with frequencies + damping times known in terms of black hole spin:

Post-Newtonian expansion

$$\text{Hamiltonian} = H_N + O(v/c) + \dots$$

Similar for radiated energy, , ...

State of the art: mostly $(v/c)^7$

$$h = \sum_{l,m} e^{i\omega_{lm}t} e^{-t/\tau_{lm}}$$

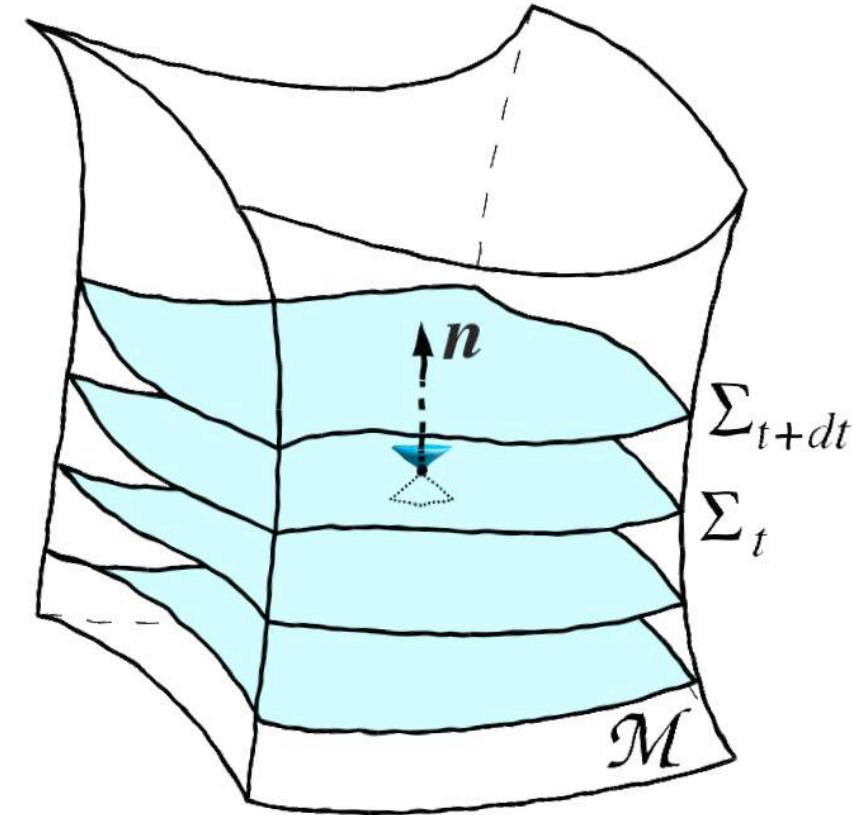
“holy grail” problem: numerically evolve BHs!

$$G_{ab} = \frac{8\pi G}{c^4} T_{ab} \quad \text{--- starting 1950's --->}$$

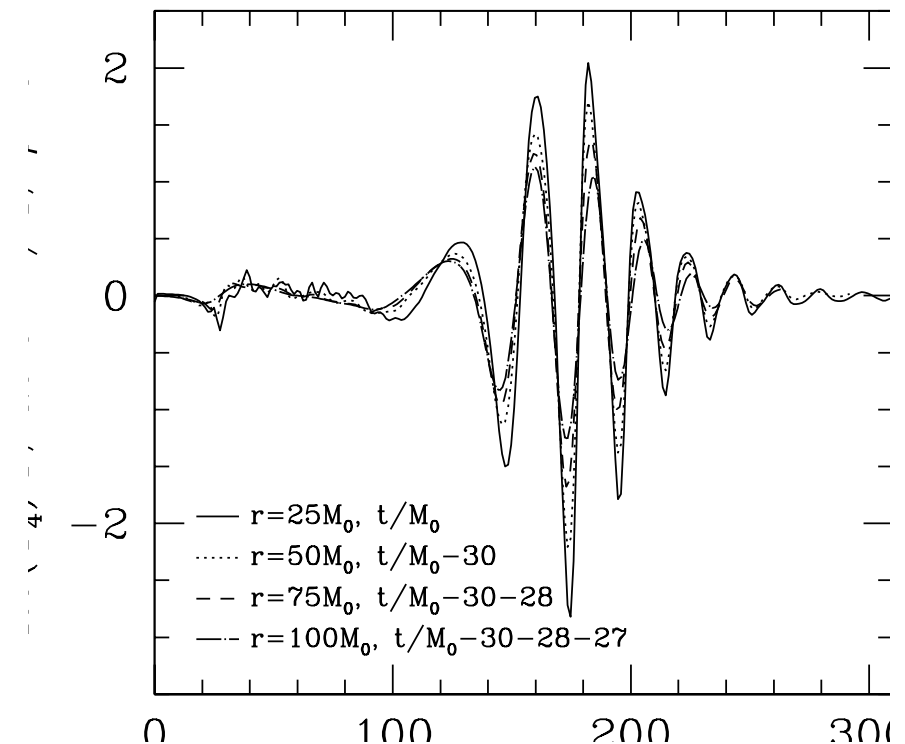
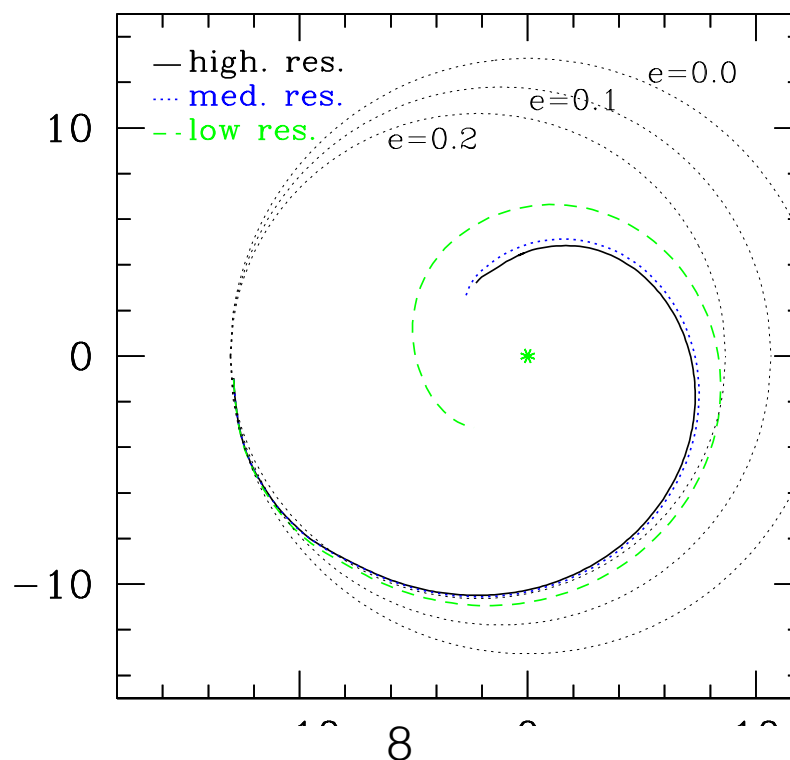
Choose coordinates for spacetime =>
 ~ 10 coupled nonlinear wave eqs., complex sources.

- GR is a gauge theory like E&M, Yang-Mills.

Preserving constraints numerically well understood for E&M, not GR.

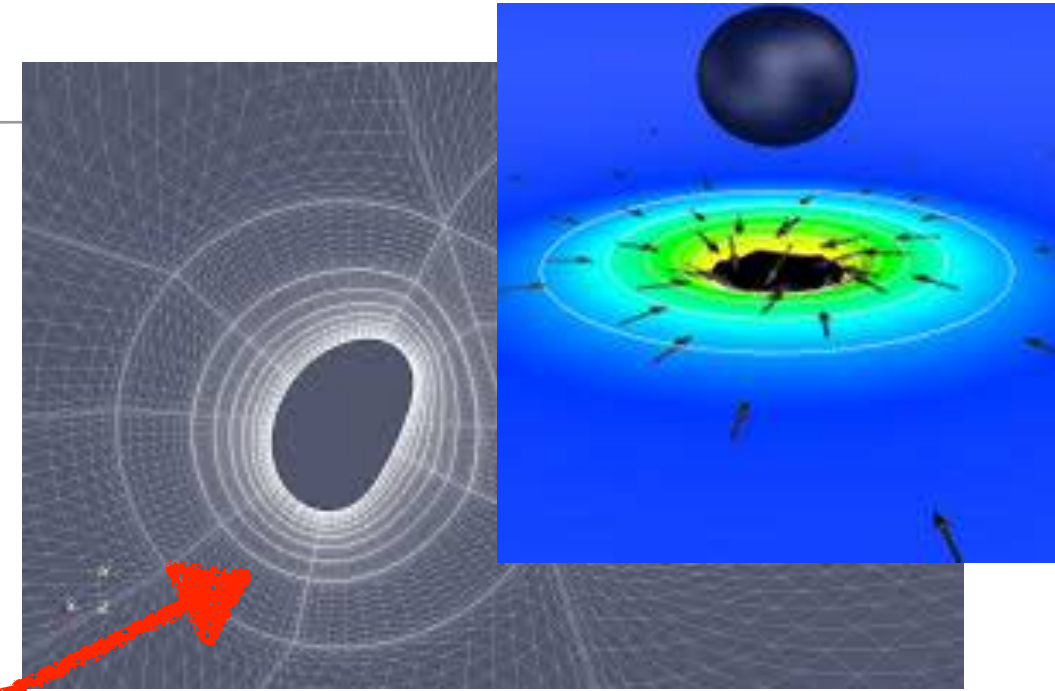


- **First orbit + GWs:**
Frans Pretorius 2005
- Surprise breakthrough after 4 decades of unstable formulations.
- => Gold-rush of improved methods and results.



Singularities and Black Holes

BHs are quintessential objects of GW physics: coalescence, end product of neutron star mergers or supernovae.



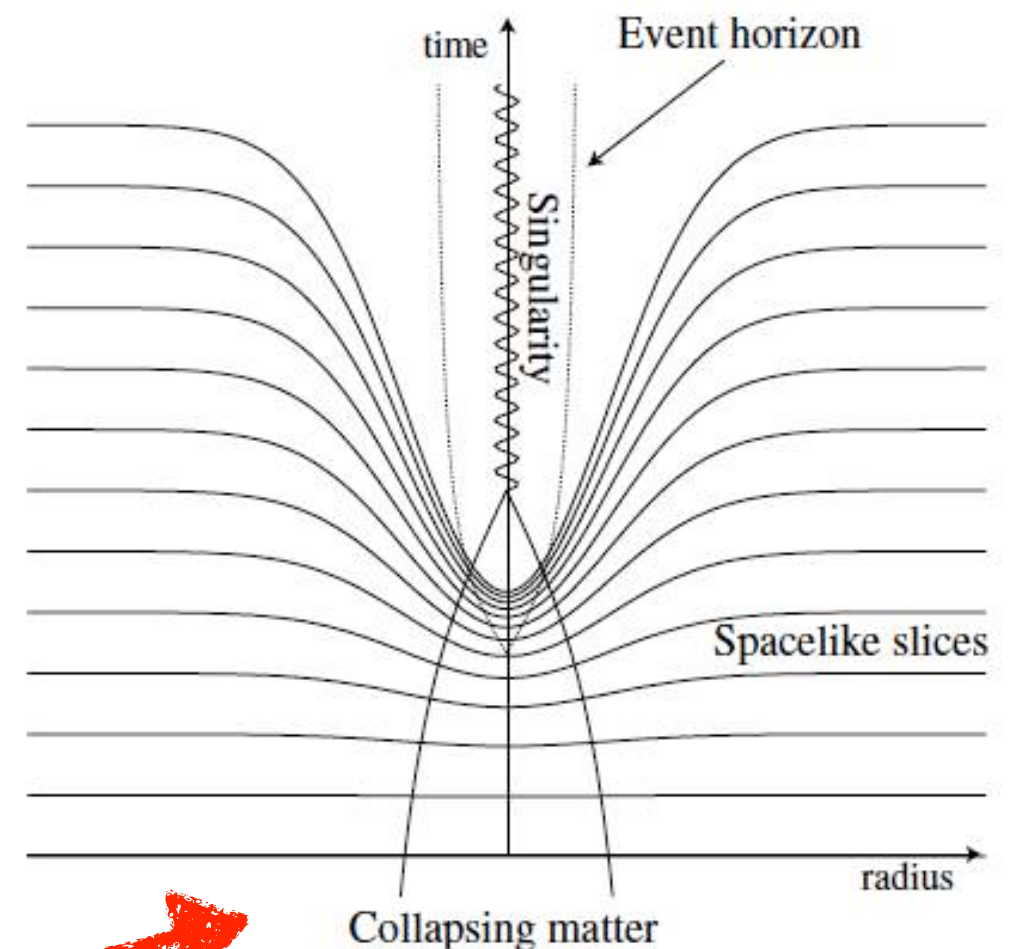
- Need to avoid simulating singular BH interior!

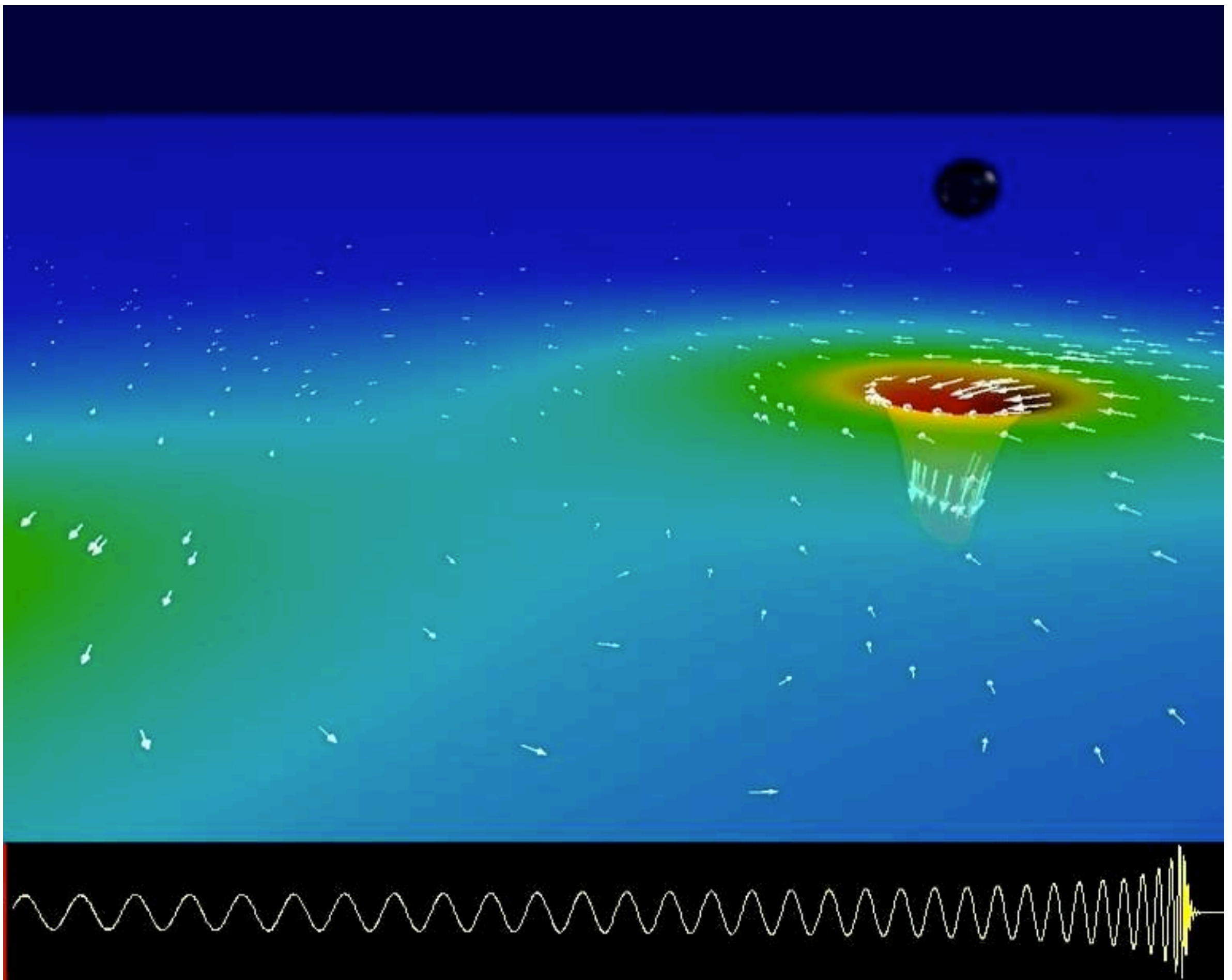
- **Excision technique:** don't evolve values inside a pure outflow boundary ("apparent" horizon)

Control systems keep excision surface (hole in domain) in place.

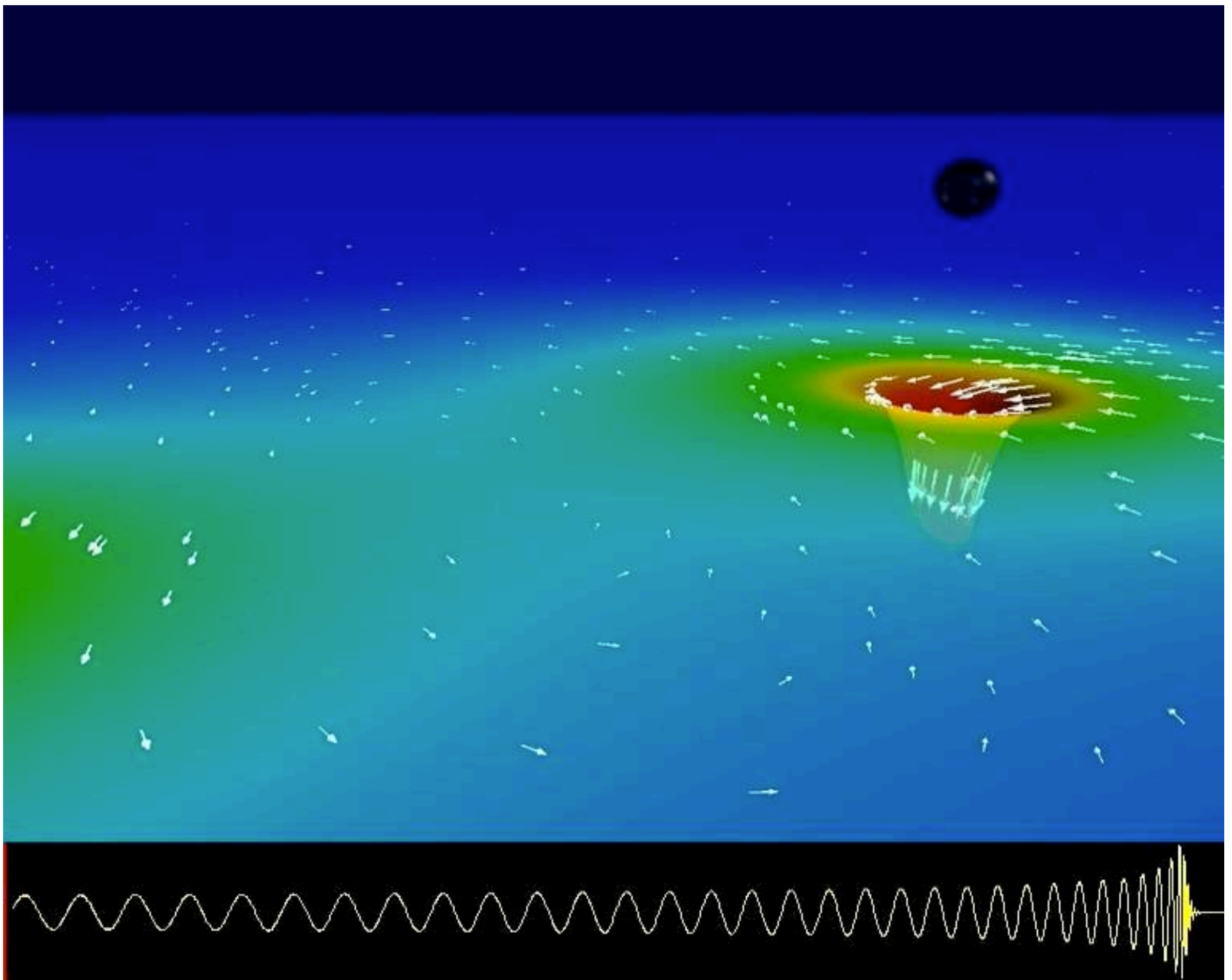
SpEC code / SXS collaboration

- **Singularity avoiding slicings:** Choose time coordinate to never reach physical singularity => no holes in computational domain.
Several finite difference codes.

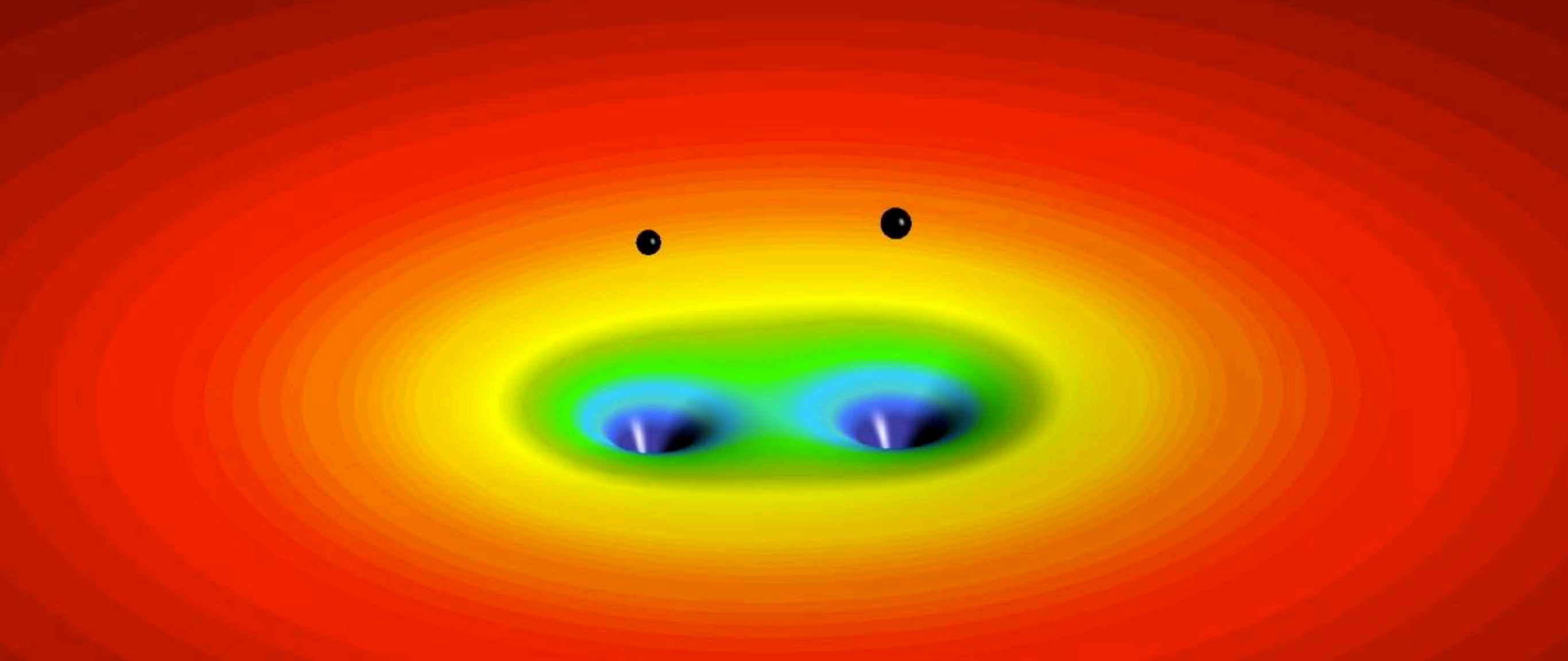




Visualizacion: SXS collaboration



Visualizacion: SXS collaboration

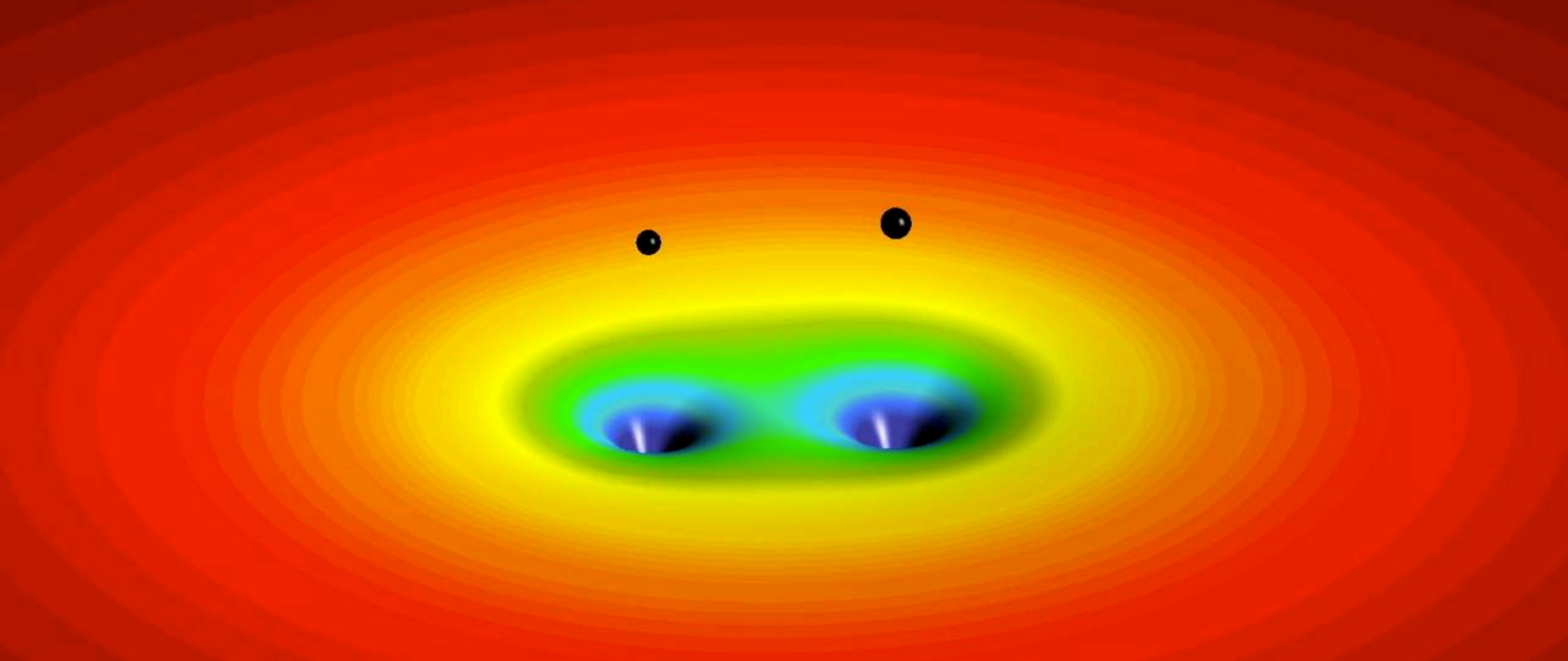


time(ms)=287.5



Visualización: Rafel Jaume Amengual, UIB

During the inspiral phase and after the merger, the geometry presents several approximate symmetries, a successful numerical scheme must be based on the coordinates that make these symmetries manifest..



time(ms)=287.5

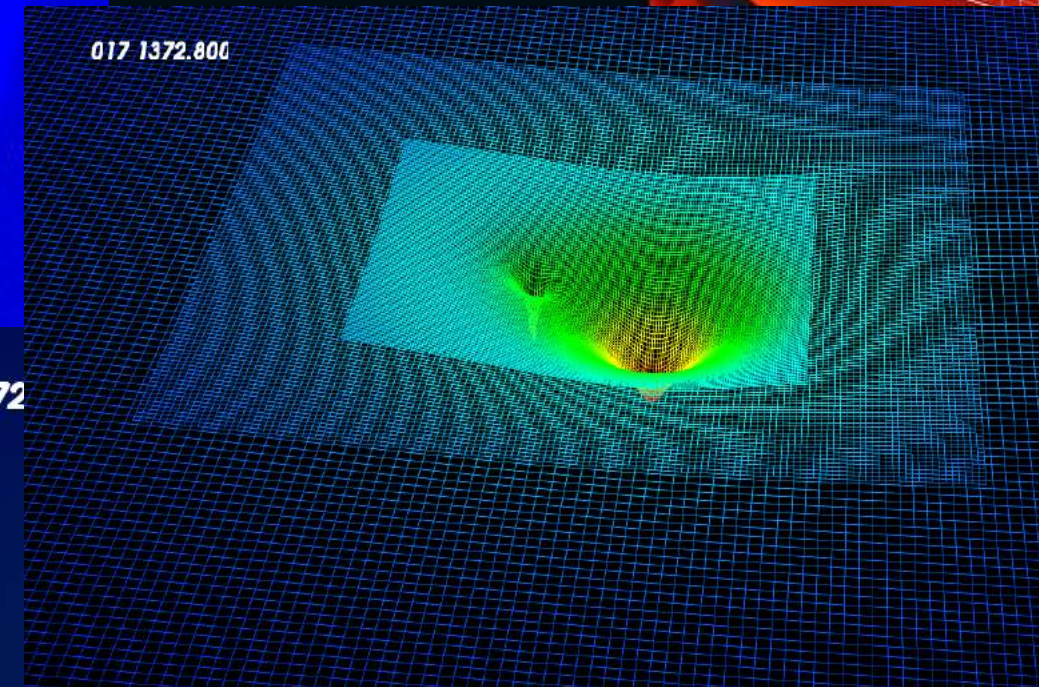
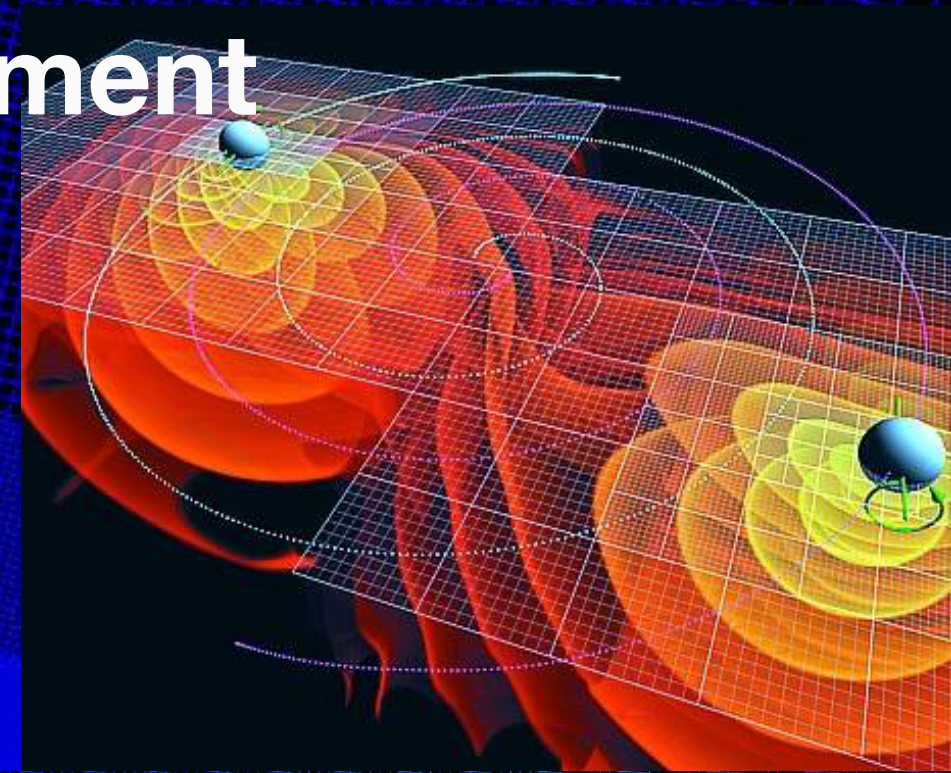


Visualización: Rafel Jaume Amengual, UIB

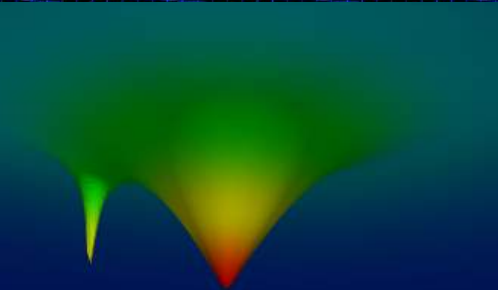
During the inspiral phase and after the merger, the geometry presents several approximate symmetries, a successful numerical scheme must be based on the coordinates that make these symmetries manifest..

Numerics, Scales & mesh refinement

- Solutions are smooth without matter: high order finite differencing or spectral methods.
- Several length & time scales:
 - individual compact objects
 - orbital scale
 - wave frequency increases \sim factor of 10
 - causally isolate boundaries
- Need spatial and temporal mesh refinement,
- Simulations $\sim 10^5 - 10^6$ core hours, $\sim 10^9$ core hours in total so far



017 1372

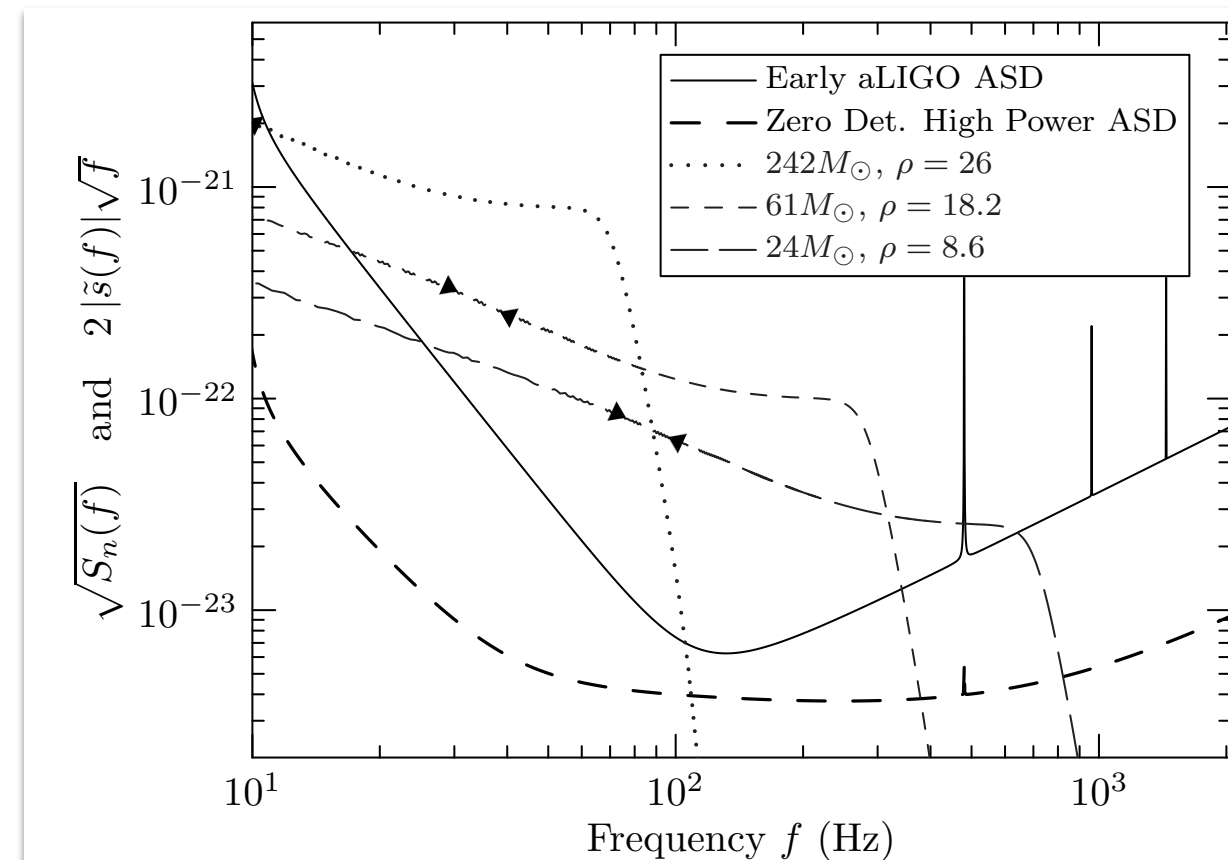
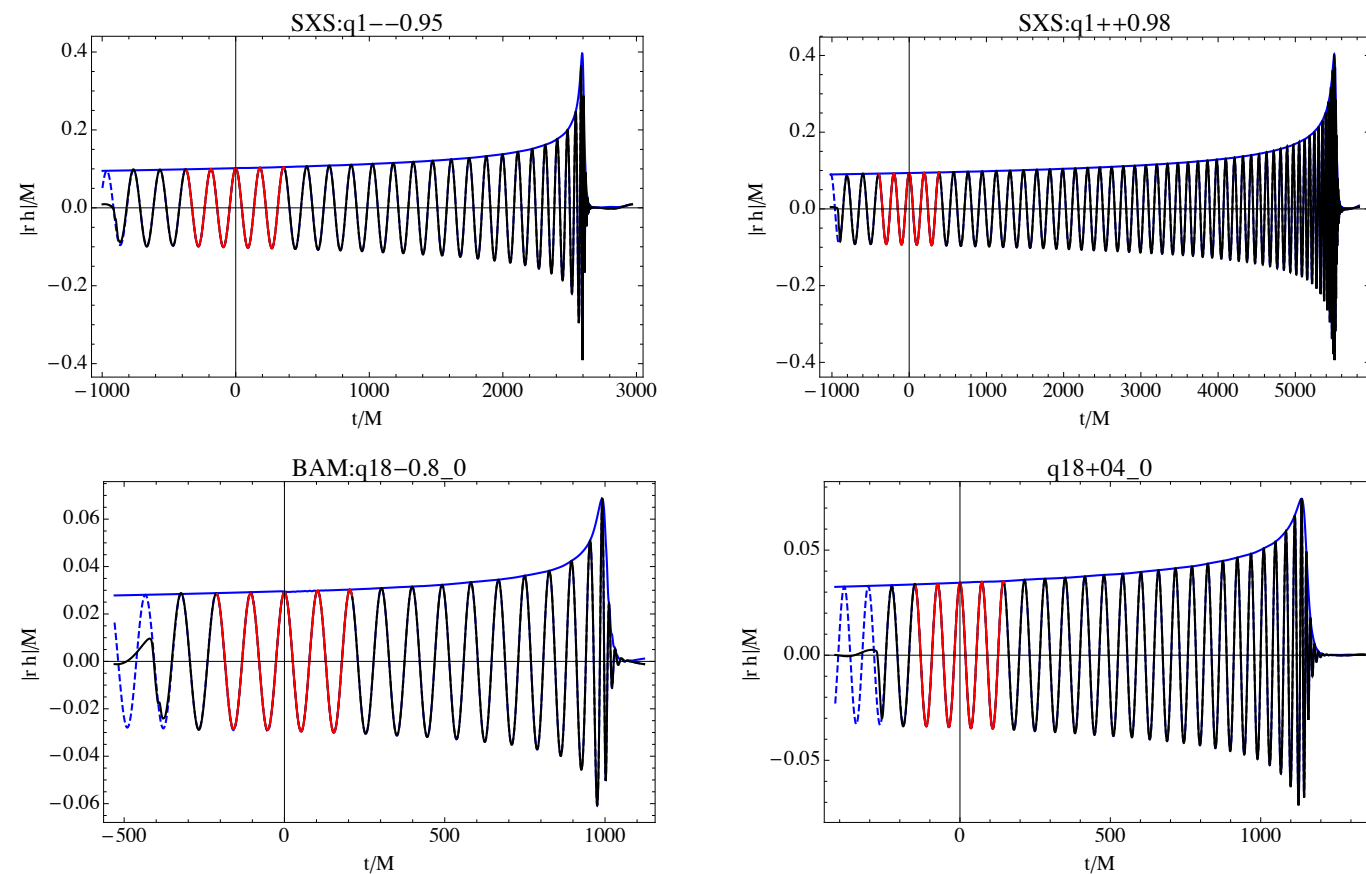


Gluing PN + NR: Hybrid waveforms

- Extending NR to low frequencies is very expensive!

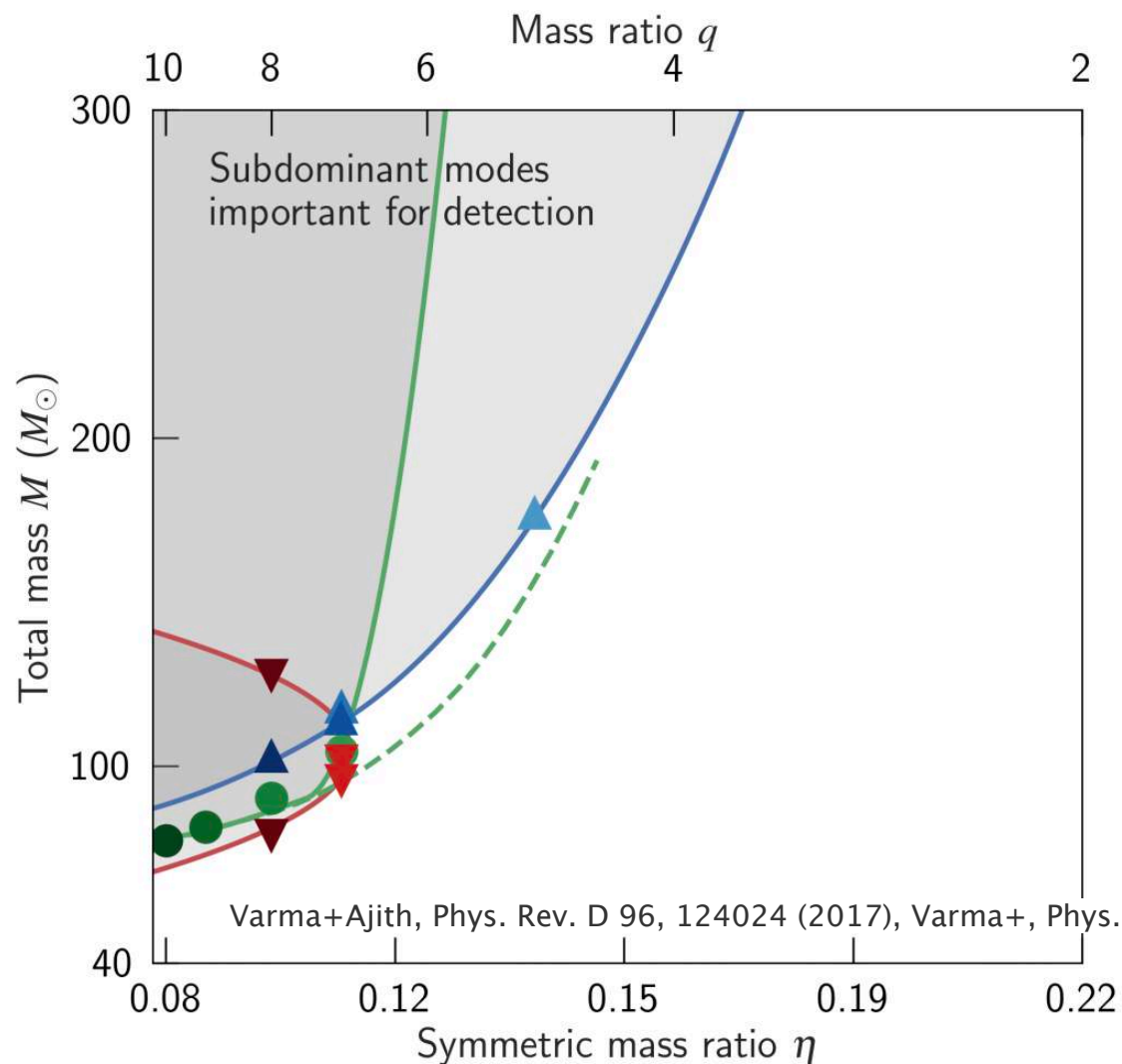
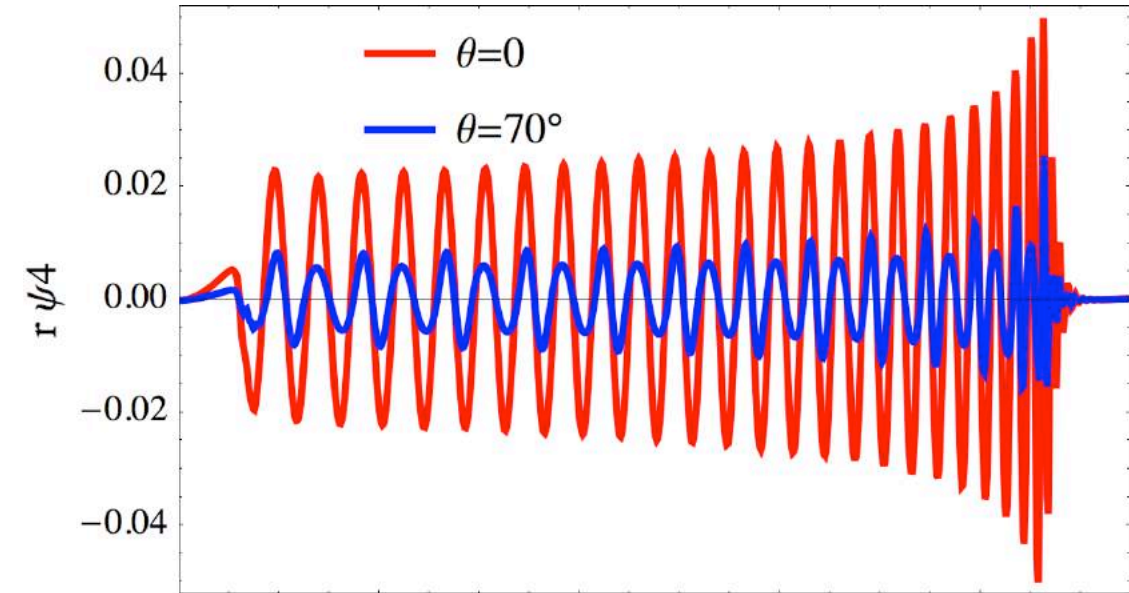
$$T_{\text{coalescence}} \approx \eta^{-1} f_{\text{initial}}^{-8/3} \quad \eta = \frac{m_1 m_2}{(m_1 + m_2)^2}$$

- -> hybridise (glue) with post-Newtonian waveforms: input data to calibrate waveform models.

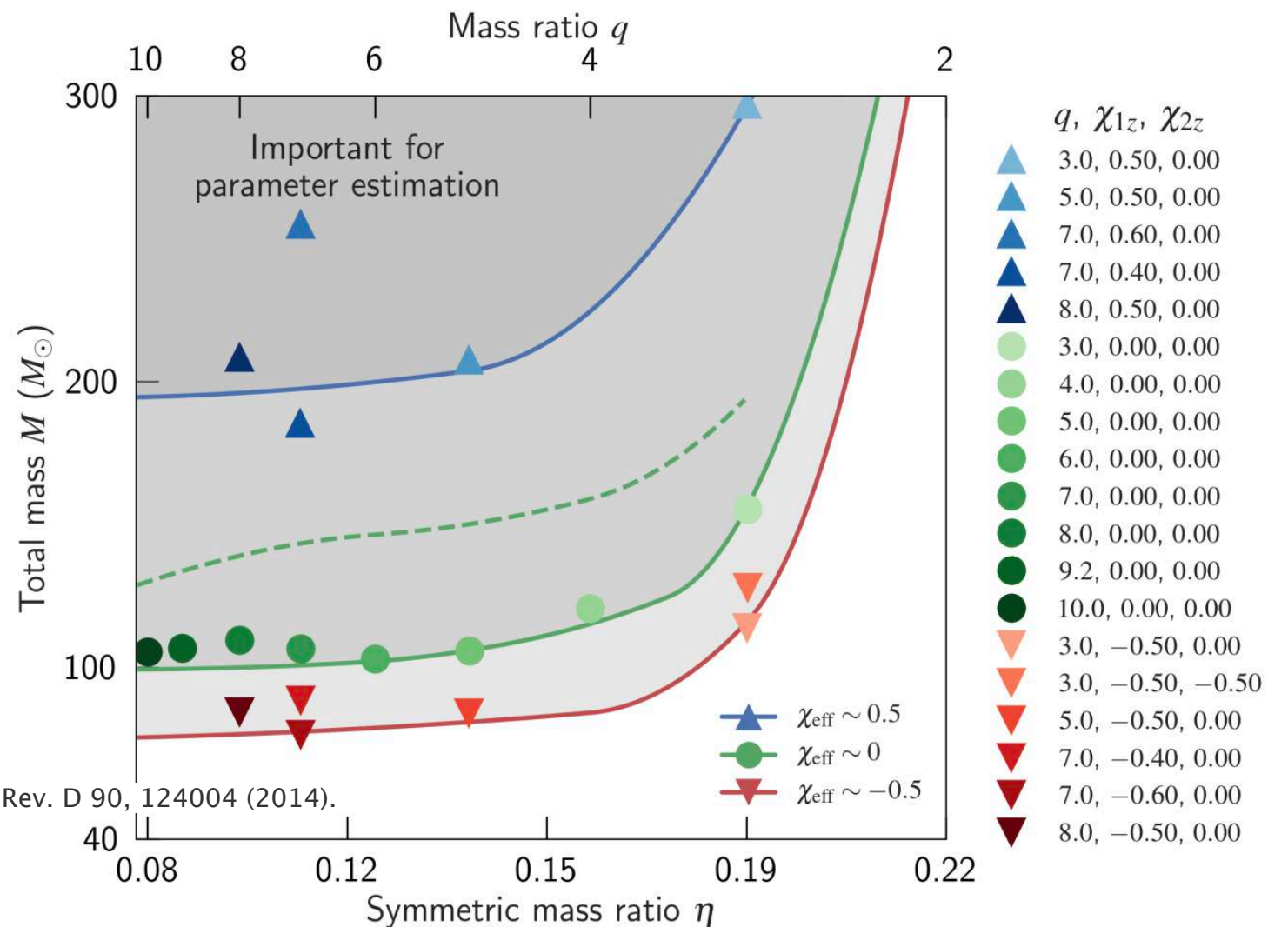


Subdominant spherical harmonics

- Data analysis used to only use $l=|m|=2$.
- Several efforts to incorporate harmonics into data analysis for O3 -> *poster by C. García*.
- [London+, PRL 2018, Cotesta+, PRD 2018]



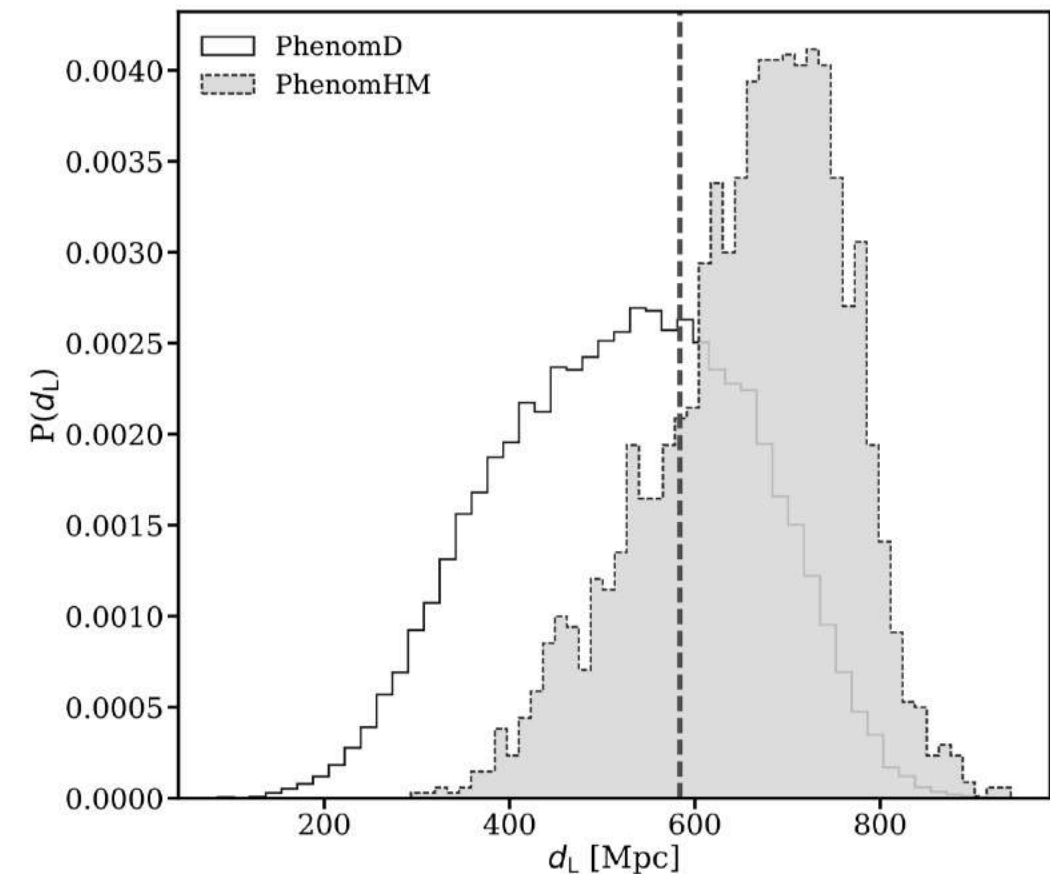
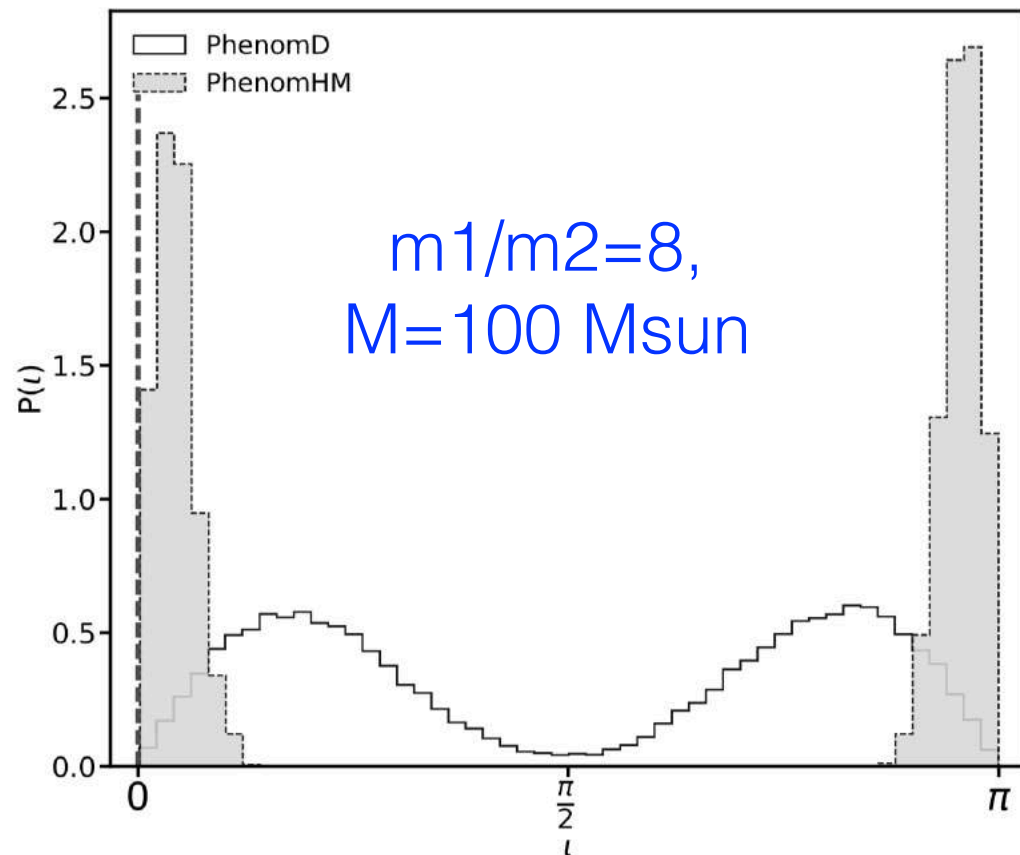
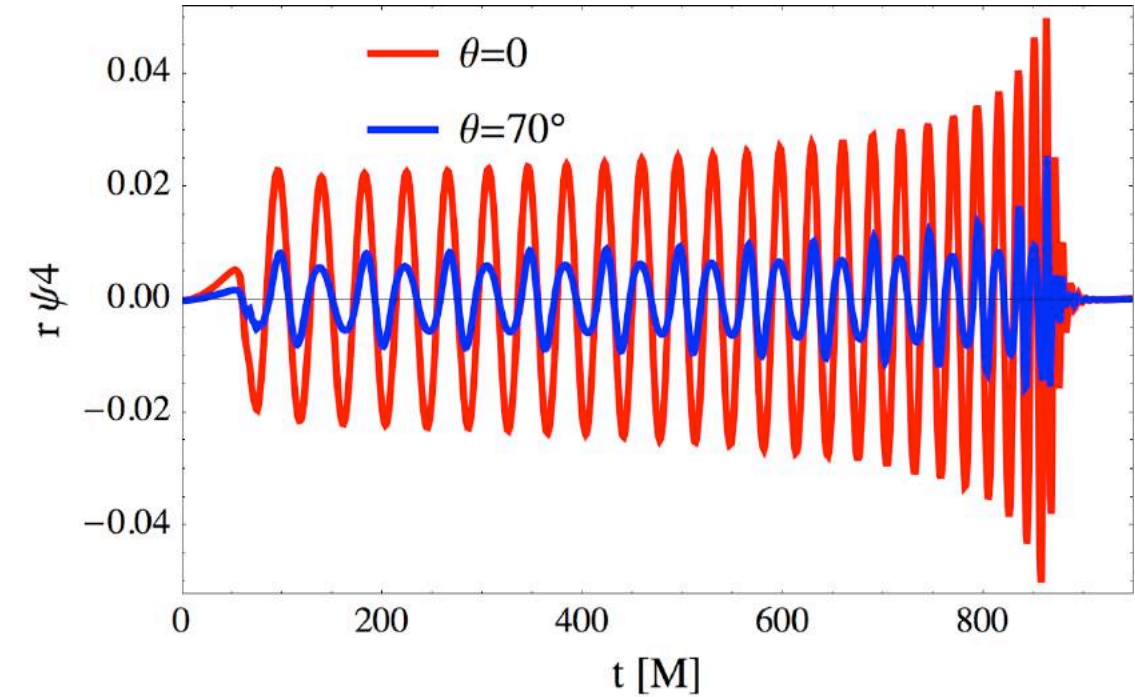
(a) For detection



(b) For parameter estimation

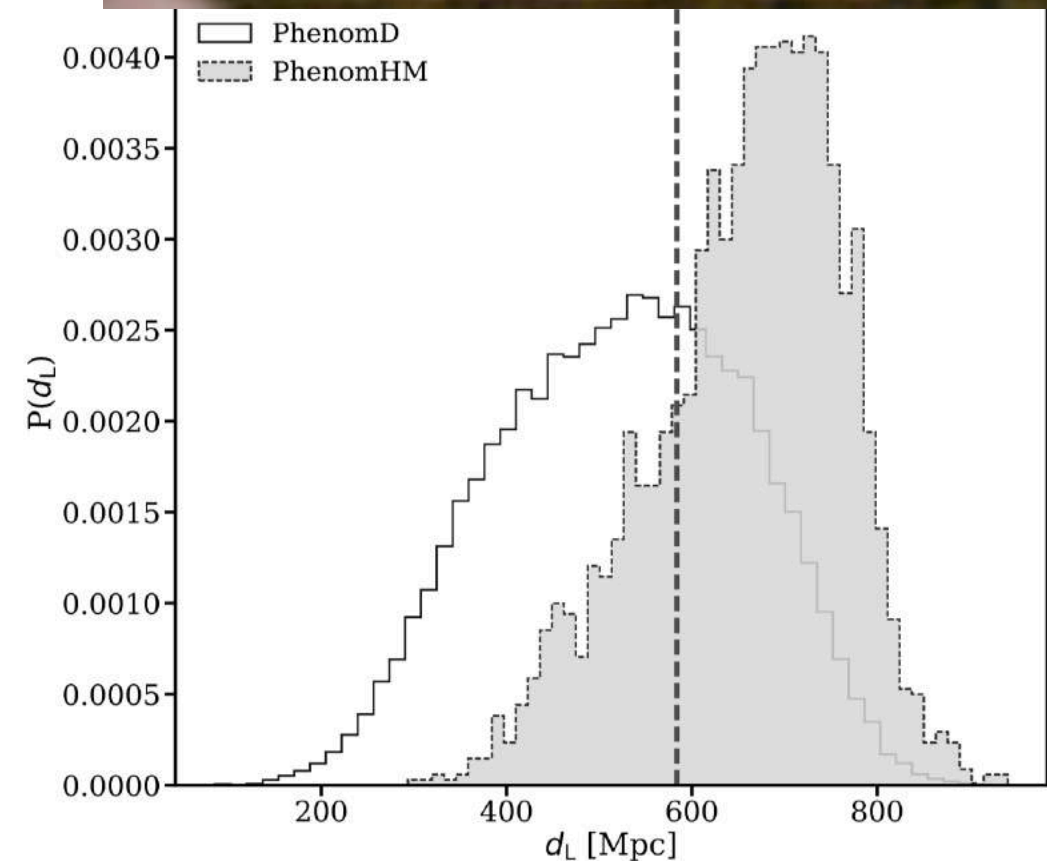
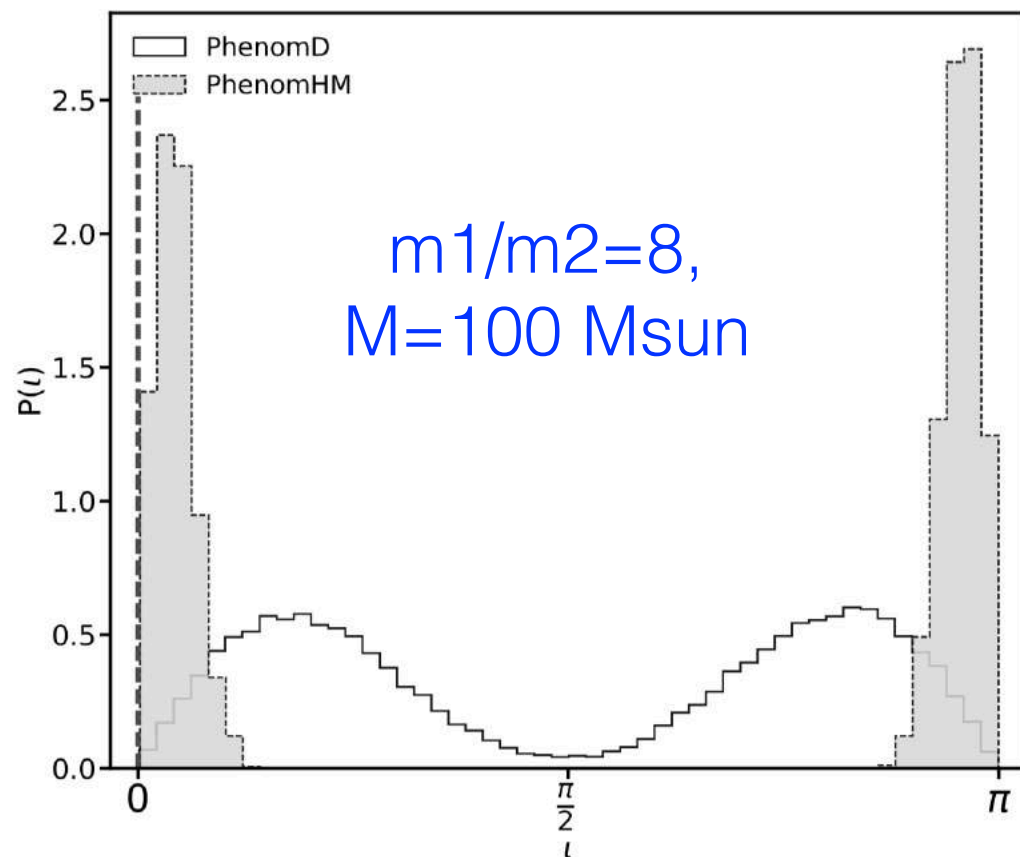
Subdominant spherical harmonics

- Data analysis used to only use $l=|m|=2$.
- Several efforts to incorporate harmonics into data analysis for O3 -> *poster by C. García*.
- [London+, PRL 2018, Cotesta+, PRD 2018]



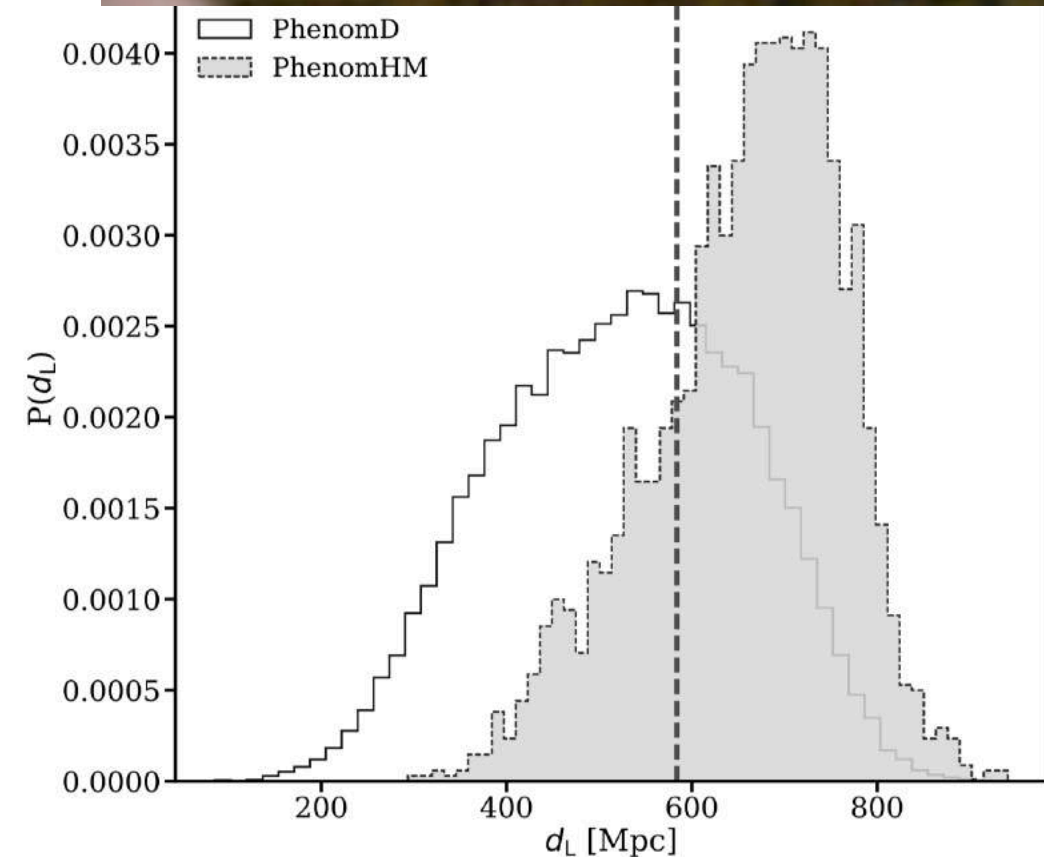
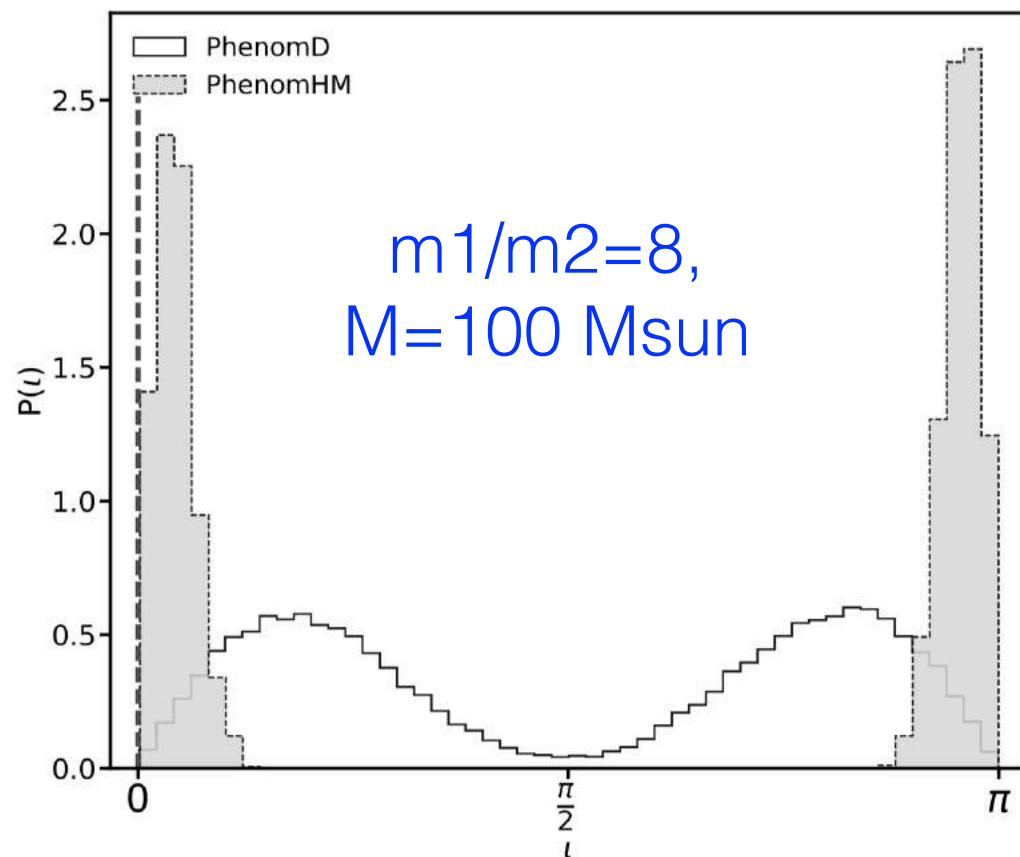
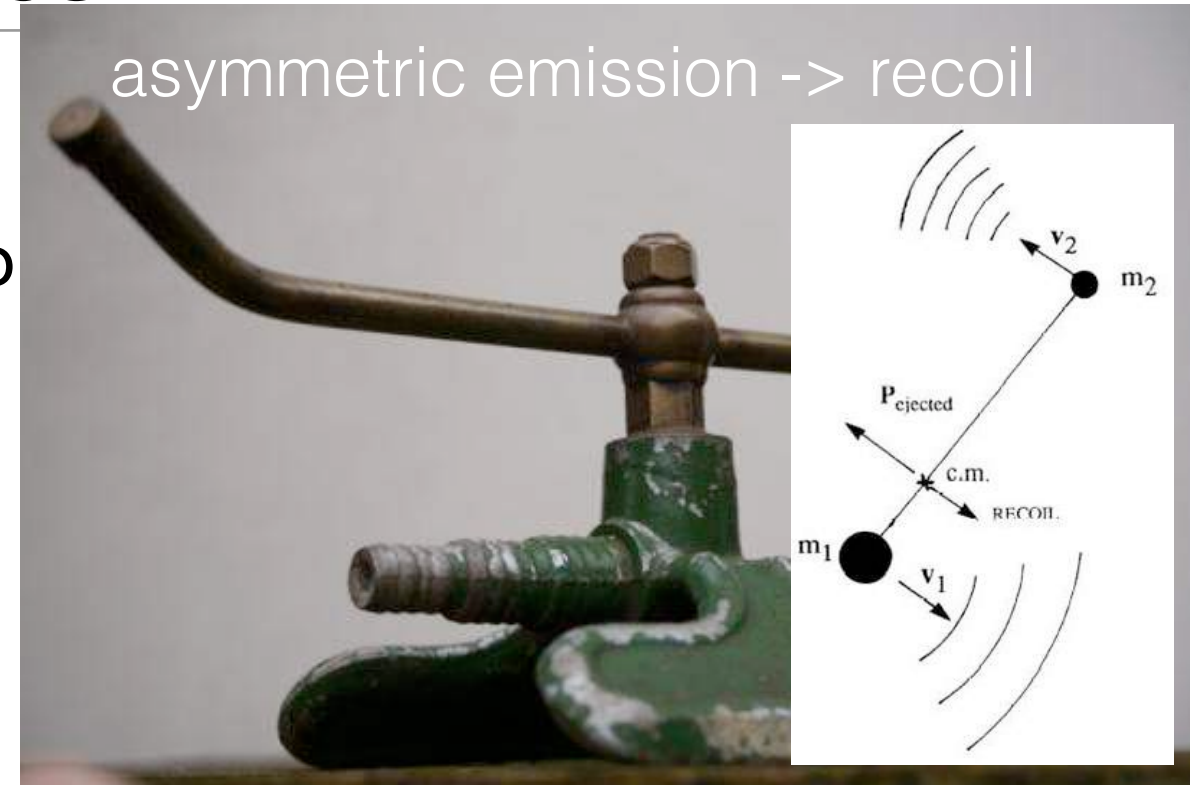
Subdominant spherical harmonics

- Data analysis used to only use $l=|m|=2$.
- Several efforts to incorporate harmonics into data analysis for O3 -> *poster by C. García*.
- [London+, PRL 2018, Cotesta+, PRD 2018]



Subdominant spherical harmonics

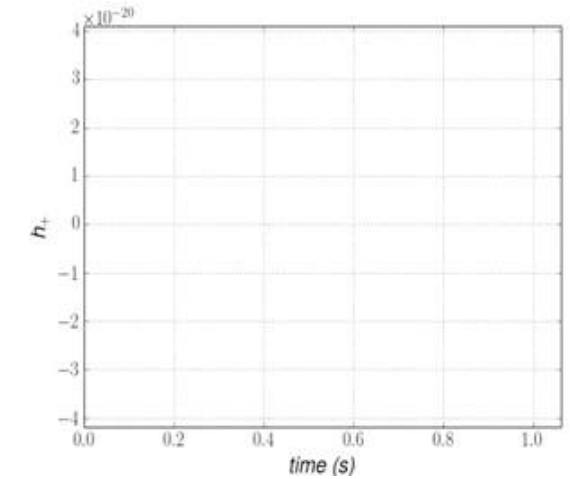
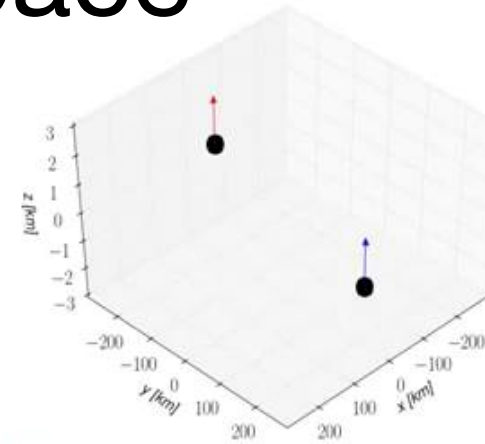
- Data analysis used to only use $l=|m|=2$.
- Several efforts to incorporate harmonics into data analysis for O3 -> *poster by C. García*.
- [London+, PRL 2018, Cotesta+, PRD 2018]



Spins & the BBH parameter space

- **Leading order PN spin effect: spin-orbit**

$$H_{SO} = 2 \frac{\vec{S}_{\text{eff}} \cdot \vec{L}}{r^3} \quad \dot{S} = -2 \frac{\vec{S}_{\text{eff}} \times \vec{L}}{r^3}$$

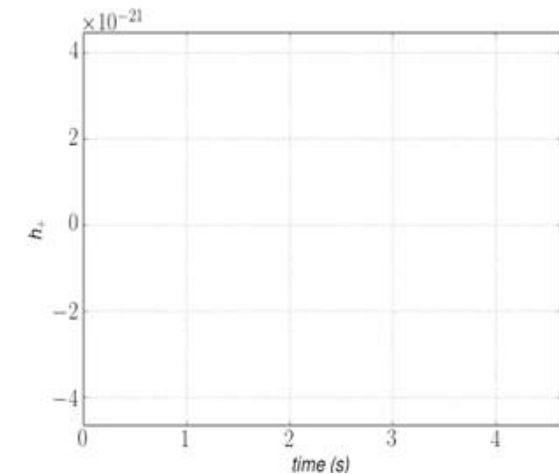
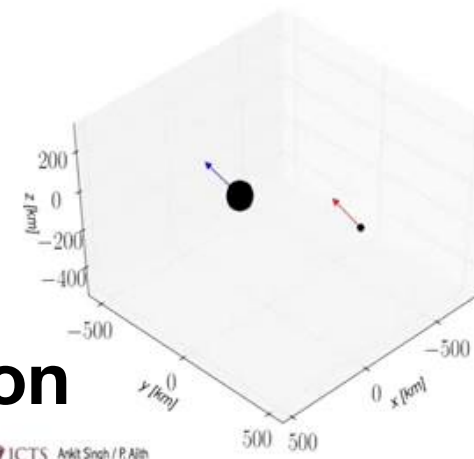


- **Spins orthogonal to orbital plane: plane preserved.**

- 3-dimensional parameter space: dominant “average” spin

$$\chi_{\text{eff}} = \frac{\vec{S}_1 \cdot \hat{L}/m_2 + \vec{S}_2 \cdot \hat{L}/m_1}{m_1 + m_2} \quad \text{measure ok}$$

- subdominant: spin difference **not yet**



- **Spin components in orbital plane: precession**

7 dimensions (9 with eccentricity)

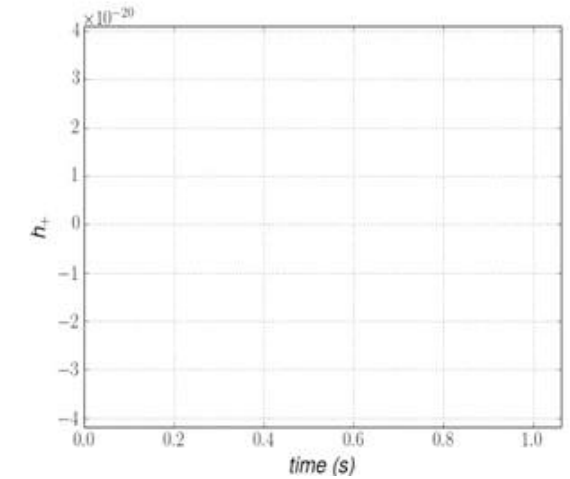
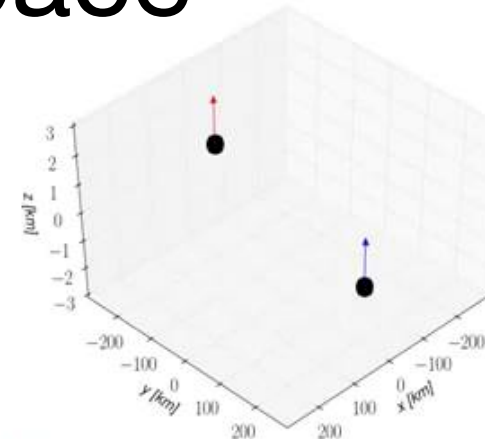
- Dominant precession effective spin [Hannam+ PRL 2013, Schmidt+ PRD2014]

$$A_1 = 2 + \frac{3m_2}{2m_1} \quad \chi_p = \frac{\max(A_1 S_{1\perp}, A_2 S_{2\perp})}{A_2 m_2^2} \quad \text{measure poorly}$$

Spins & the BBH parameter space

- **Leading order PN spin effect: spin-orbit**

$$H_{SO} = 2 \frac{\vec{S}_{\text{eff}} \cdot \vec{L}}{r^3} \quad \dot{S} = -2 \frac{\vec{S}_{\text{eff}} \times \vec{L}}{r^3}$$

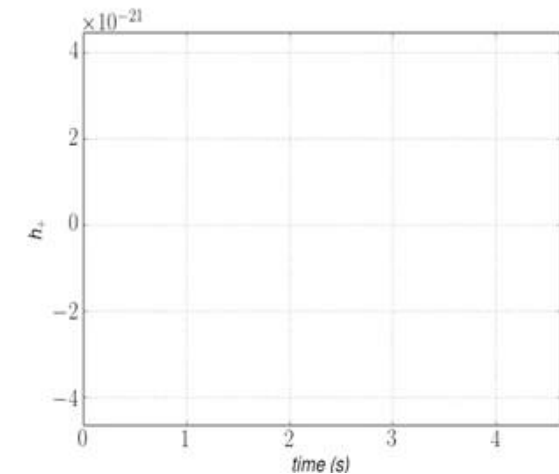
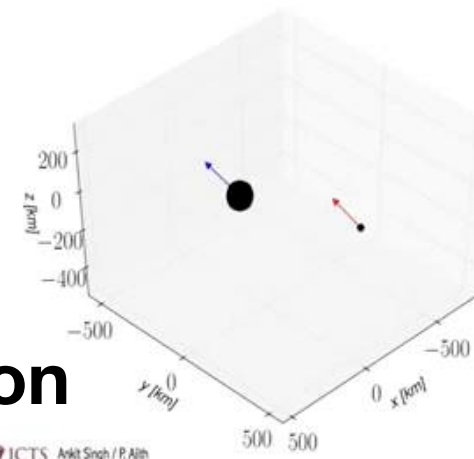


- **Spins orthogonal to orbital plane: plane preserved.**

- 3-dimensional parameter space: dominant “average” spin

$$\chi_{\text{eff}} = \frac{\vec{S}_1 \cdot \hat{L}/m_2 + \vec{S}_2 \cdot \hat{L}/m_1}{m_1 + m_2} \quad \text{measure ok}$$

- subdominant: spin difference **not yet**



- **Spin components in orbital plane: precession**

7 dimensions (9 with eccentricity)

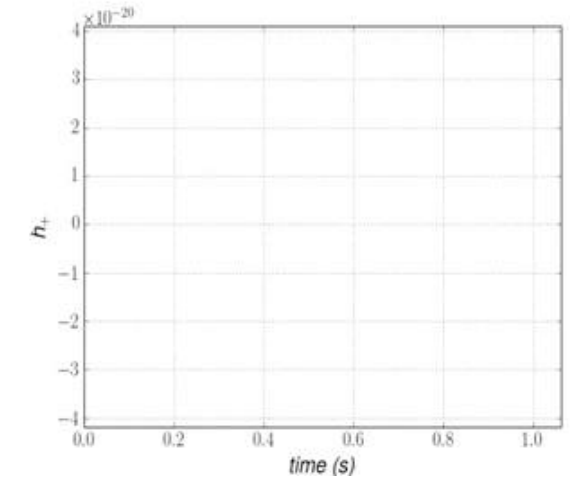
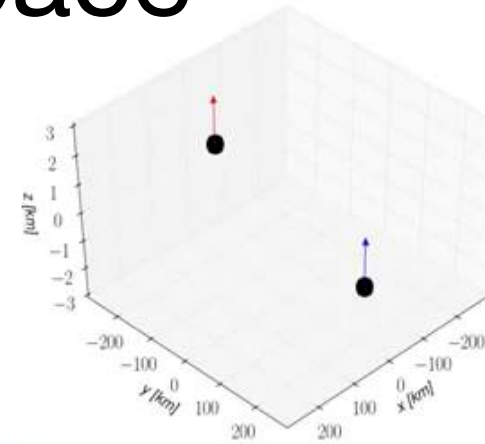
- Dominant precession effective spin [Hannam+ PRL 2013, Schmidt+ PRD2014]

$$A_1 = 2 + \frac{3m_2}{2m_1} \quad \chi_p = \frac{\max(A_1 S_{1\perp}, A_2 S_{2\perp})}{A_2 m_2^2} \quad \text{measure poorly}$$

Spins & the BBH parameter space

- **Leading order PN spin effect: spin-orbit**

$$H_{SO} = 2 \frac{\vec{S}_{\text{eff}} \cdot \vec{L}}{r^3} \quad \dot{S} = -2 \frac{\vec{S}_{\text{eff}} \times \vec{L}}{r^3}$$

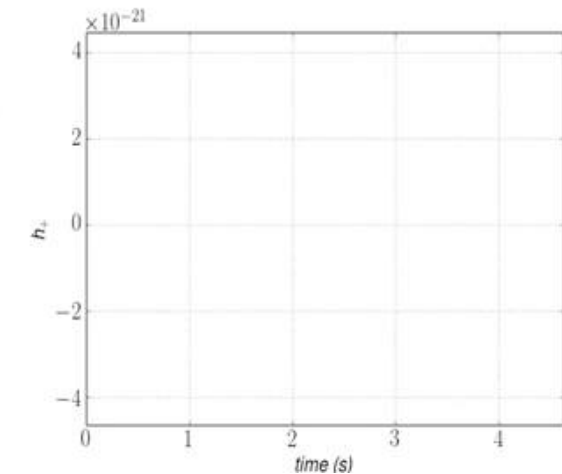
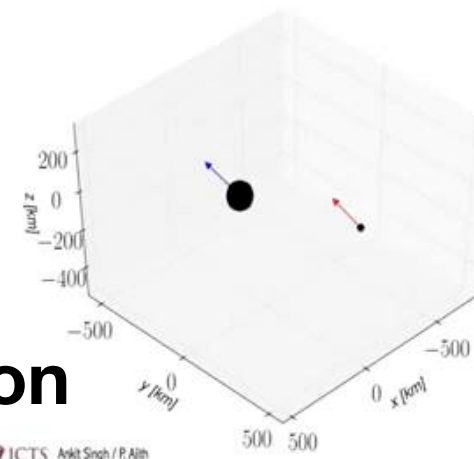


- **Spins orthogonal to orbital plane: plane preserved.**

- 3-dimensional parameter space: dominant “average” spin

$$\chi_{\text{eff}} = \frac{\vec{S}_1 \cdot \hat{L}/m_2 + \vec{S}_2 \cdot \hat{L}/m_1}{m_1 + m_2} \quad \text{measure ok}$$

- subdominant: spin difference **not yet**



- **Spin components in orbital plane: precession**

7 dimensions (9 with eccentricity)

- Dominant precession effective spin [Hannam+ PRL 2013, Schmidt+ PRD2014]

$$A_1 = 2 + \frac{3m_2}{2m_1} \quad \chi_p = \frac{\max(A_1 S_{1\perp}, A_2 S_{2\perp})}{A_2 m_2^2} \quad \text{measure poorly}$$

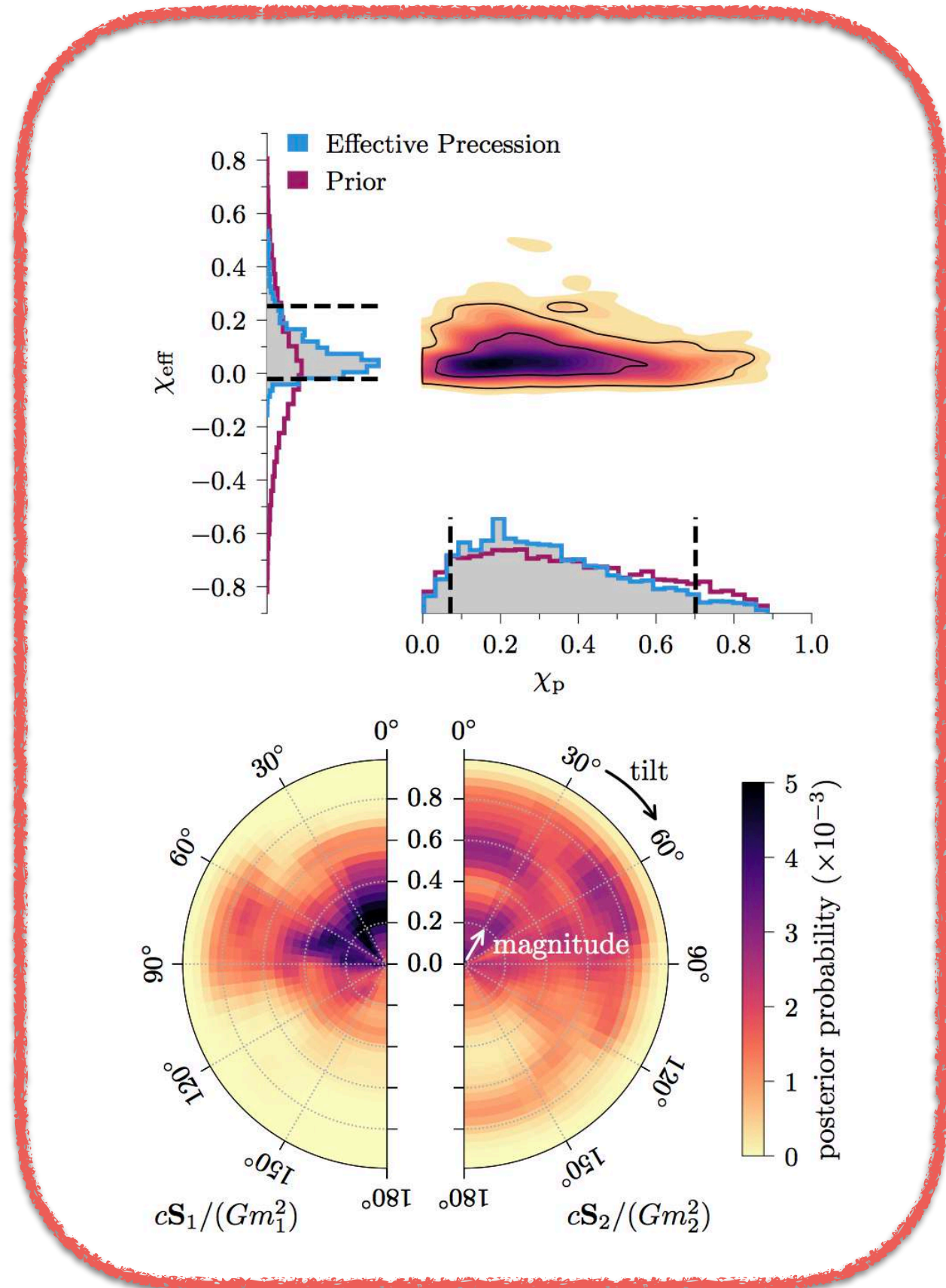
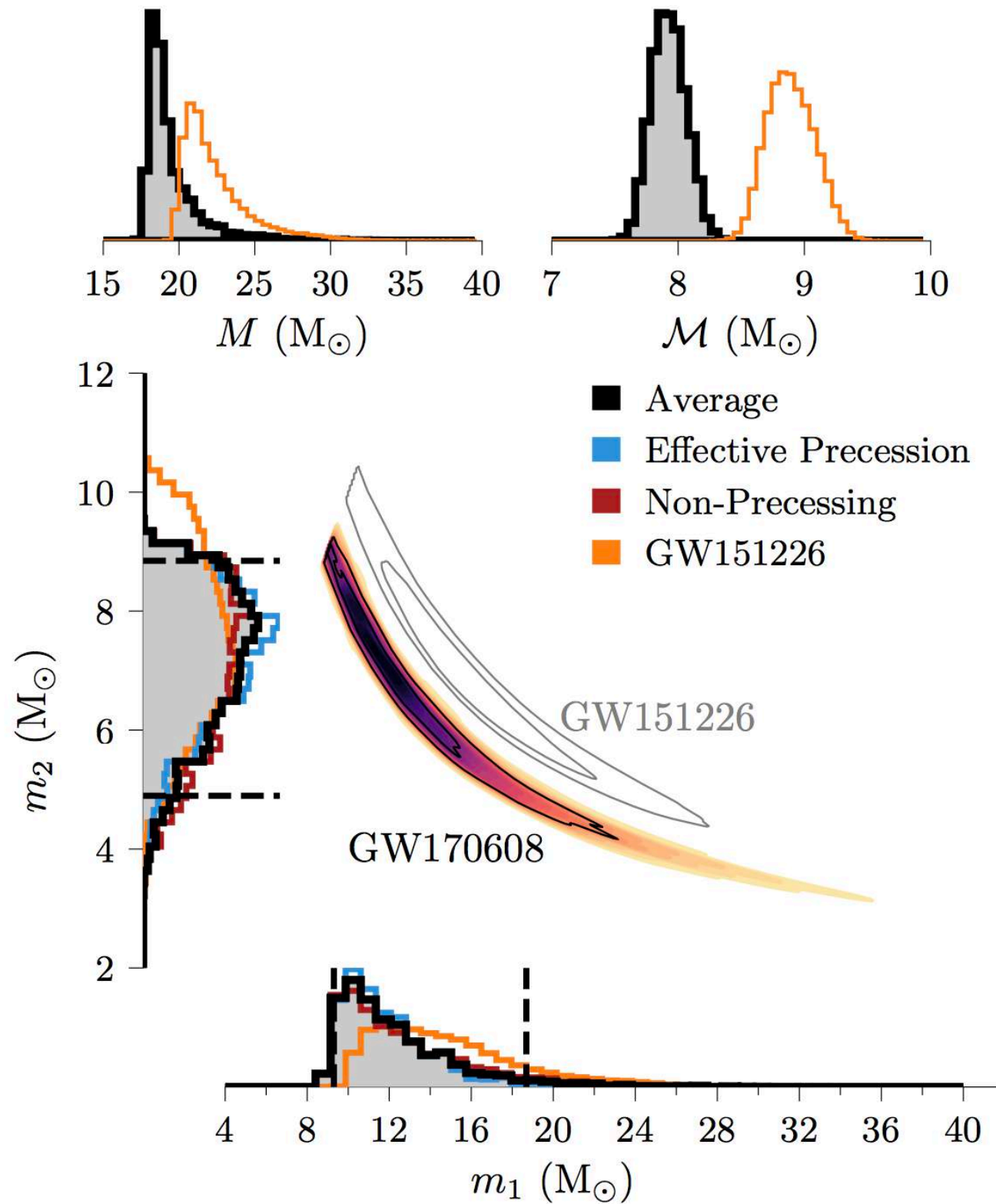
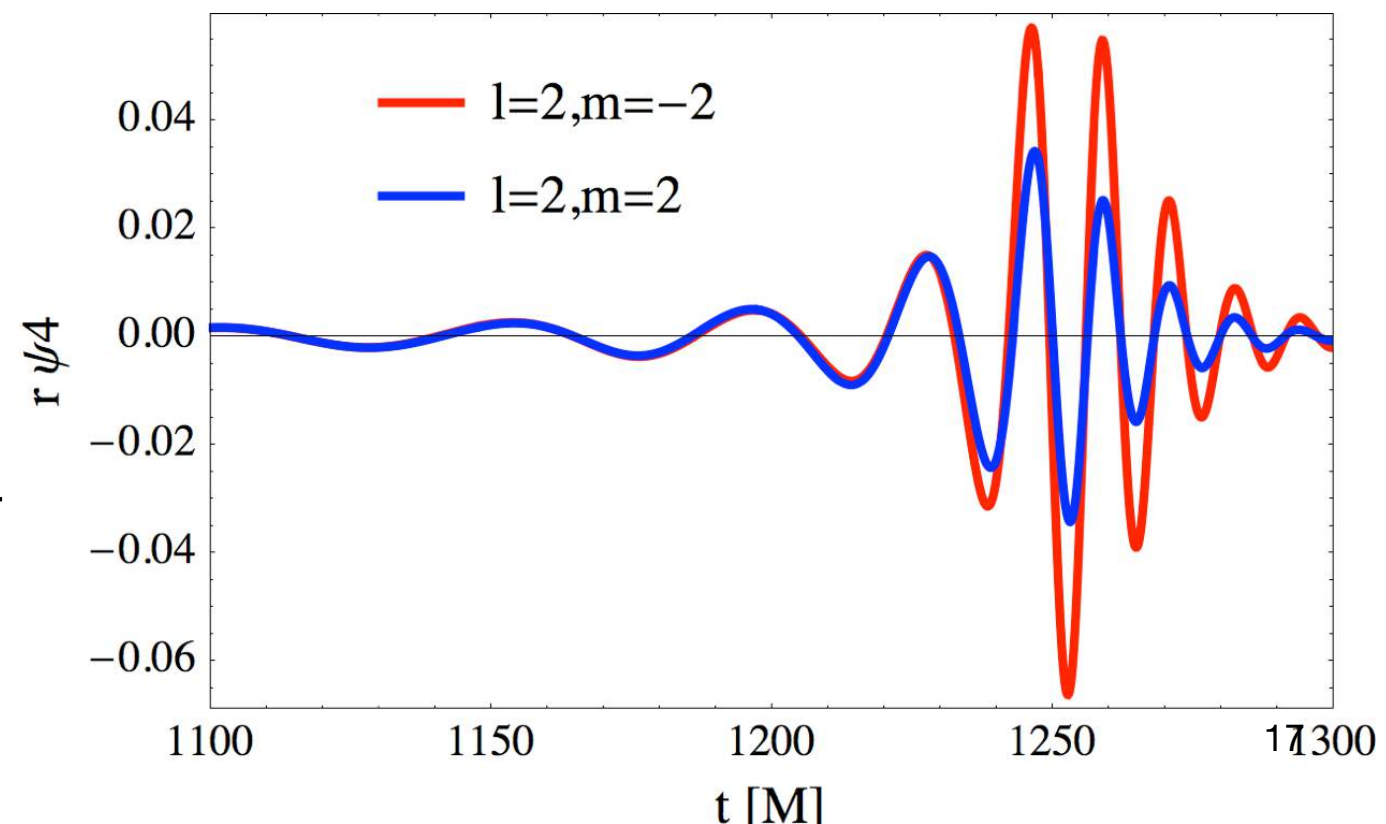
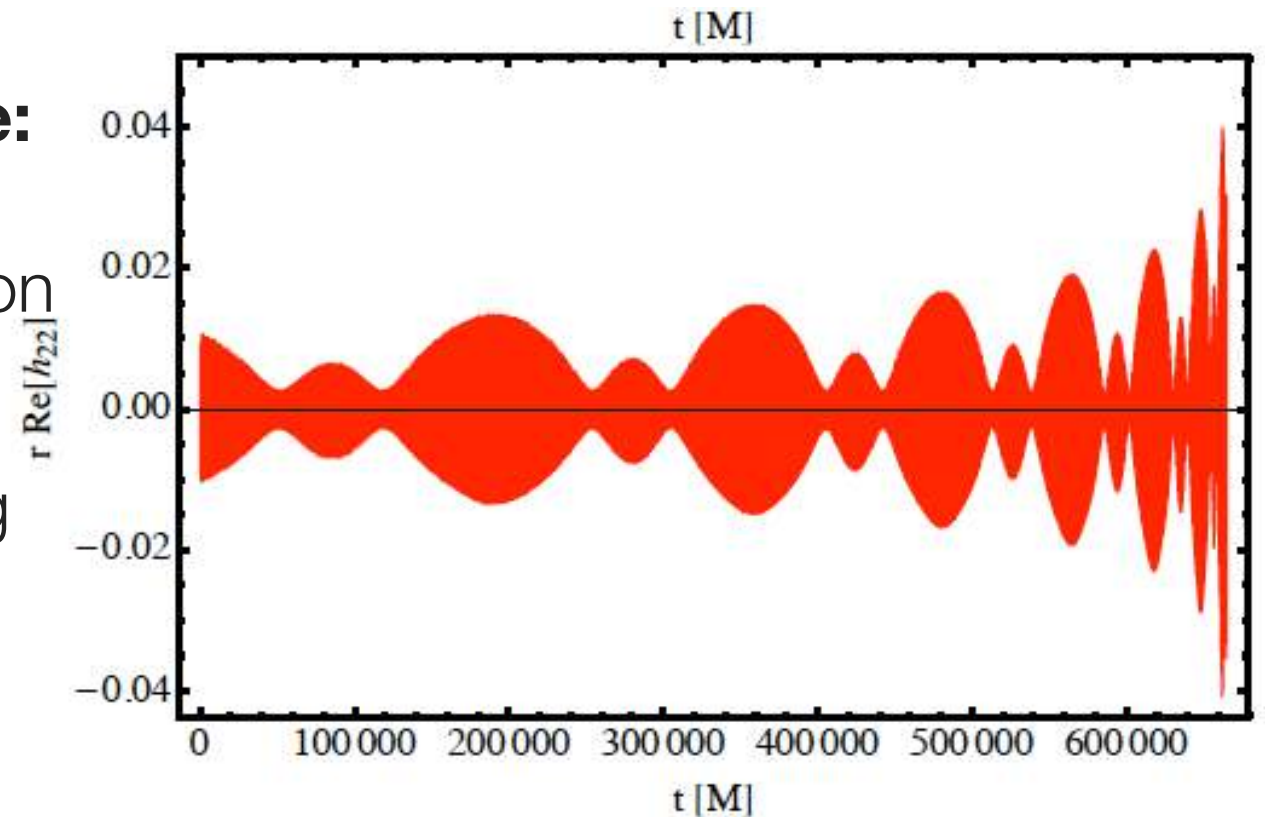
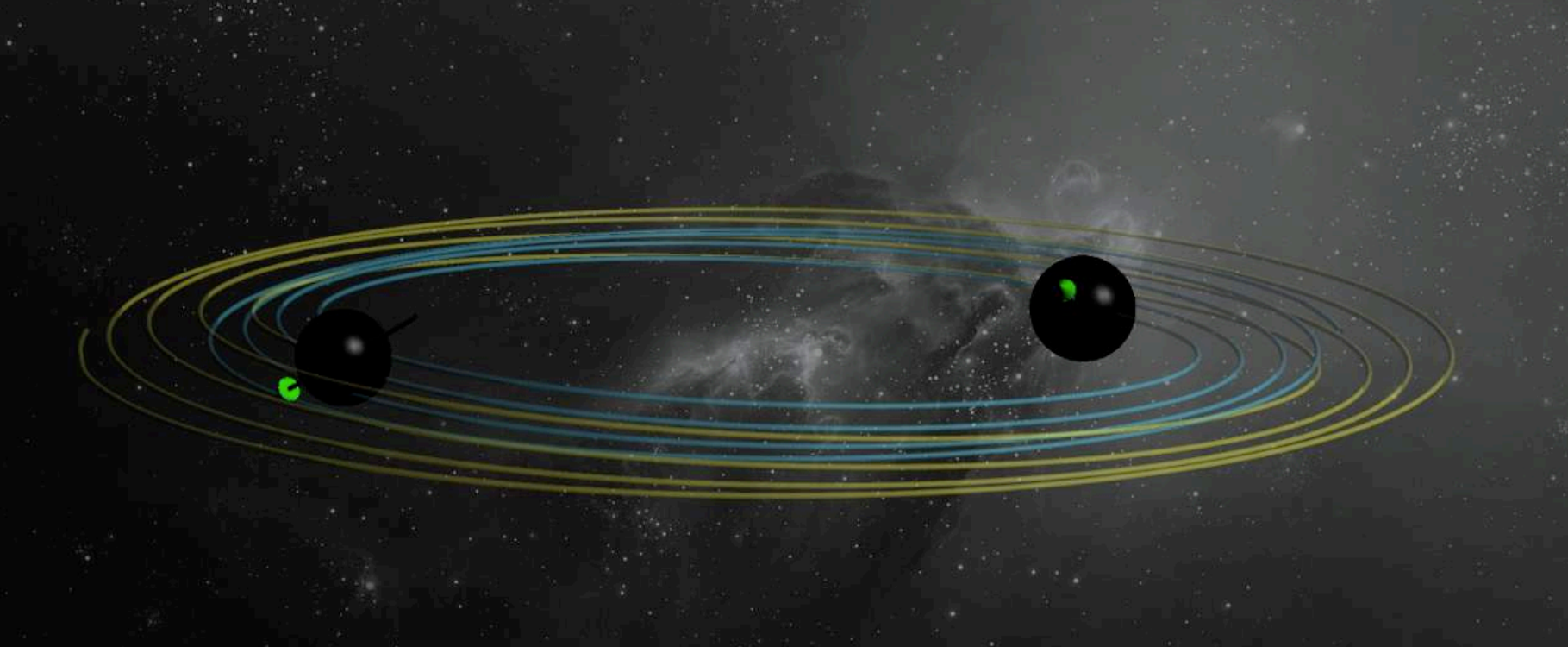


Figure 2. Posterior probability densities for binary component masses (m_1 , m_2), total mass (M), and chirp mass

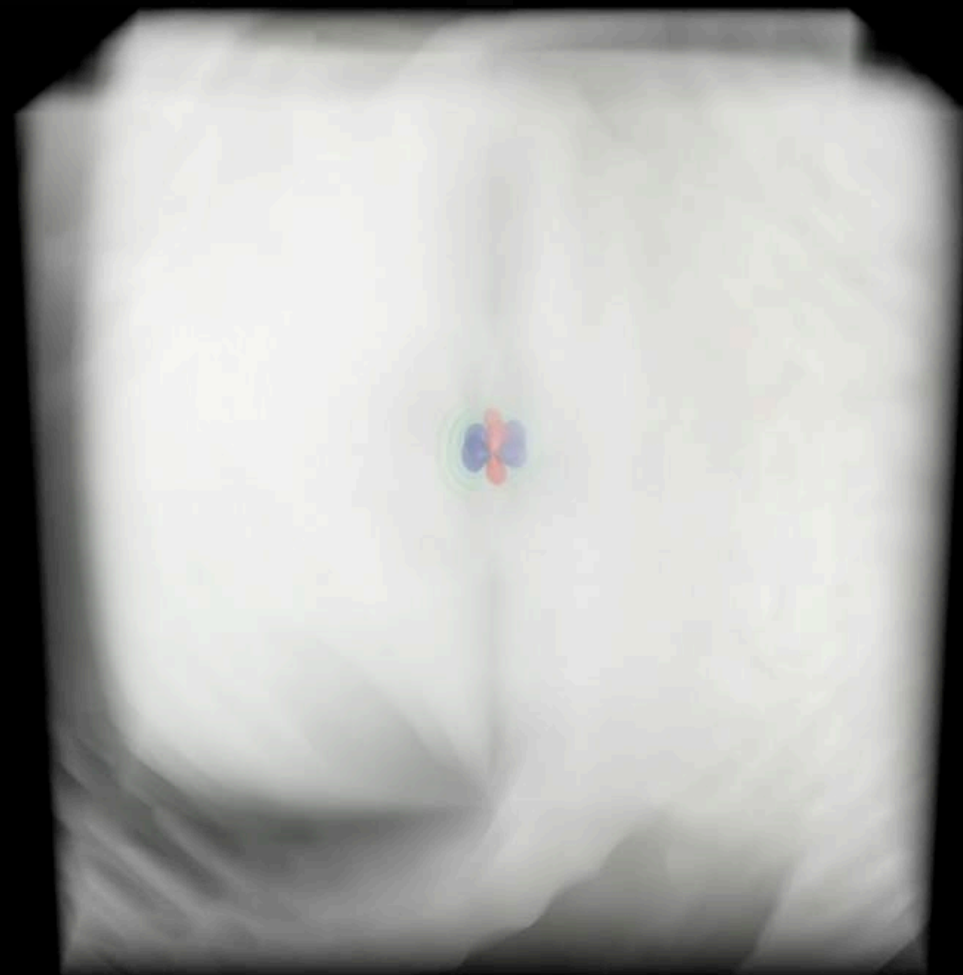
Shortcuts toward precession & subdominant harmonics

- **orbital time scale \ll precession scale:**
Co-rotating frame: phasing and radiated energy essentially unaffected by precession
[Schmidt+ PRD 2011]
- \rightarrow approximate map from non-precessing to precessing:
“twist up” non-precessing model with “post-Newtonian” Euler angles.
[Schmidt+ PRD 2012, Hannam+ PRL 2013]
 - Missing: north/south asymmetry responsible for large recoil
[Brügmann+PRD 2008]
- [London+2018]
Use perturbation theory arguments for approximate map from 22-mode to other spherical harmonic modes.



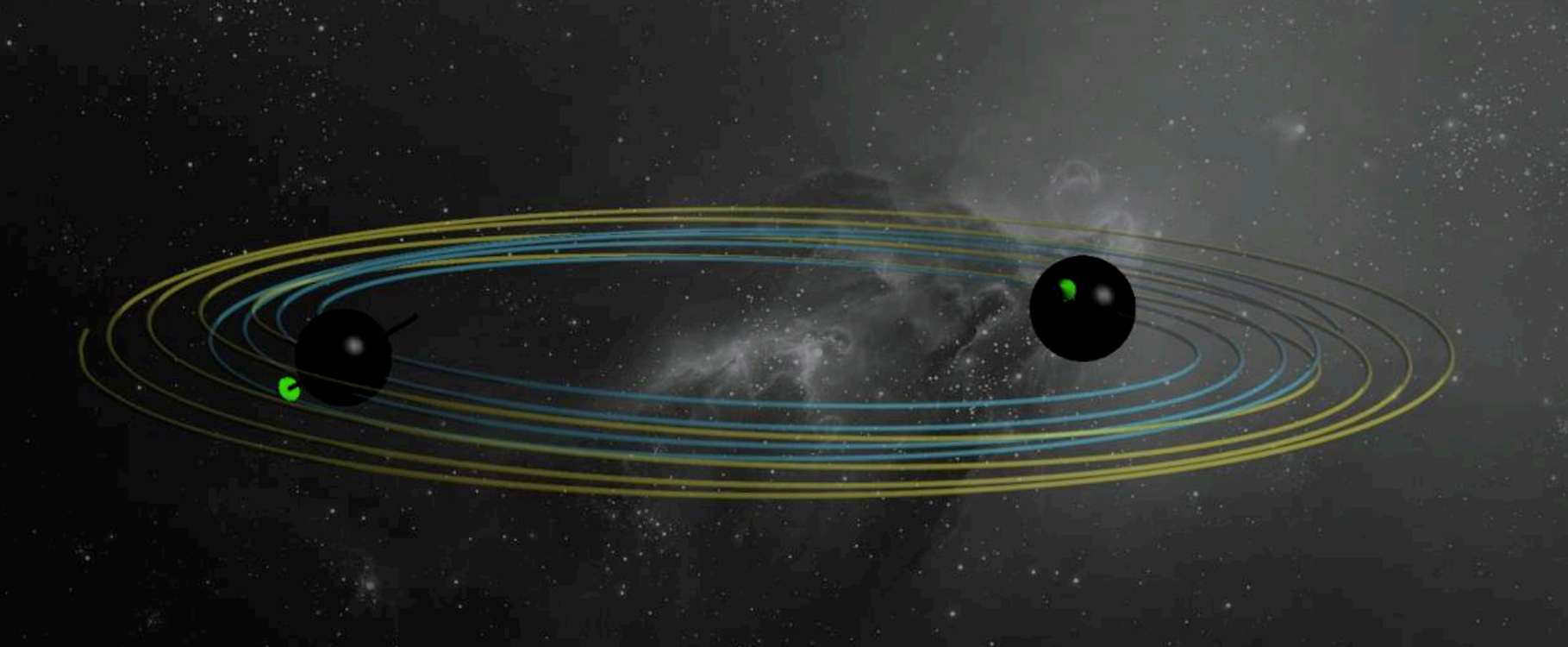


time(ms)=265.5

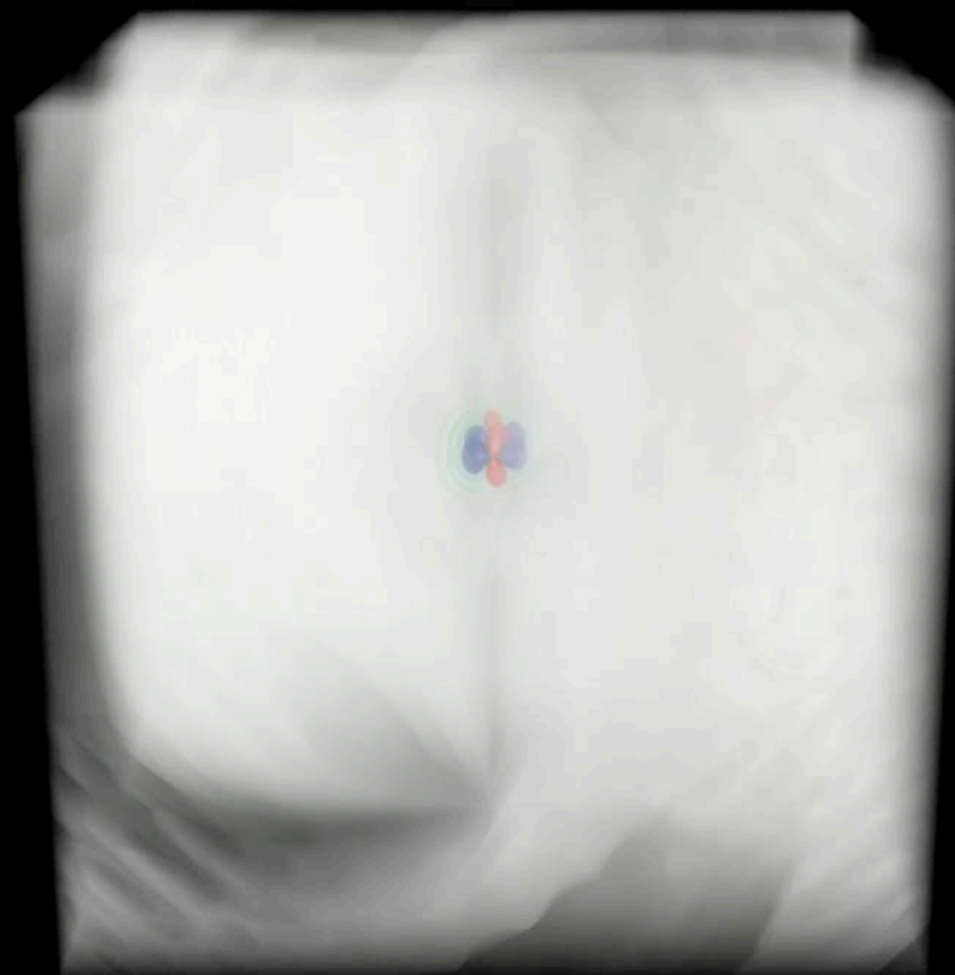


Simulaciones: Sascha Husa
Visualización: Rafel Jaume, UIB



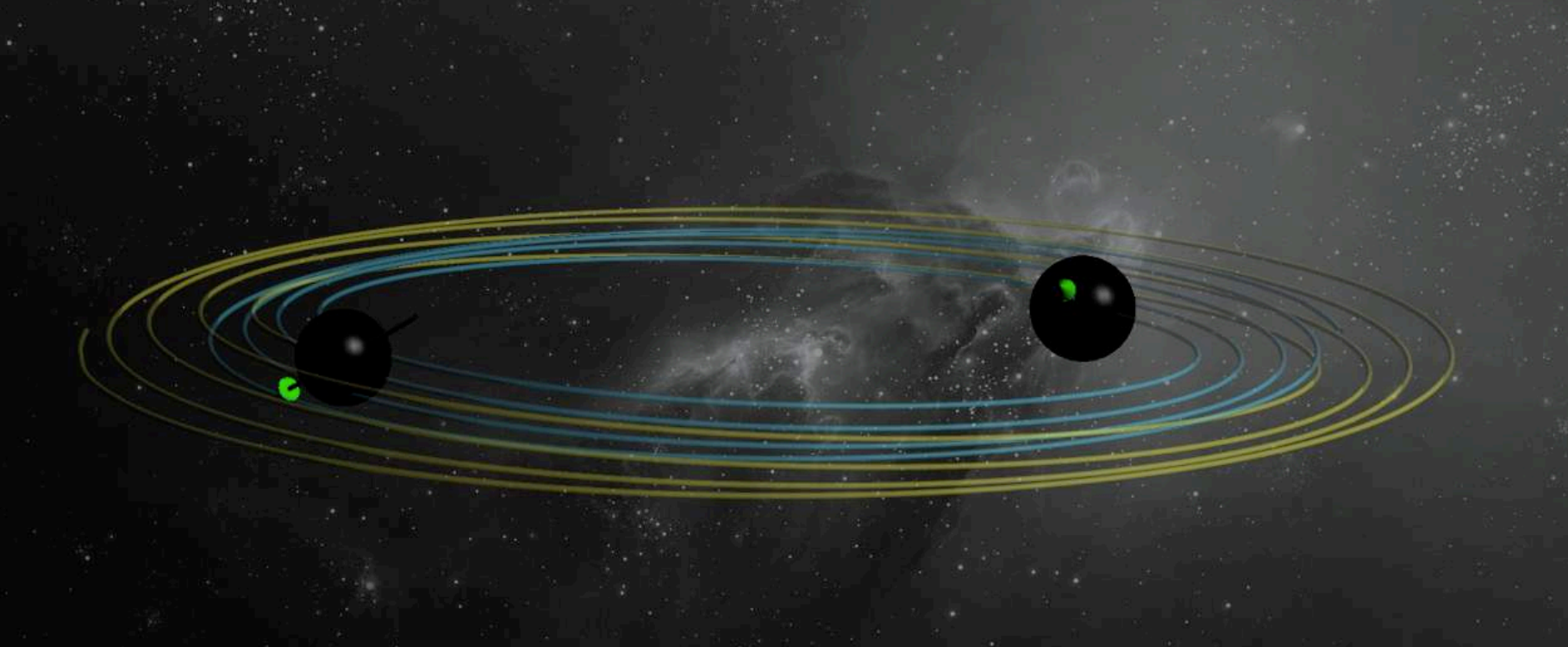


time(ms)=265.5

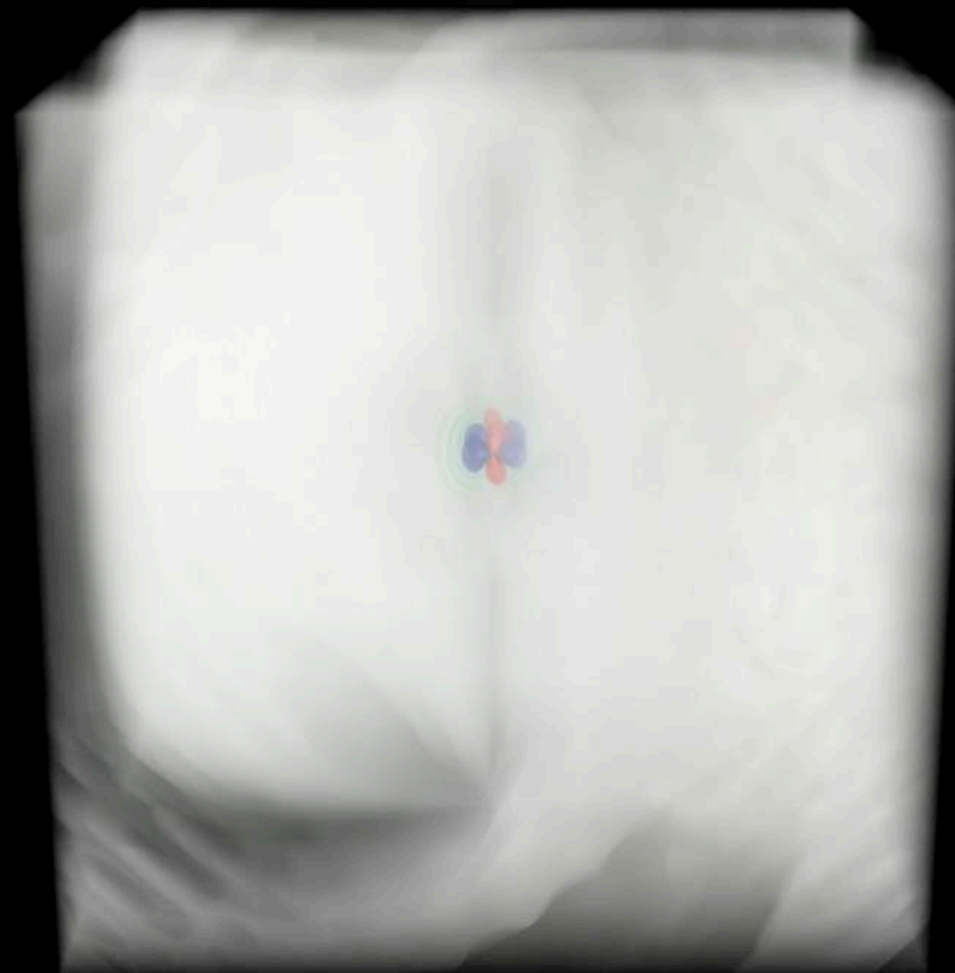


Simulaciones: Sascha Husa
Visualización: Rafel Jaume, UIB



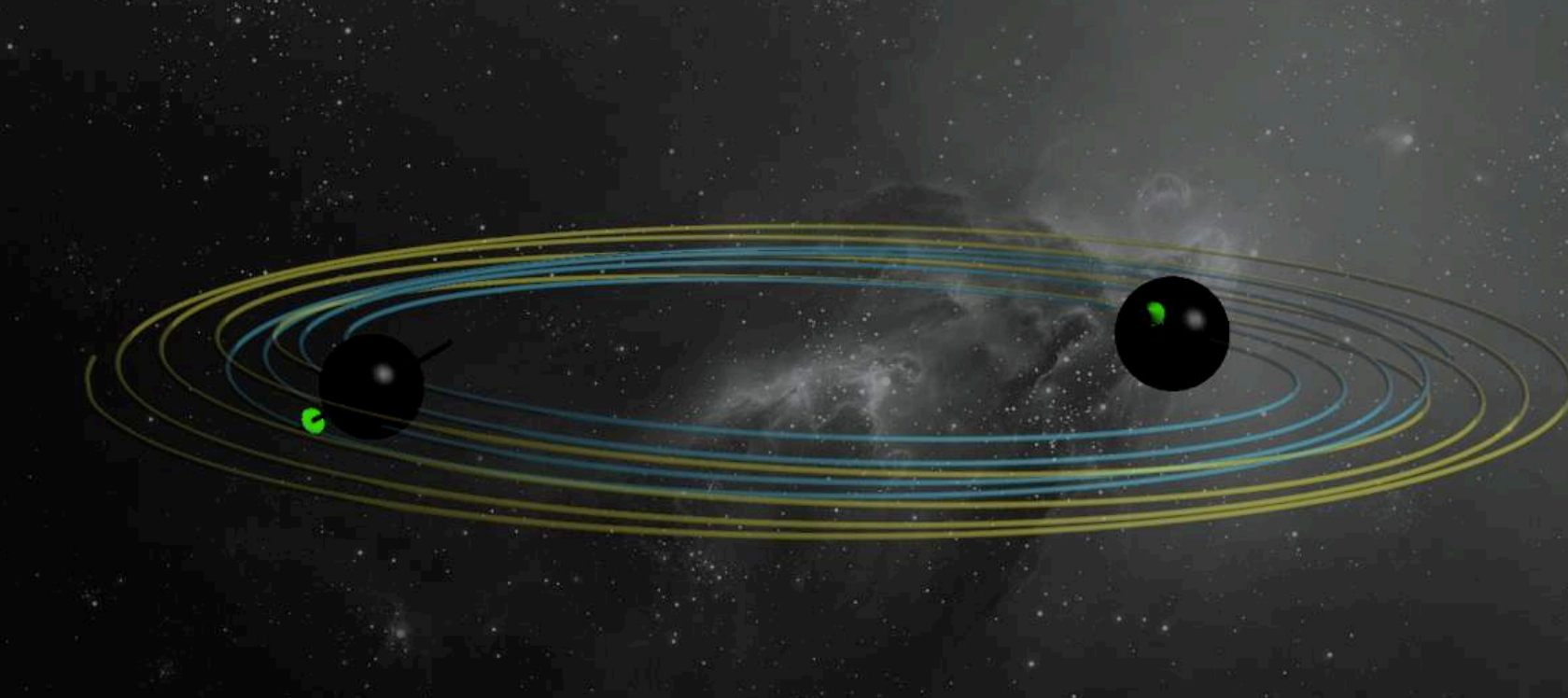


time(ms)=265.5

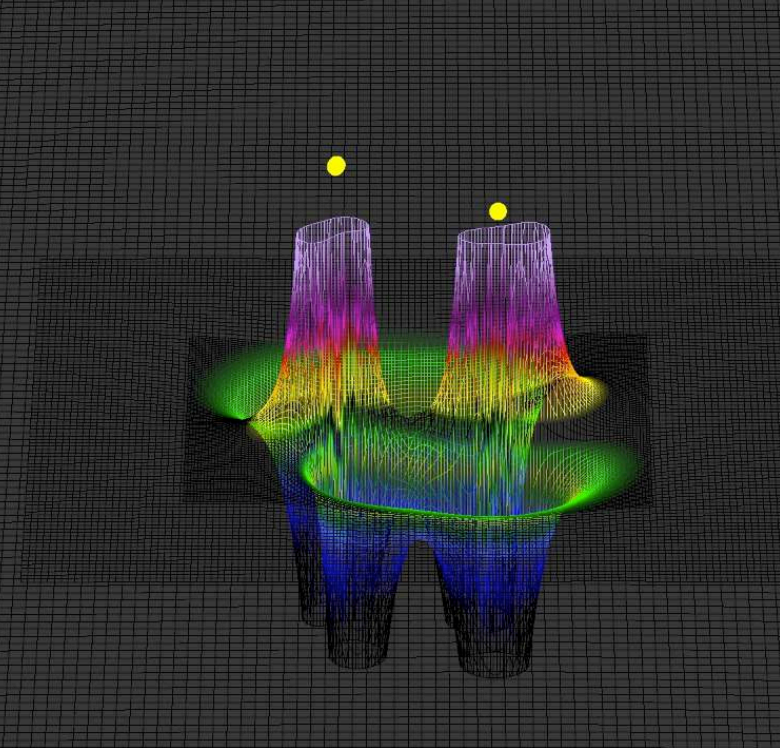


Simulaciones: Sascha Husa
Visualización: Rafel Jaume, UIB

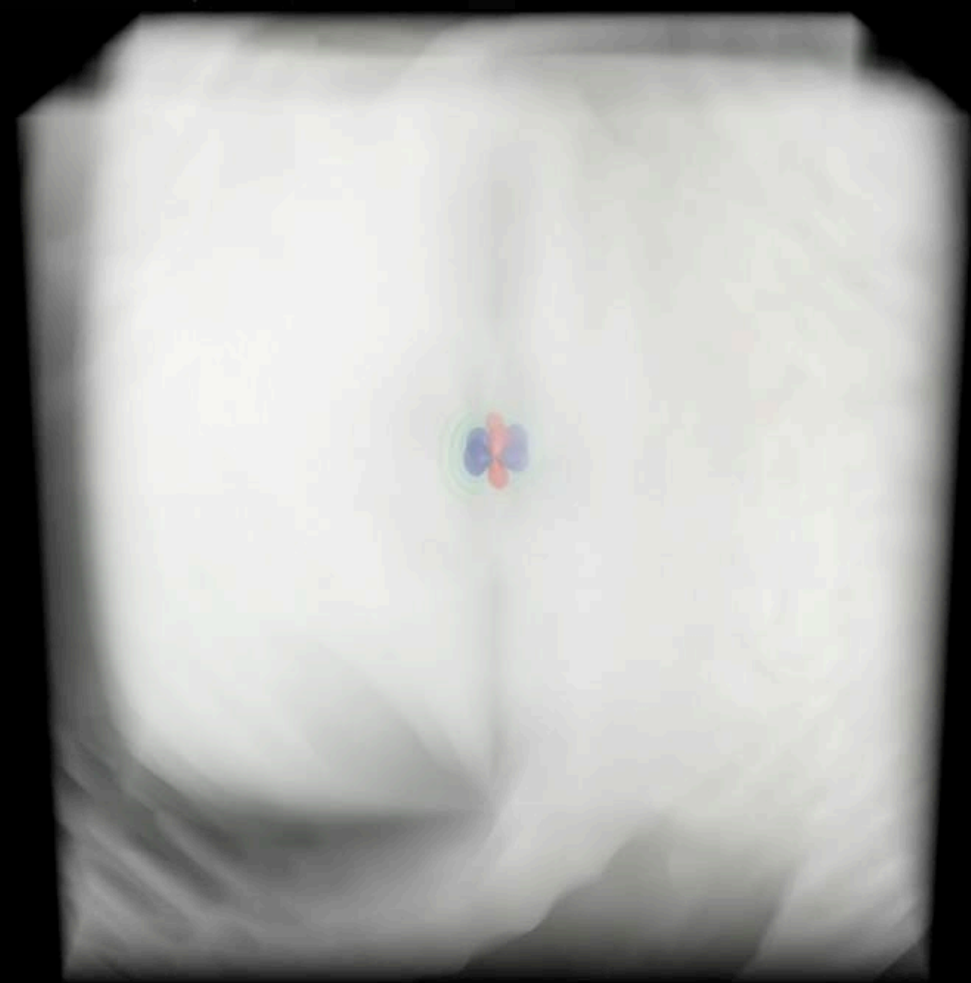




time(ms)=450



time(ms)=265.5



Simulaciones: Sascha Husa
Visualización: Rafel Jaume, UIB



Waveform Modelling strategies I

- **Model simple functions:**

e.g. split waveform into amplitude & phase.

- Frequency or time domain:

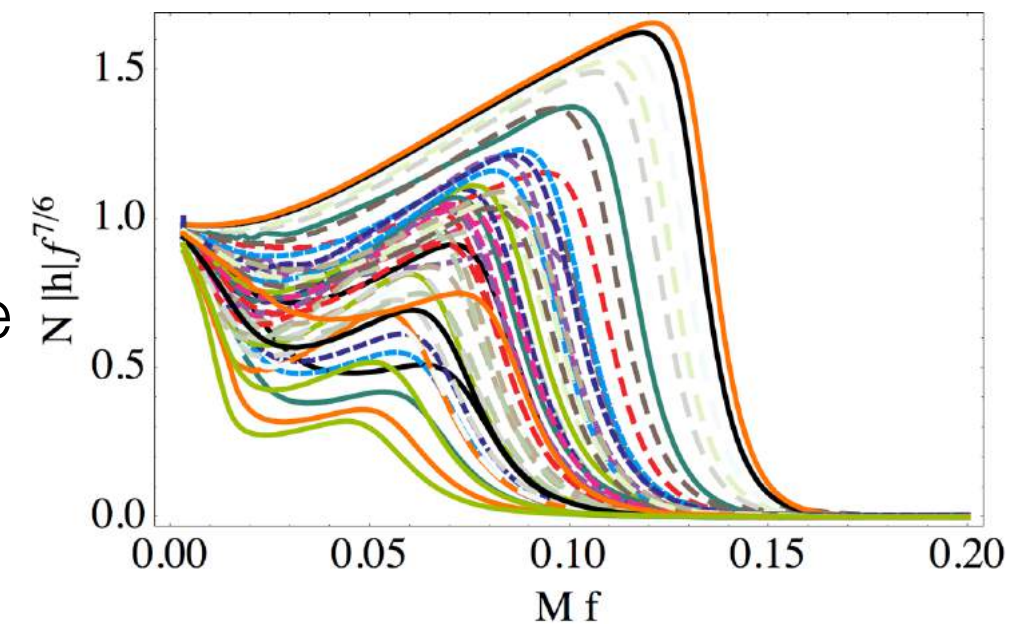
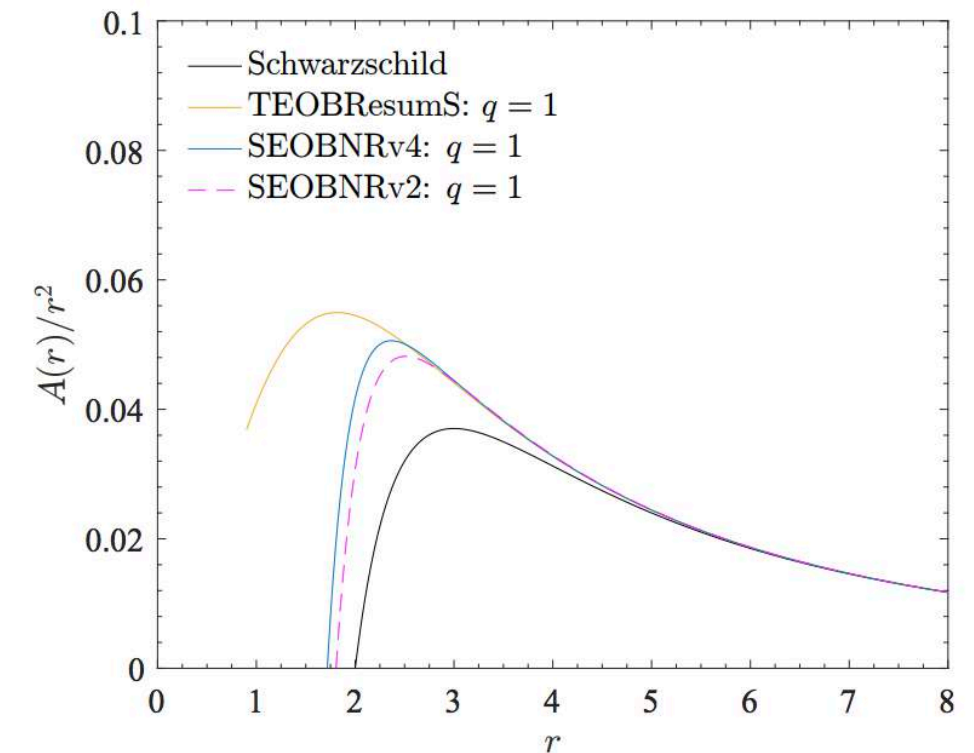
- TD naturally suited for modelling dynamics
- FD often more efficient for data analysis.

- **Discretize functions:**

reduce to coefficients in some phenomenological ansatz, grid up, construct basis functions from waveforms.

- **Example:**

- ~ 30 frequency points grid for amplitude and phase
- polynomial interpolation in parameter space
- reconstruct WF as spline



- **Avoid underfitting + overfitting to noise & systematic errors.**

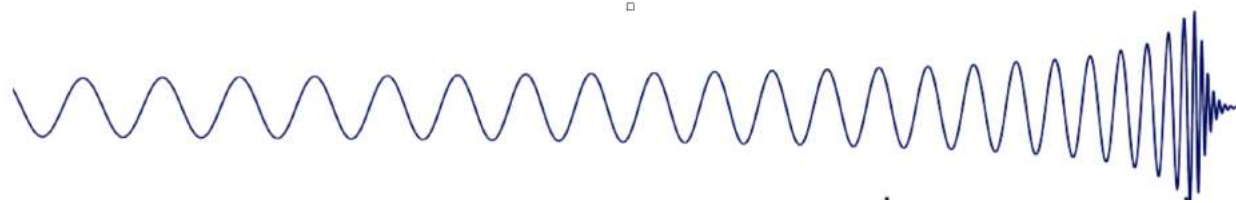
Waveform Modelling strategies II

- Currently 3 main strategies with **different emphasis**:
- effective one body (EOB) - **push perturbative methods as far as possible**
 - model the energy and flux of a particle inspiral in an effective metric, then integrate ODEs numerically.
 - Slow - need a fast model of the phenomenological EOB model.
- phenomenological (frequency domain) models - **phenomenological understanding**
 - piecewise closed form expressions - fast
- “Surrogate models:” ROM for numerical data - **algorithms to interpolate large parameter spaces**
 - No intermediate phenomenological model, can use the same methods as for fast evaluation of EOB.
- Phenomenological + EOB: Make a physically motivated ansatz in terms of suitable parameters, fit to each waveform, then fit coefficients across parameter space.

Hierarchical Strategy to conquer parameter space

Model directions in parameter space in order of importance.

- Start with $l=|m|=2$ spherical harmonic mode (1 harmonic), no spins - 1D physical parameter space

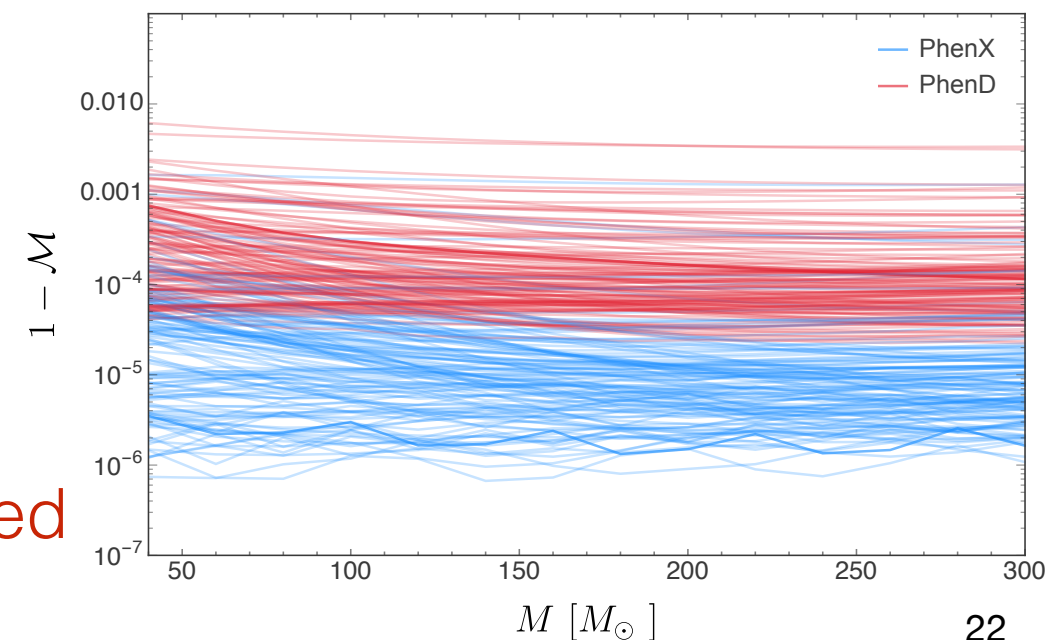


- Non-precessing spins: single effective spin - 1 harmonic, 2D
- Leading precession effects via PN - 5 harmonics, \cong 3D
- Non-precessing spins - 1 harmonic, 3D
- Non-precessing spins higher modes: handful of harmonics, 3D
- Extend to matter (incorporate some neutron star tidal effects)
- Eccentricity: non-spinning 22 mode - 2D
- NR calibration of leading precession effects - 7 D
- Generic black holes - 9 D

beyond GR

Phenomenological waveforms program

- Collaboration of UIB, Cardiff U, MPI Hannover, ICTS Bangalore, U of Zurich.
 - Numerical simulations based on MareNostrum machines during last decade.
- PhenomD / PhenomP: UIB contribution to compact binary discoveries.
- @UIB: [X. Jiménez Forteza](#), [David Keitel](#), Geraint Pratten, Marta Colleoni, Leila Haegel, *Cecilio García*, *Toni Ramos*, *Hector Estellés*, [SH](#).
- Recent work:
 - PhenomX ~ 100 accuracy improvement
 - Calibrate subdominant harmonics to NR

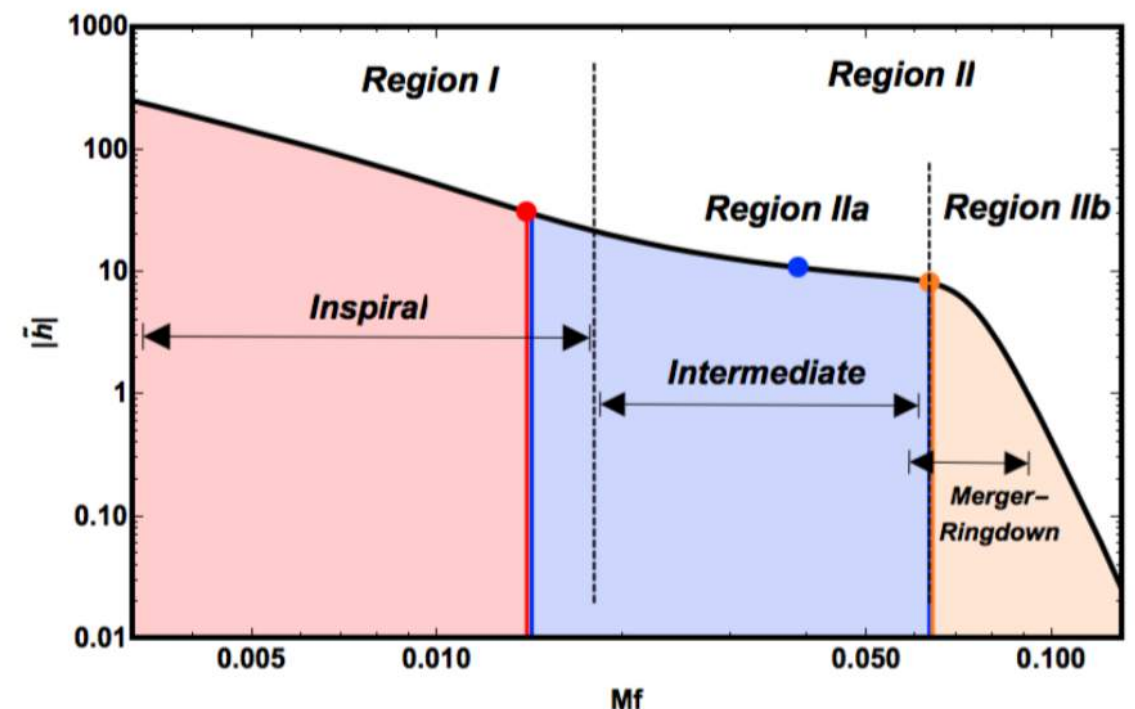
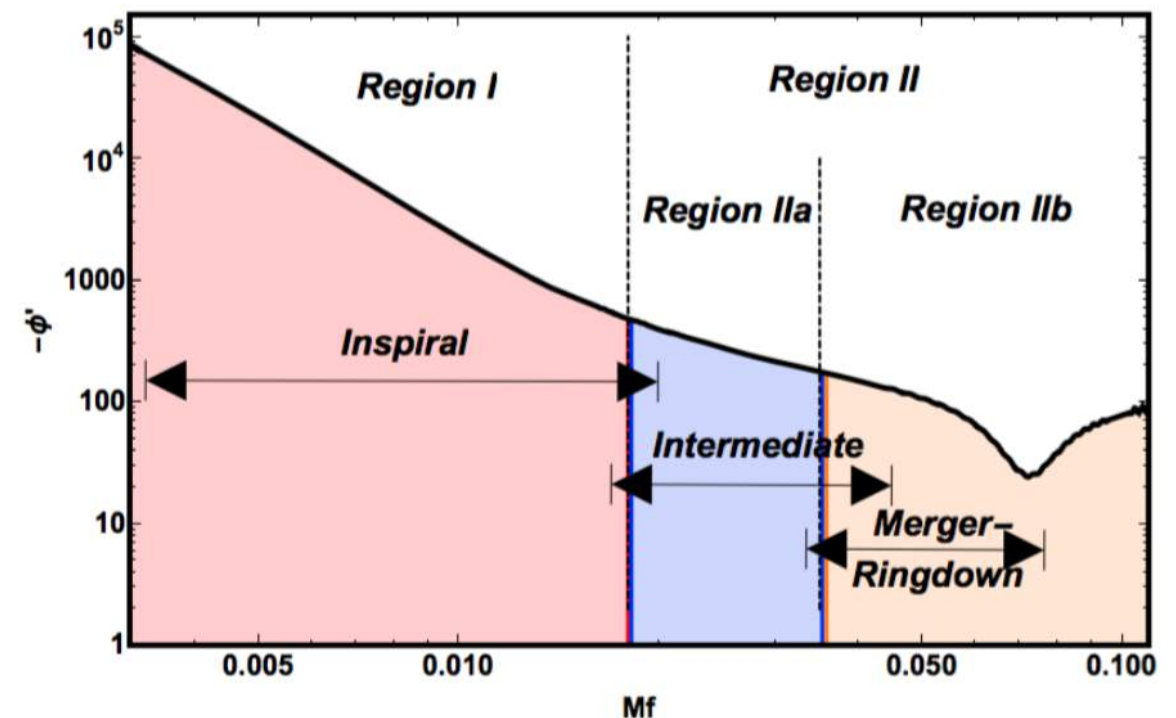


Mismatch in part due to NR inaccuracy - need more accurate input waveforms \longrightarrow

Phenom*: Modelling the dominant spherical harmonic mode from non-precessing binaries

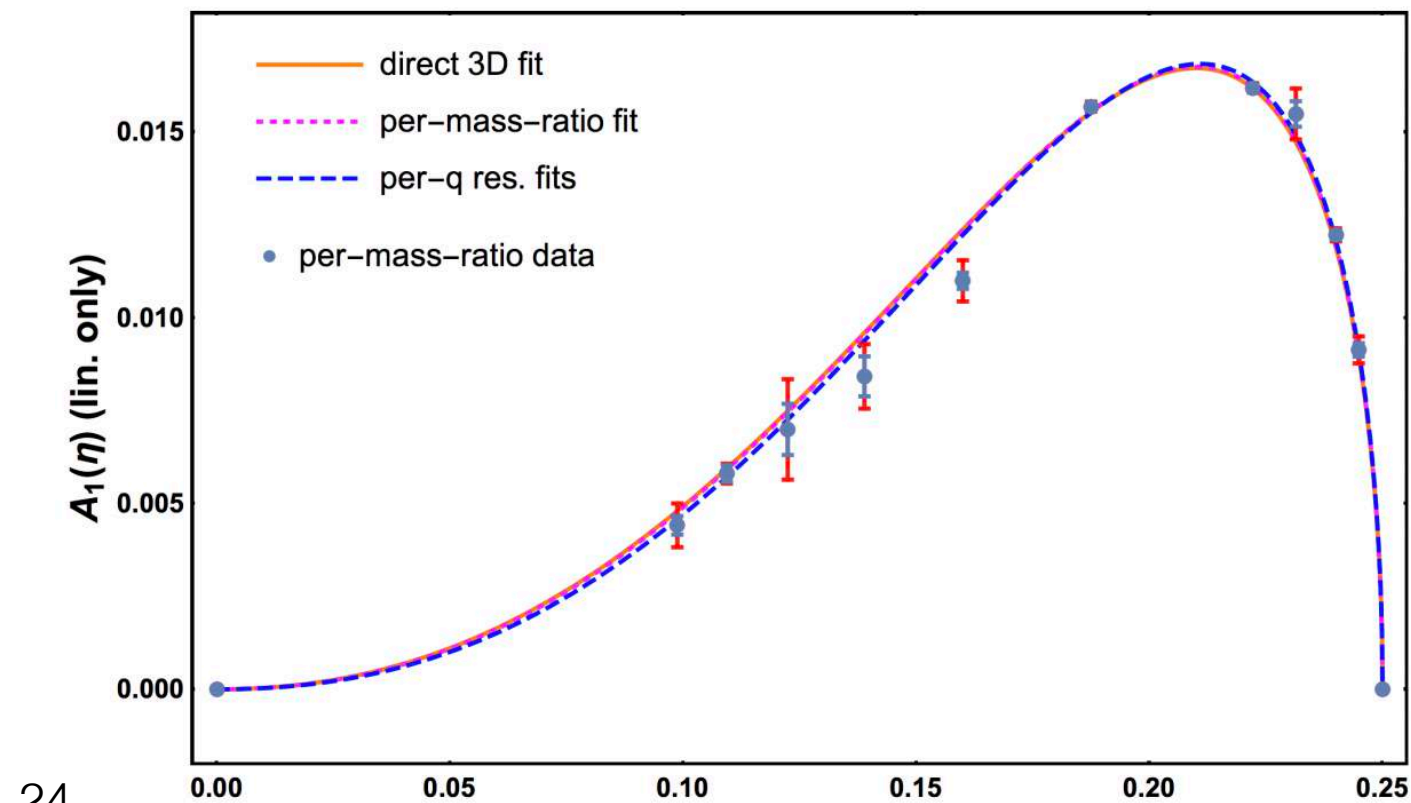
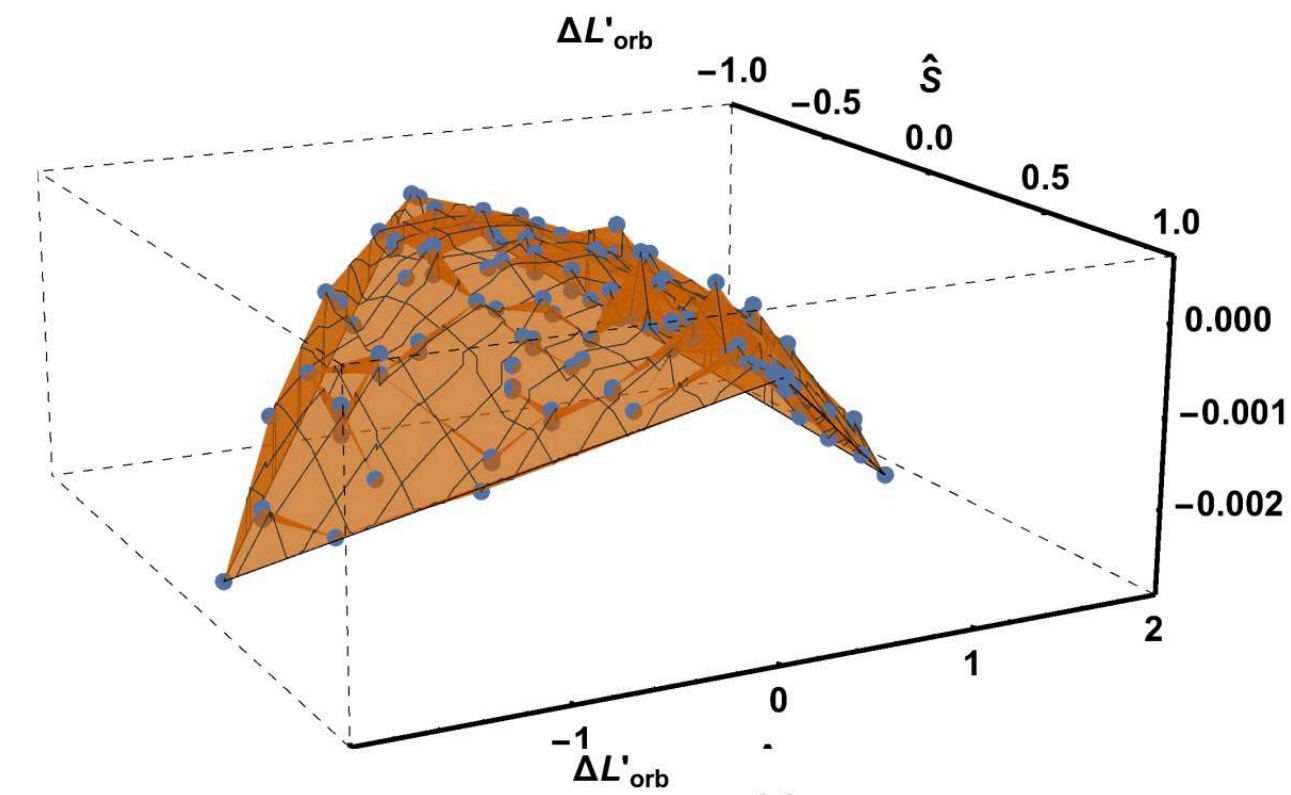
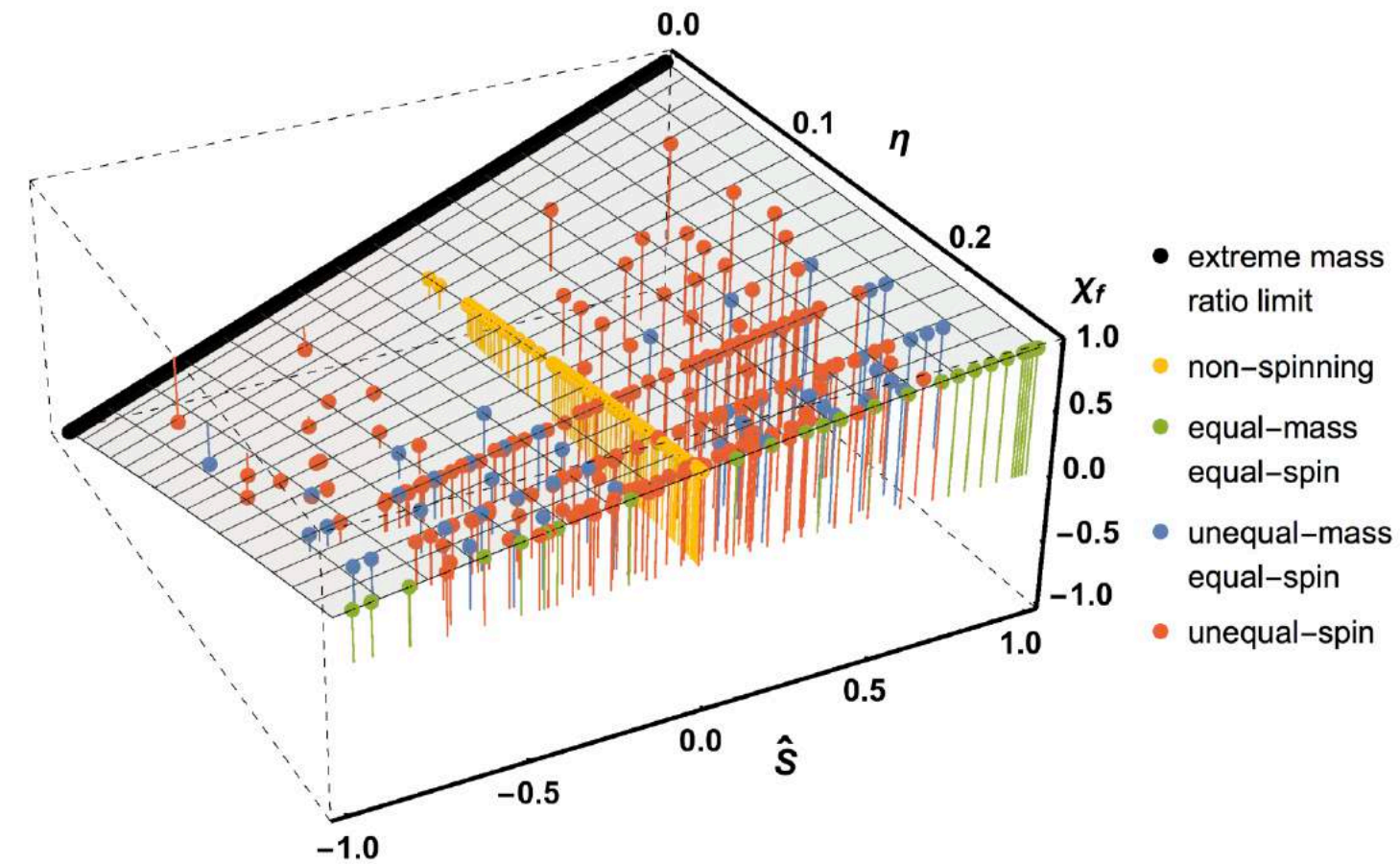
Divide and conquer:

- Split waveform into amplitude + phase, model simple non-oscillatory functions.
- Simplicity of modelling increases with the number of frequency-regions.
- Actual: ~ 10 parameters per function.
- Our choice: - 3 regions, ~ 3 params. each
 - inspiral (use PN intuition)
 - merger
 - ringdown (use perturbative intuition)



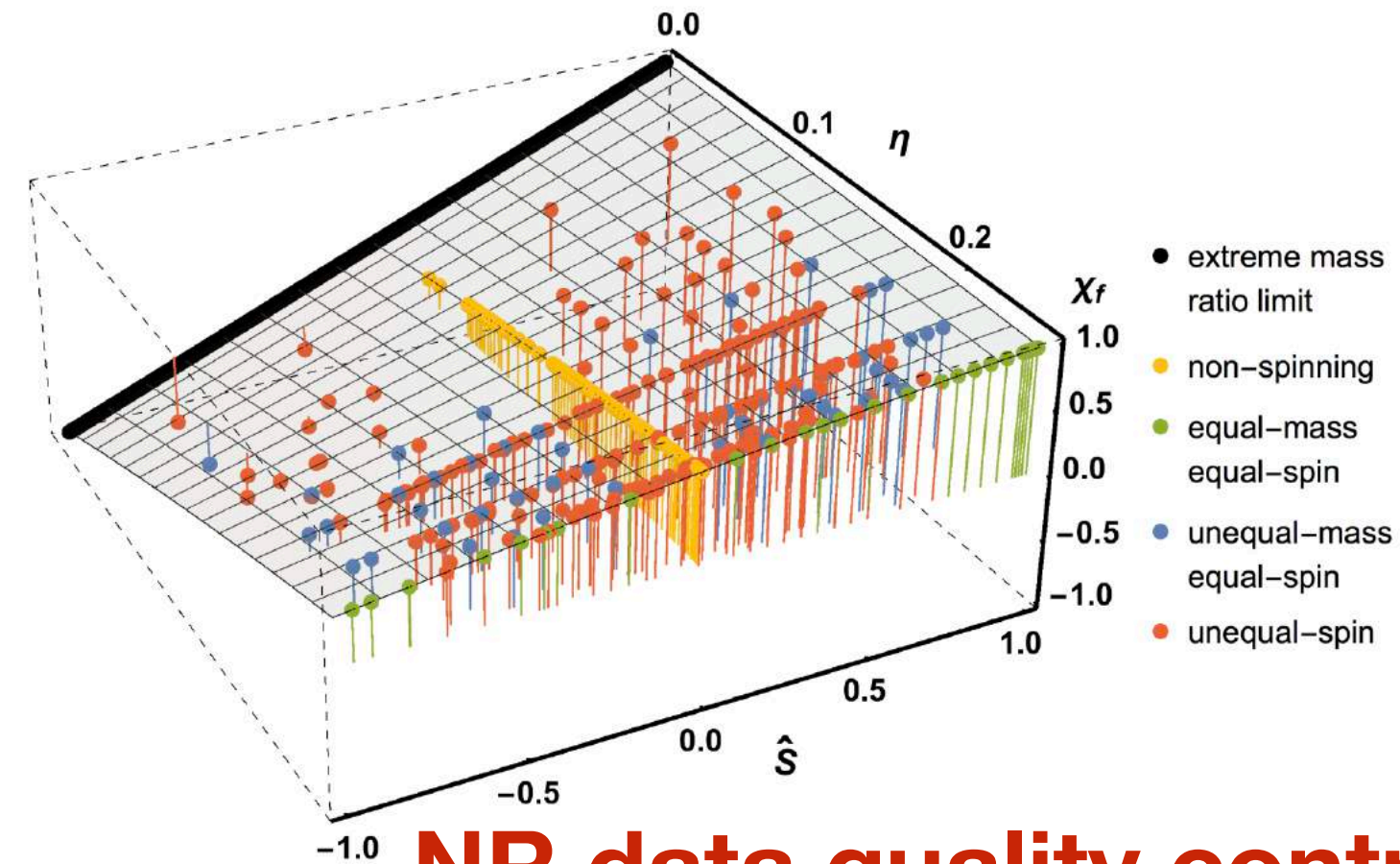
Hierarchical modelling: Final spin example

- Proceed to find fitting ansatz in hierarchical way: 1D, 2D, 3D
- Work with residuals after subtracting previous step,
- Always work on 1D or 2D problems only.
- Combine data from different NR codes , with different numerical artefacts.

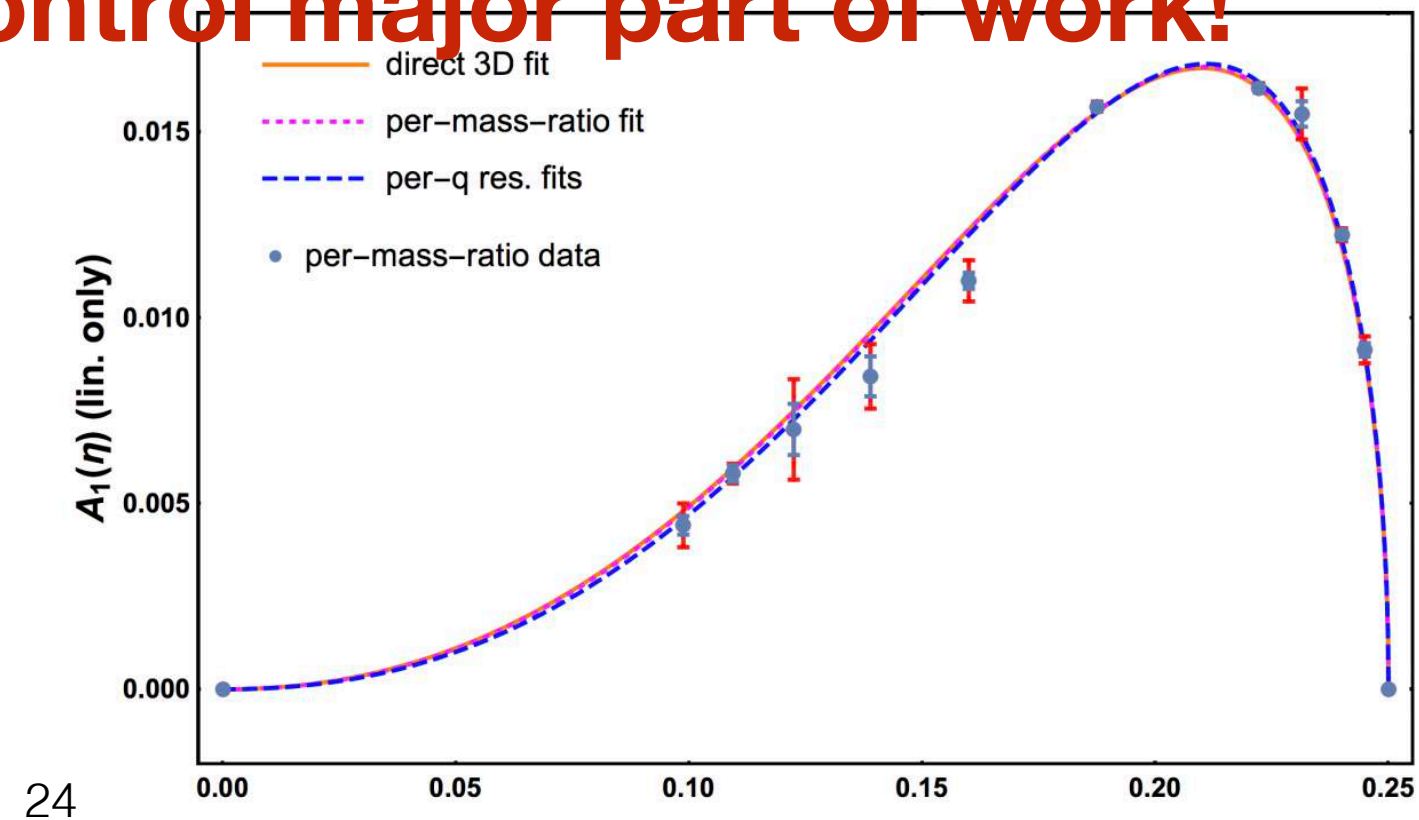
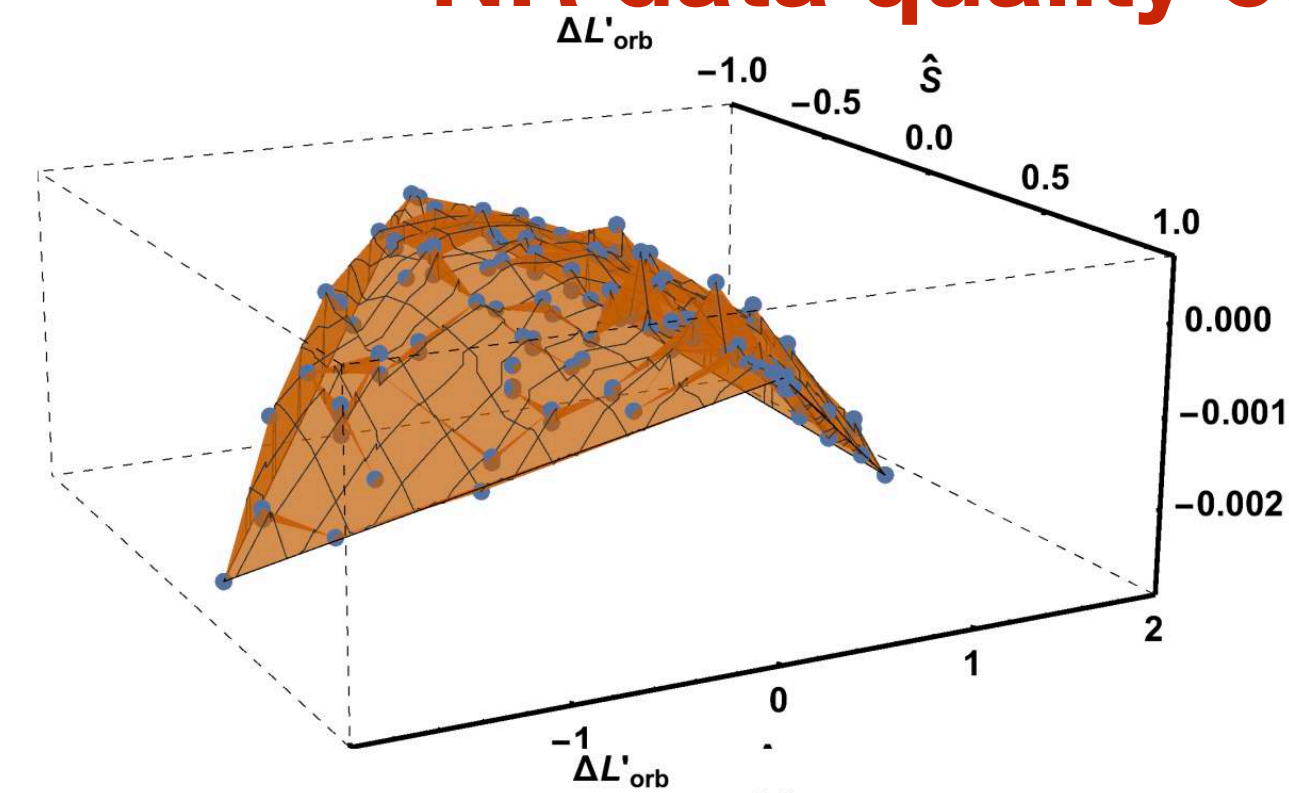


Hierarchical modelling: Final spin example

- Proceed to find fitting ansatz in hierarchical way: 1D, 2D, 3D
- Work with residuals after subtracting previous step,
- Always work on 1D or 2D problems only.
- Combine data from different NR codes , with different numerical artefacts.

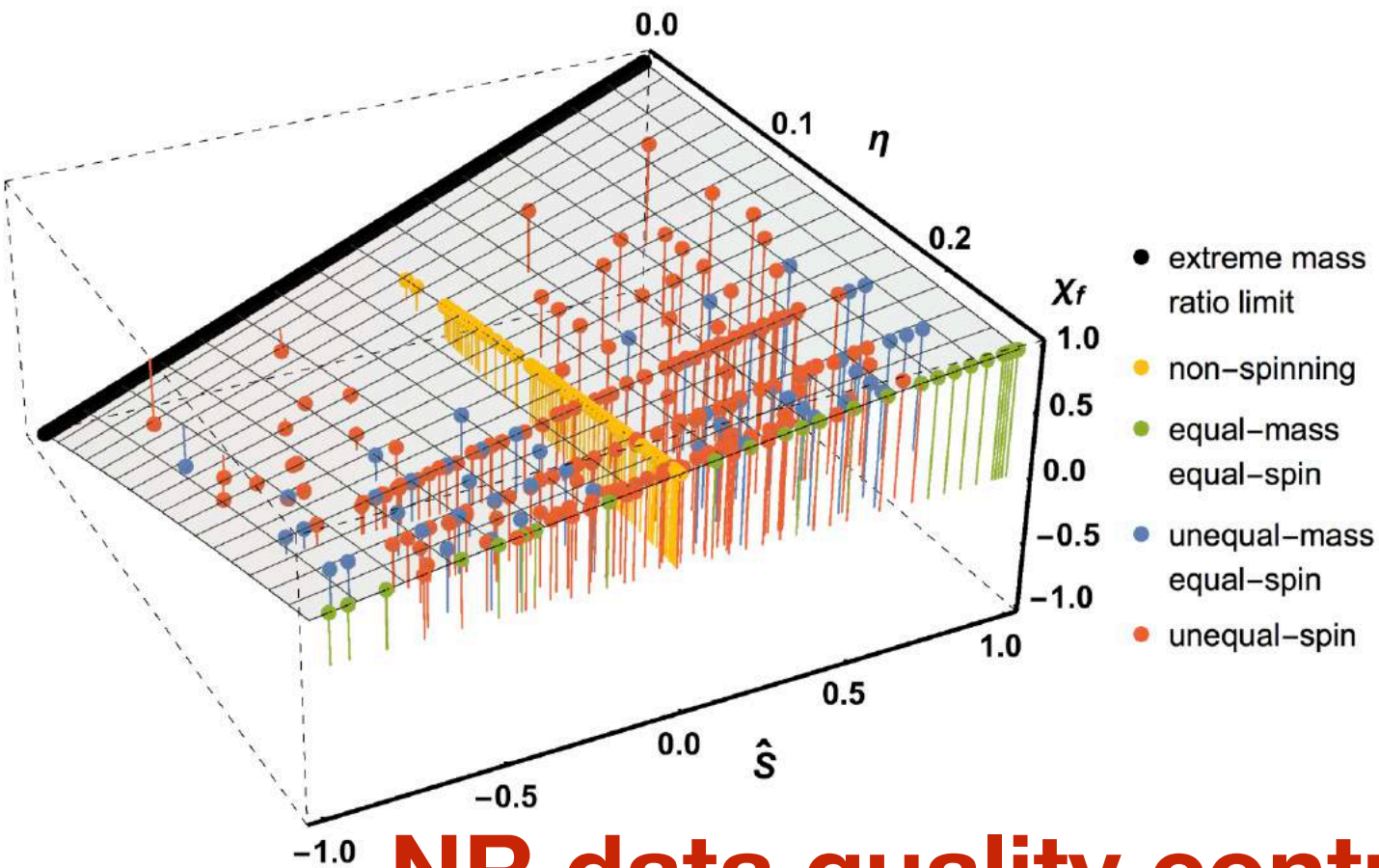


NR data quality control major part of work!

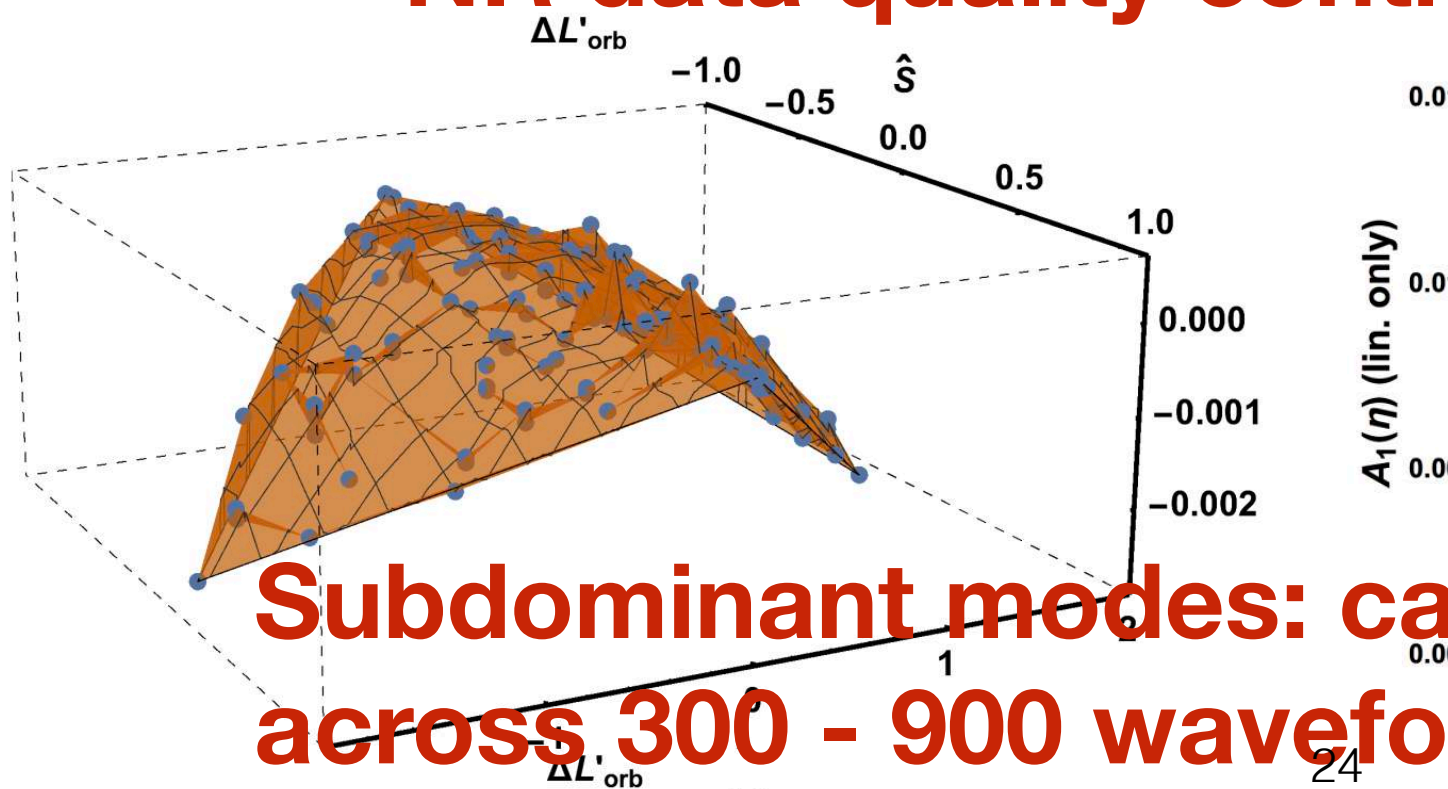


Hierarchical modelling: Final spin example

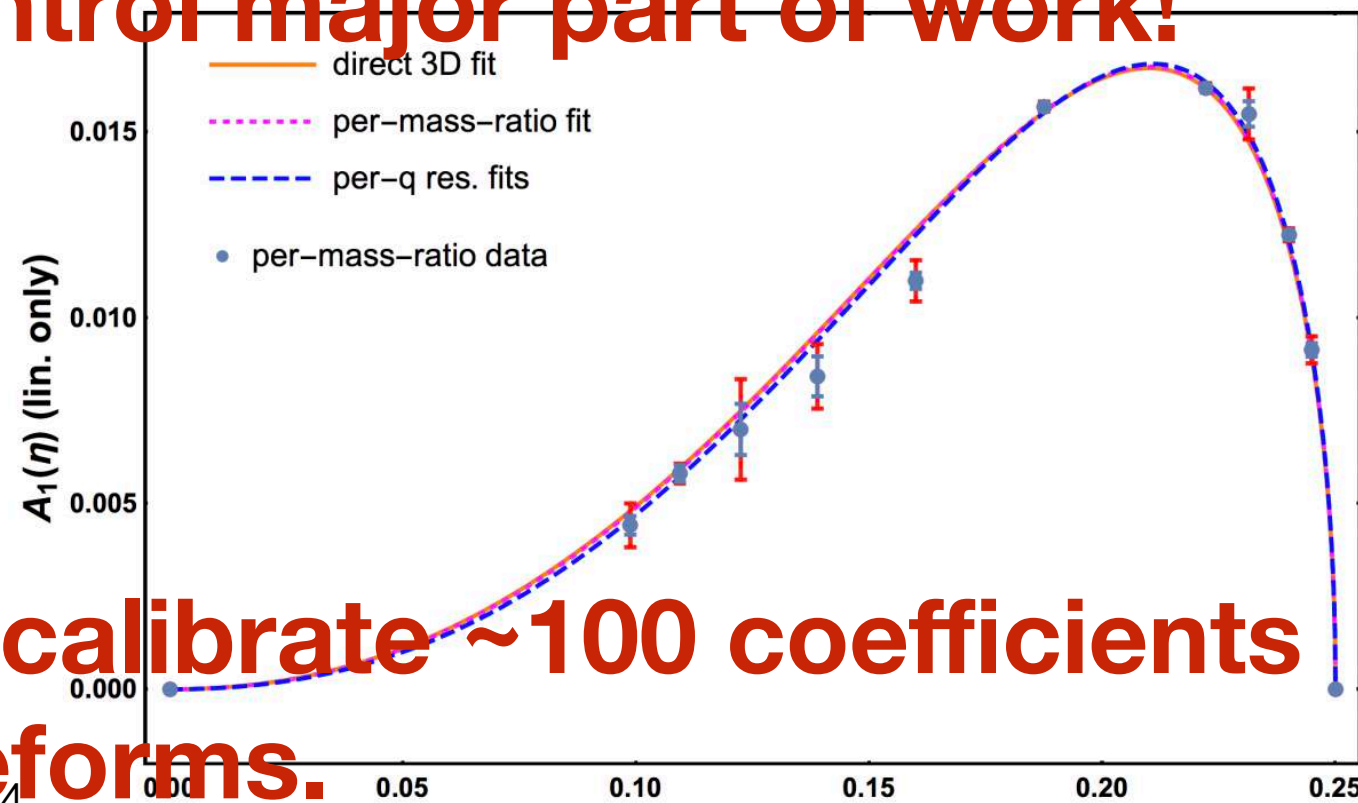
- Proceed to find fitting ansatz in hierarchical way: 1D, 2D, 3D
- Work with residuals after subtracting previous step,
- Always work on 1D or 2D problems only.
- Combine data from different NR codes , with different numerical artefacts.



NR data quality control major part of work!



Subdominant modes: calibrate ~100 coefficients across 300 - 900 waveforms.



Are models good enough for current detectors?

- Detailed study for G: inject NR waveforms into noise - contain physics that is not yet (well) modelled [Effects of wf. model systematics on the interpretation of GW150914, LIGO+Virgo, PRD2017]:
 - higher modes, precession, eccentricity.
 - Redo Bayesian parameter estimation, determine parameter bias.
 - Models good enough for first detection(s) - need to improve for O3 and beyond.

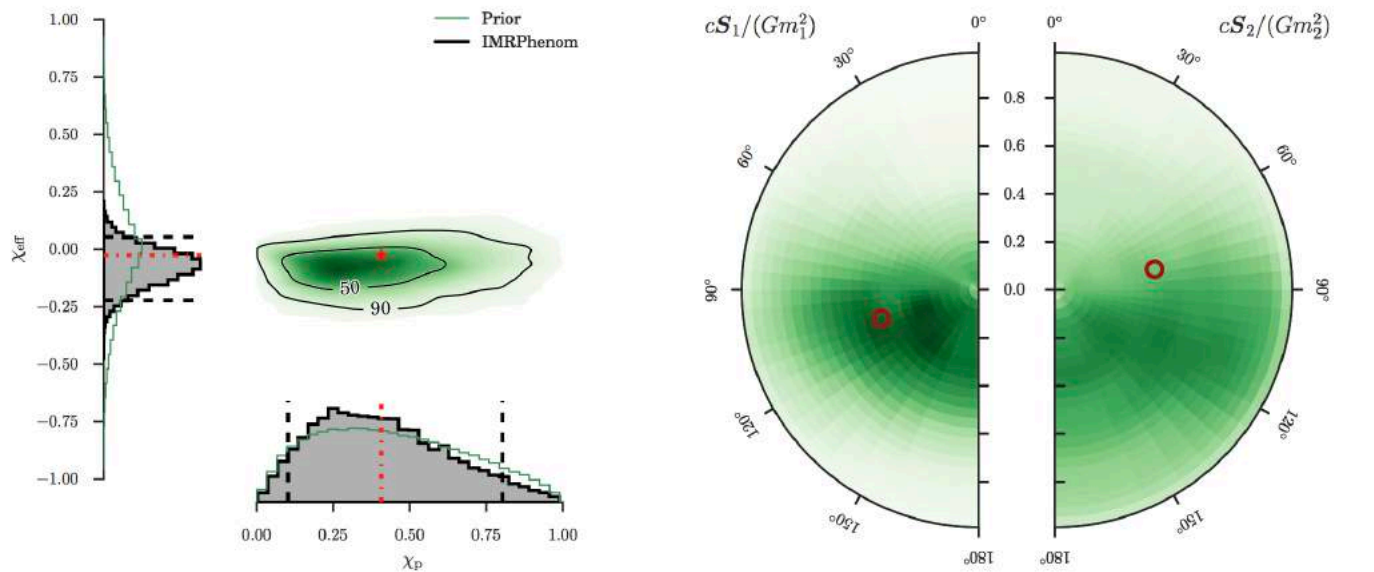
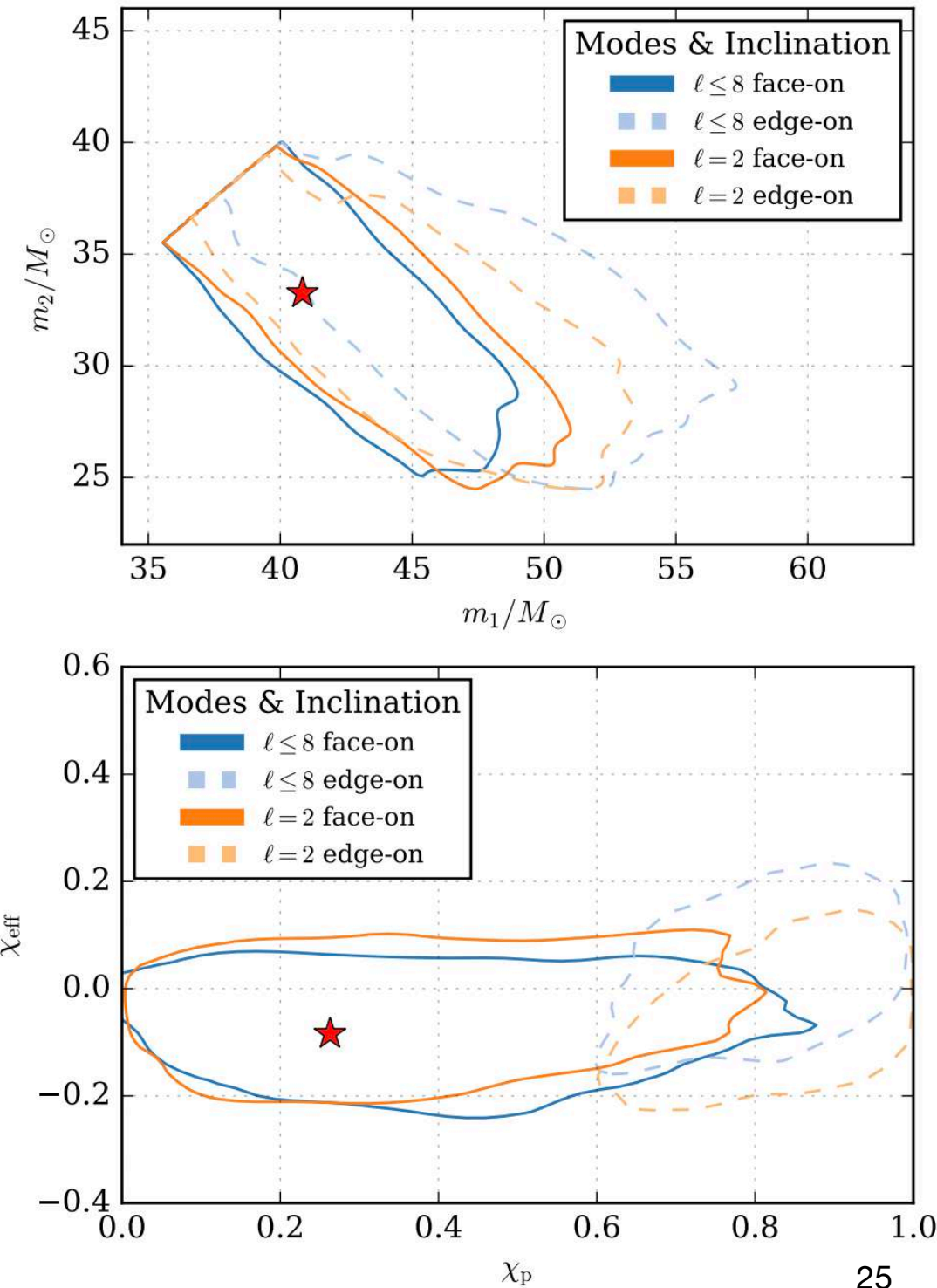


FIG. 3. Comparison of spins for the precessing NR mock signal (CFUIB0029) shown in Fig. 2. Left: PDFs for the χ_p and χ_{eff} spin parameters. The one-dimensional plots show probability contours of the prior (green) and marginalized PDF (black). The dashed vertical lines mark 90% credible intervals. The two-dimensional plot shows the contours of the 50% and 90% credible regions plotted over a color-coded PDF. The injected parameter values are shown as red dot-dashed lines and a red asterisk. Right: PDFs for the dimensionless component spins $cS_1/(Gm_1^2)$ and $cS_2/(Gm_2^2)$ relative to the normal to the orbital plane L , marginalized over uncertainties in the azimuthal angles.



Bias in recovering effective spin: Kumar+, PRD2016

Second generation

Third generation

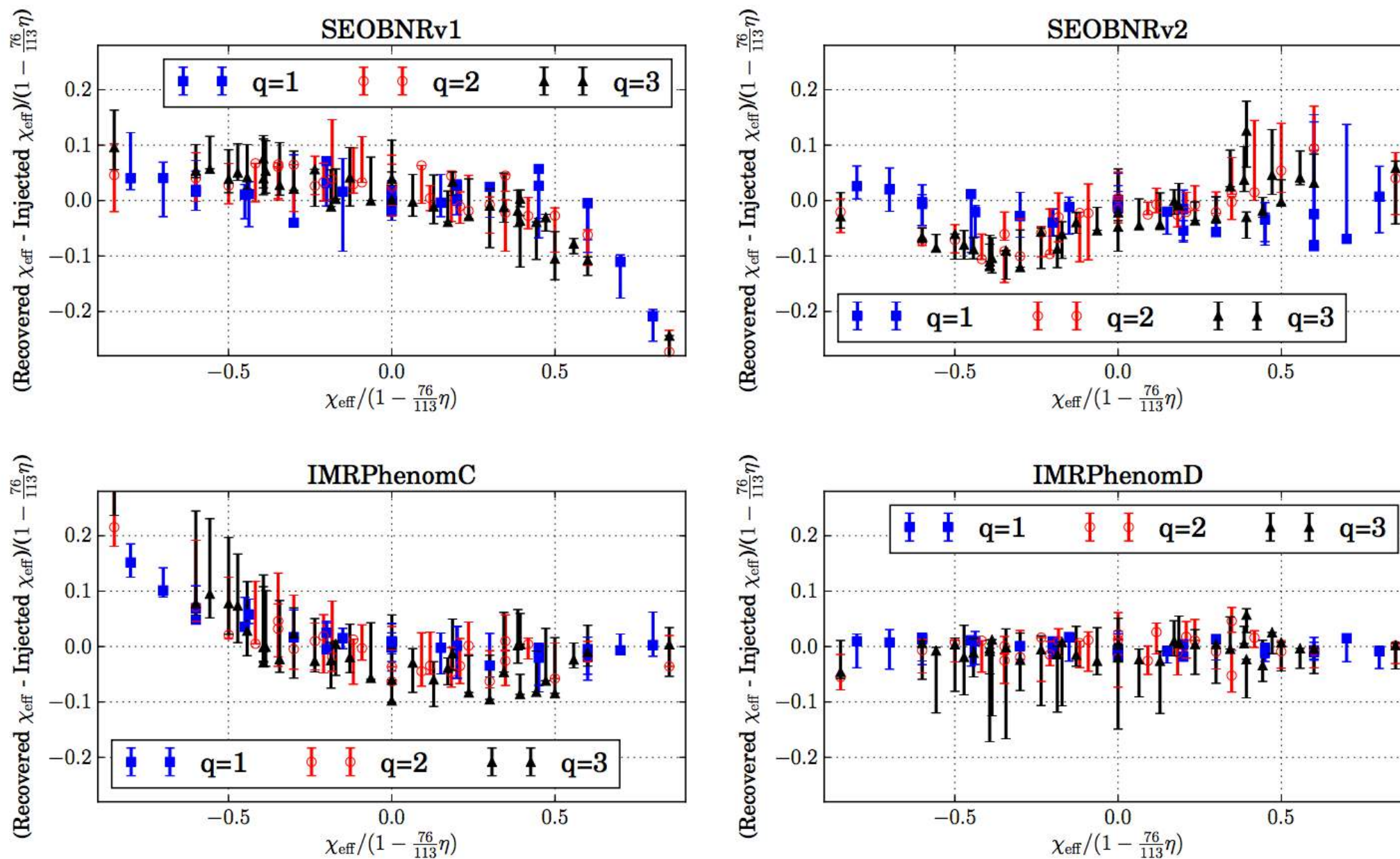


FIG. 10. Systematic bias in the recovery of the effective spin parameter χ_{eff} , as a function of the normalized effective spin of the NR waveforms. The plot-markers show the recovered χ_{eff} for a binary with total mass fixed at $80M_{\odot}$, while the “error-bars” show the range spanned by the recovered q as the injected binary mass is varied between its lowest allowed value and $150M_{\odot}$.

Fourth generation in progress ...

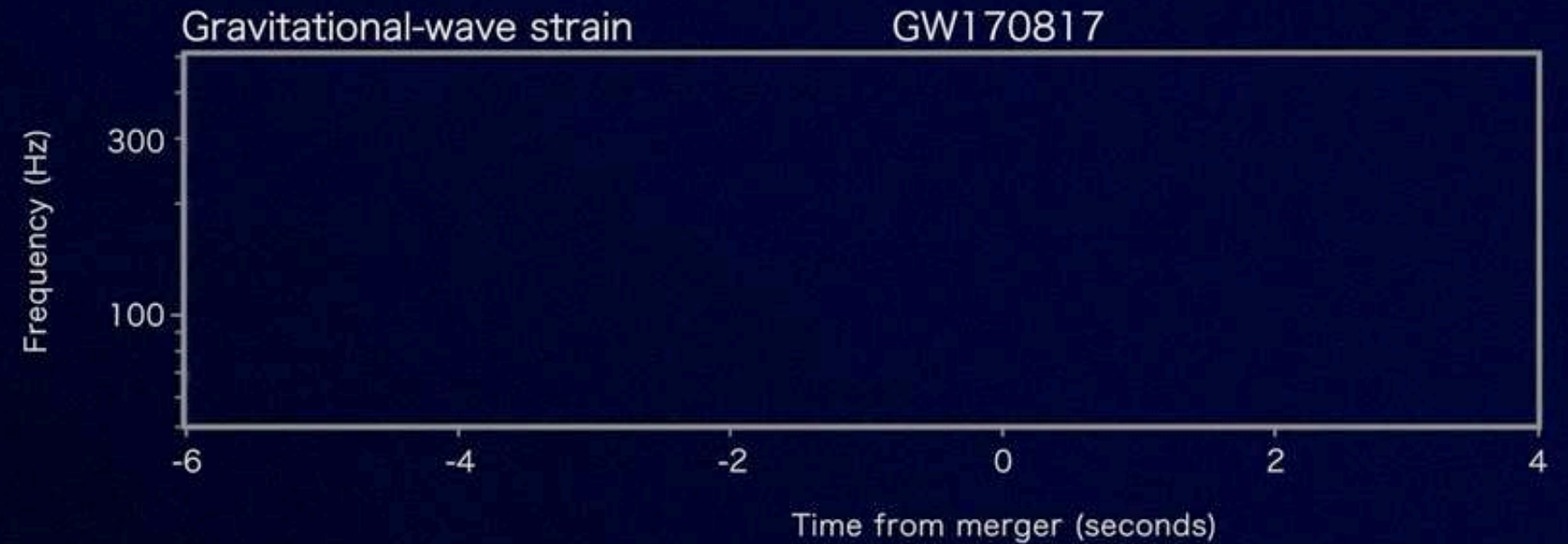
GRB 170817A y GW170817:

The beginning of multi messenger astrophysics.

Observation of GWs from the fusion of two neutron stars, short gamma ray burst and a kilonova.



LIGO



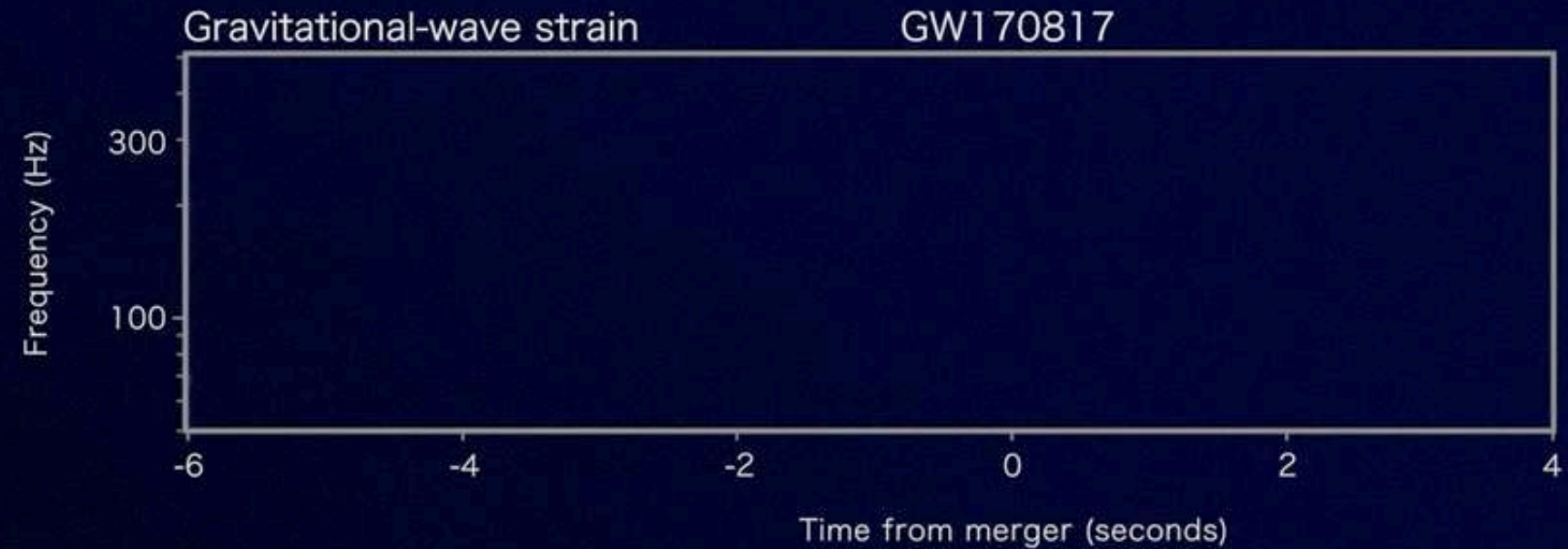
GRB 170817A y GW170817:

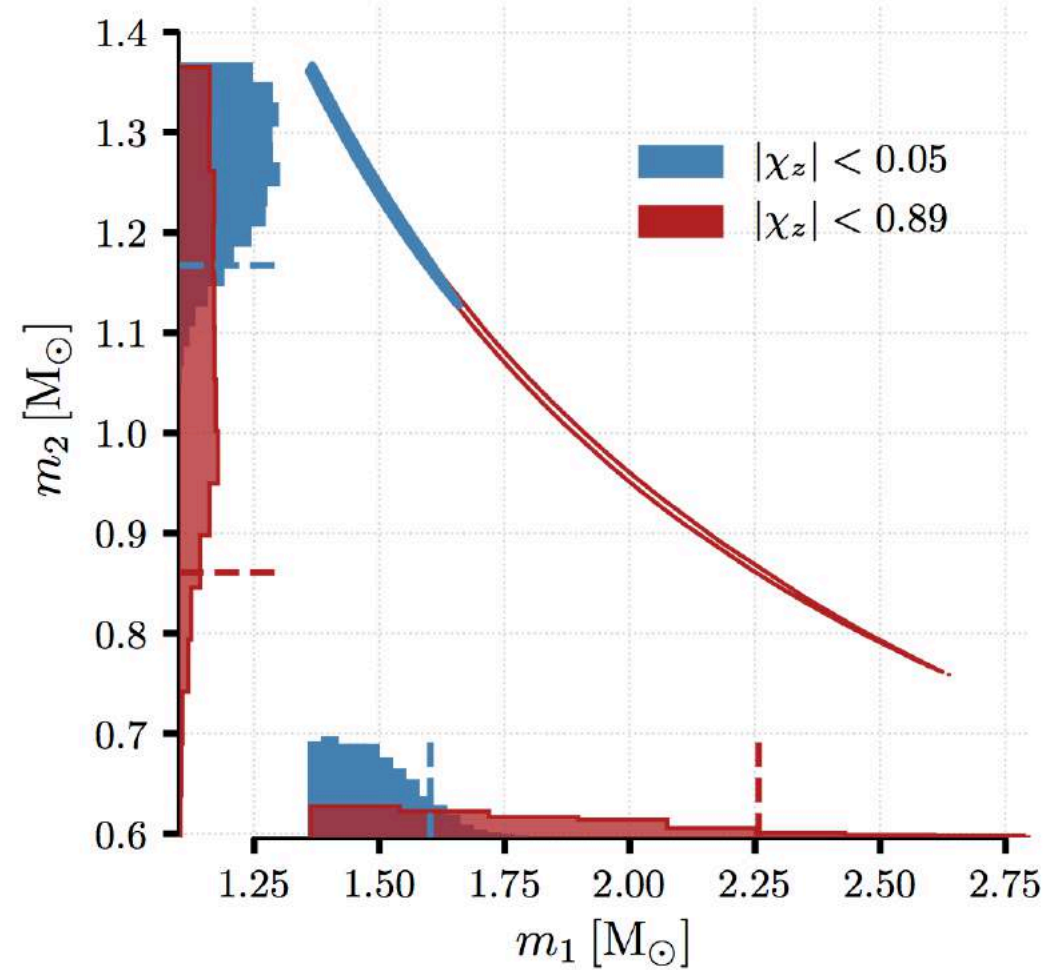
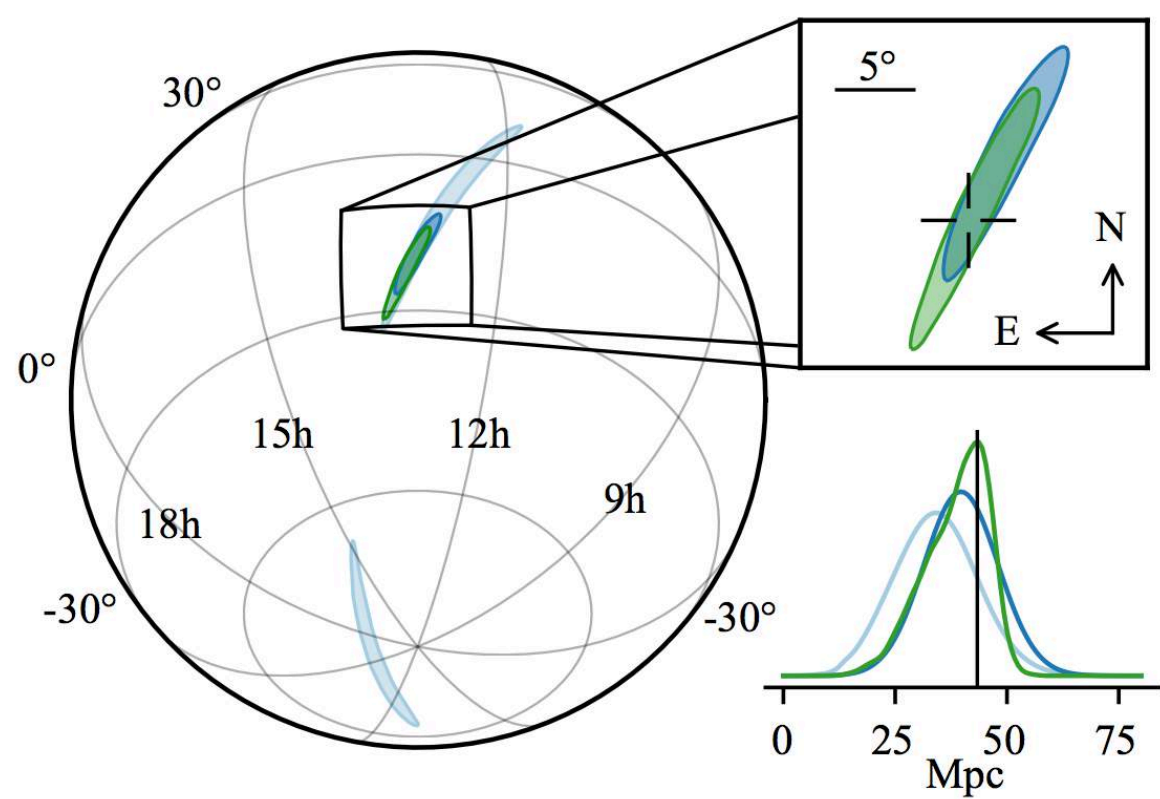
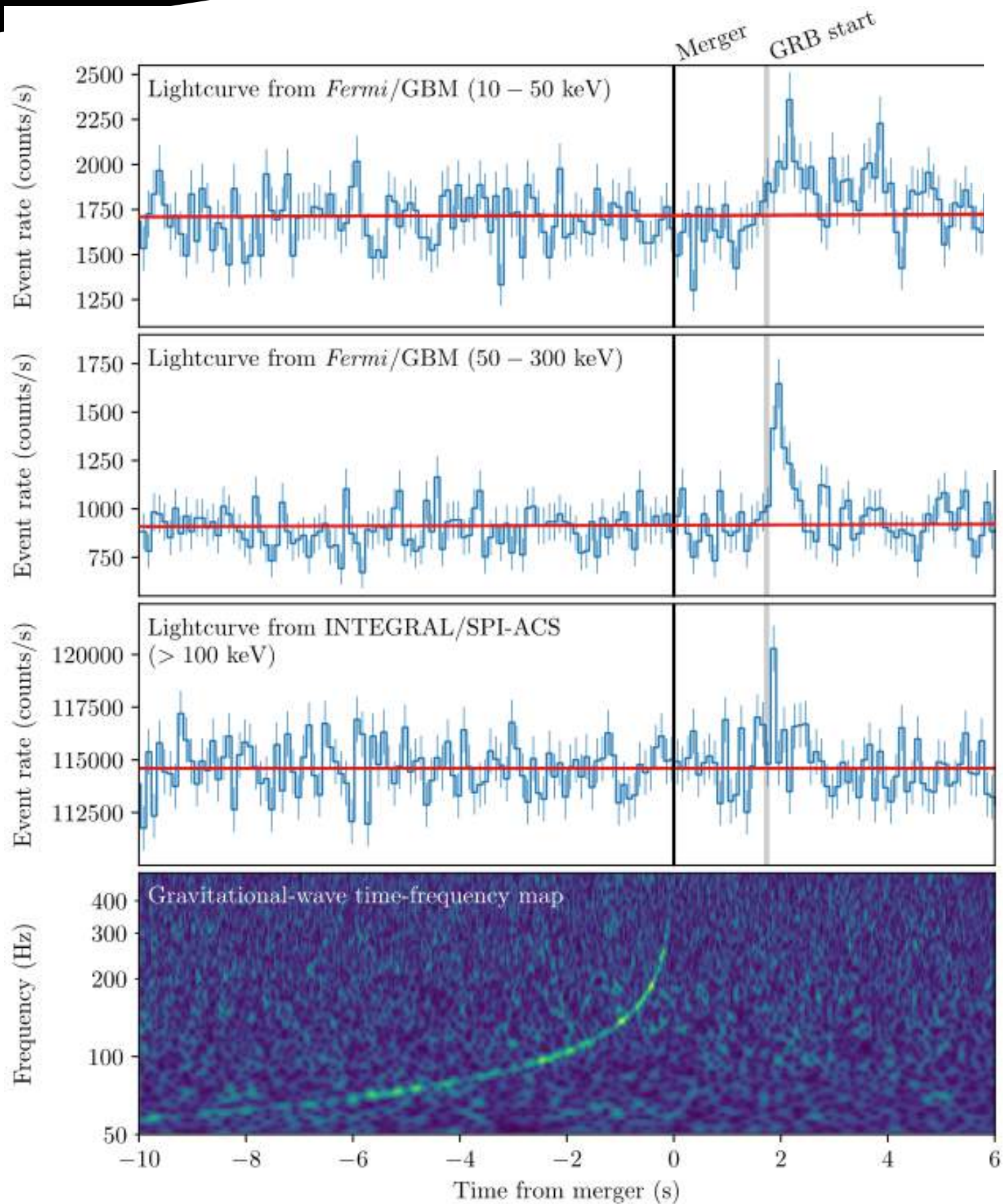
The beginning of multi messenger astrophysics.

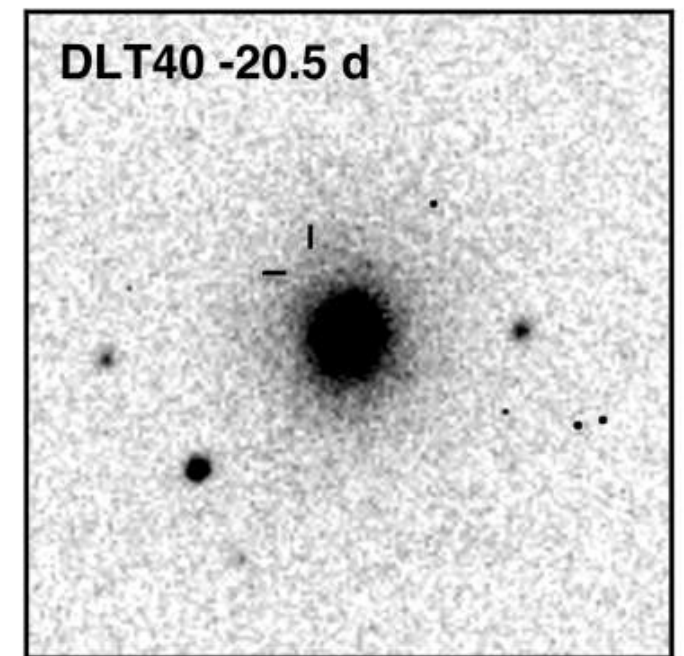
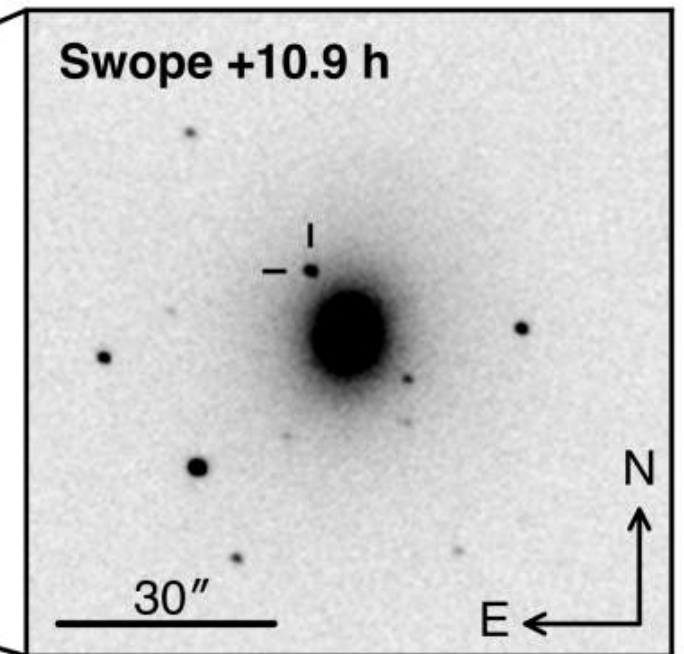
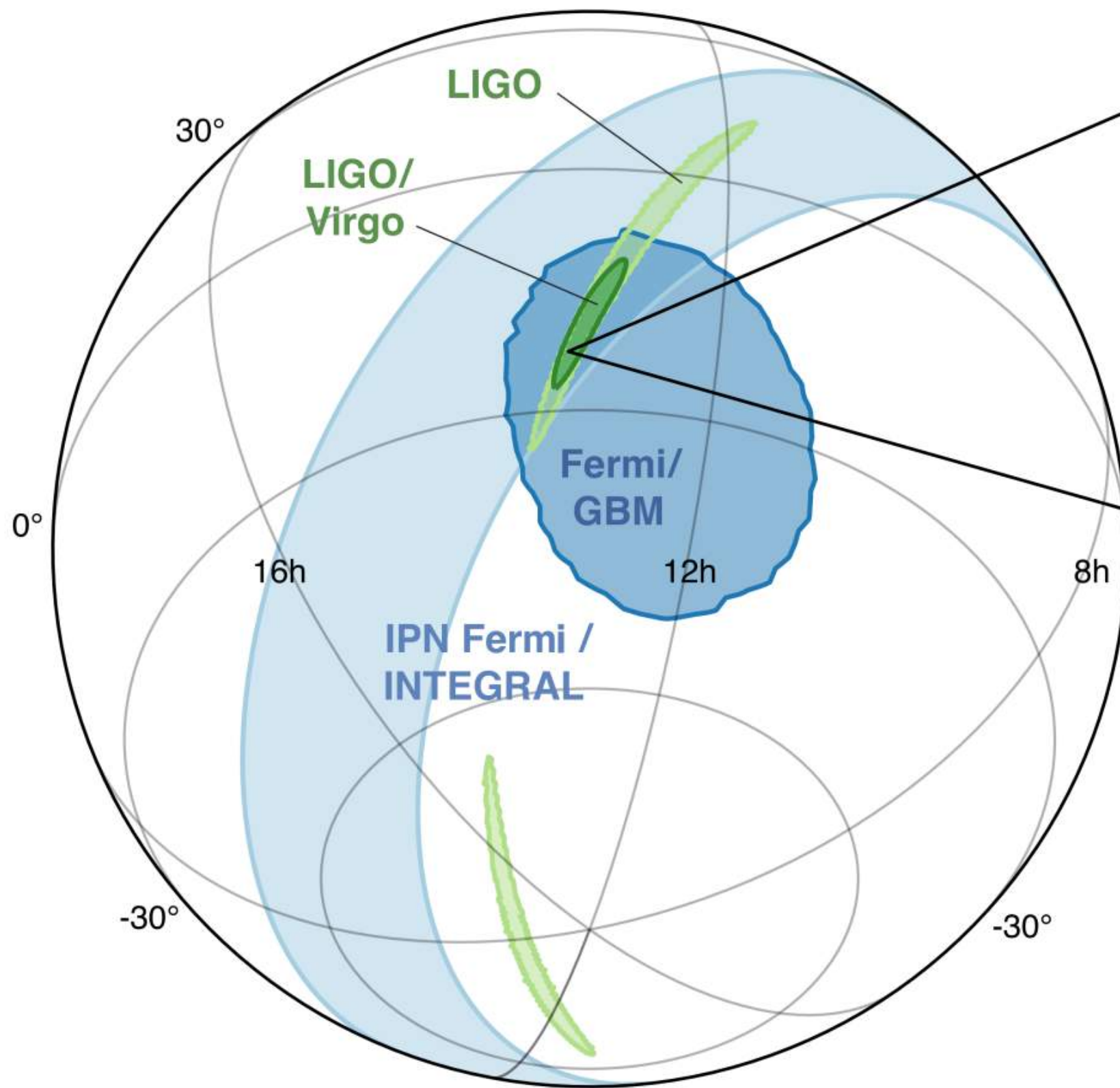
Observation of GWs from the fusion of two neutron stars, short gamma ray burst and a kilonova.



LIGO



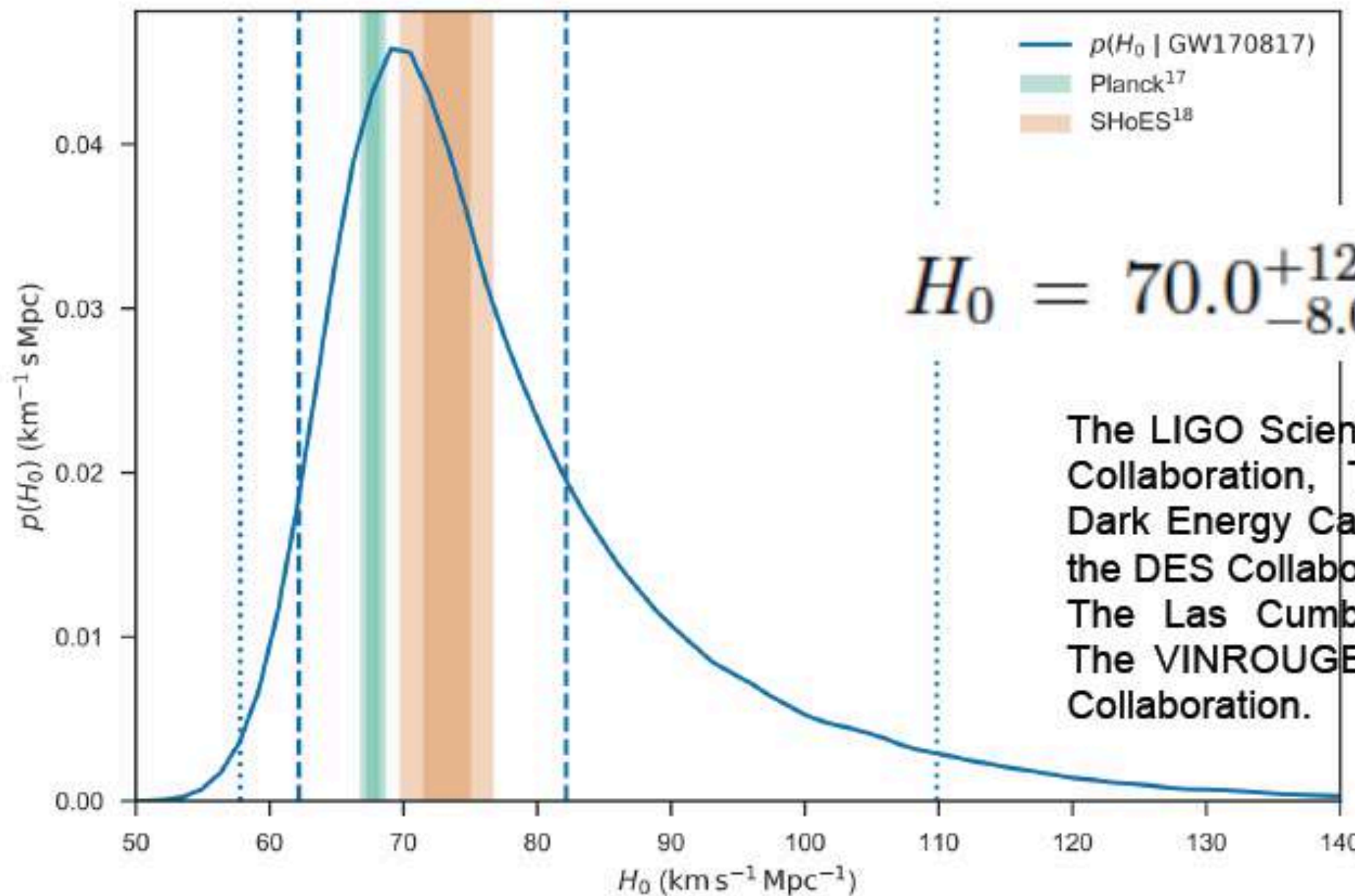




GW170817: inicio de la cosmología de GW

GW170817 puede usarse como una “**sirena estándar**”: combinando la **distancia** (inferida de la señal gravitacional) con la **velocidad** de recesión de la fuente (corrimiento al rojo; inferida de la señal electromagnética) se determina la **constante de Hubble**.

$$v_H = H_0 d$$



$$H_0 = 70.0^{+12.0}_{-8.0} \text{ km s}^{-1} \text{ Mpc}^{-1}$$

The LIGO Scientific Collaboration and The Virgo Collaboration, The 1M2H Collaboration, The Dark Energy Camera GW-EM Collaboration and the DES Collaboration, The DLT40 Collaboration, The Las Cumbres Observatory Collaboration, The VINROUGE Collaboration & The MASTER Collaboration.

Nature (2017)

GWTC-1

GWTC-1

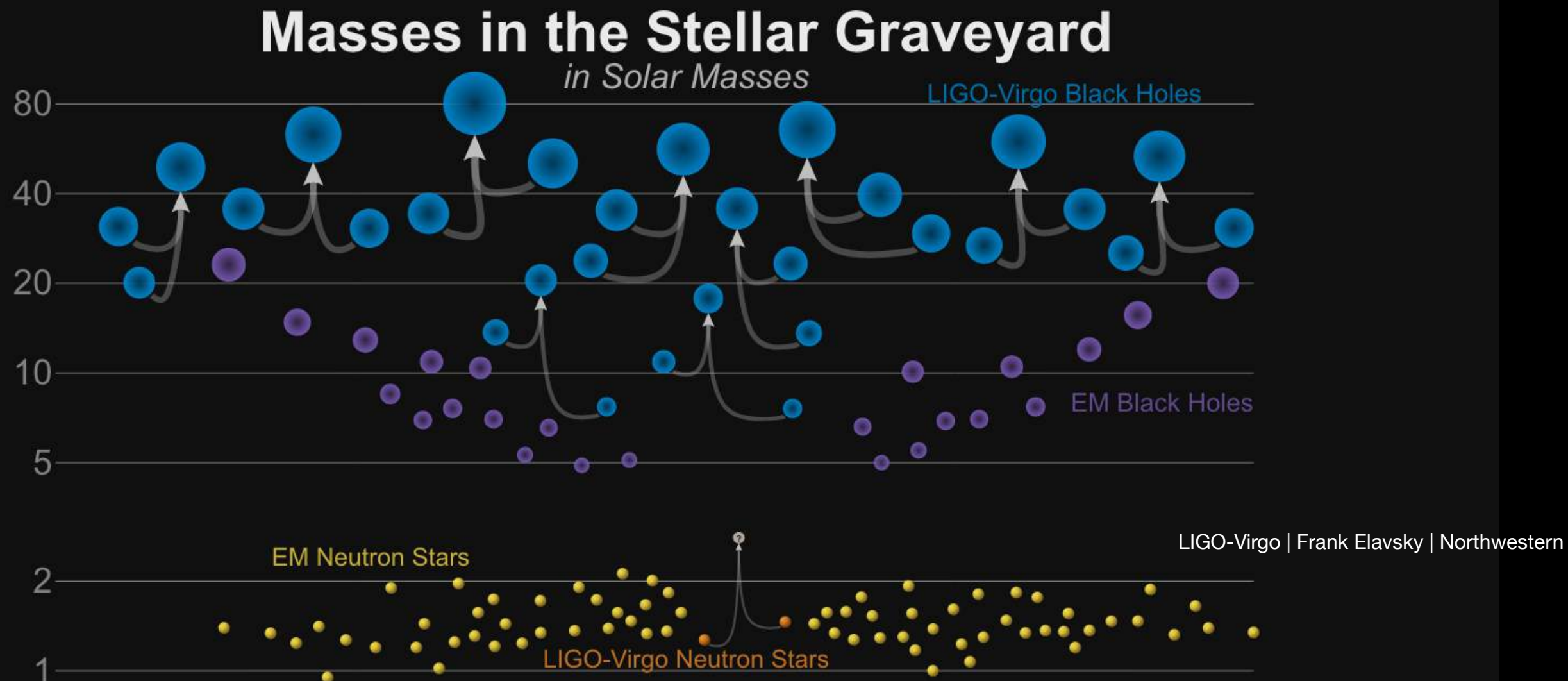
- On December 1st LIGO + Virgo have released their compact binary coalescences catalogue for the O1 + O2 observation runs: GWTC-1.
- Previously: 5 BBH GW events, 1 BBH LVT, 1 BNS

GWTC-1

- On December 1st LIGO + Virgo have released their compact binary coalescences catalogue for the O1 + O2 observation runs: GWTC-1.
- Previously: 5 BBH GW events, 1 BBH LVT, 1 BNS
- Now we go to 11: 10 BBH mergers (LVT-> GW, 4 new), 1 BNS.
- Open data + tutorials @ <https://www.gw-openscience.org/catalog>

GWTC-1

- On December 1st LIGO + Virgo have released their compact binary coalescences catalogue for the O1 + O2 observation runs: GWTC-1.
- Previously: 5 BBH GW events, 1 BBH LVT, 1 BNS
- Now we go to 11: 10 BBH mergers (LVT-> GW, 4 new), 1 BNS.
- Open data + tutorials @ <https://www.gw-openscience.org/catalog>



Event	Primary mass (M_sun)	Secondary mass (M_sun)	Effective inspiral spin	Final mass (M_sun)	Luminosity distance (Mpc)	Source redshift	Network SNR gstLAL
GW150914	35.6 ^{+4.8} _{-3.0}	30.6 ^{+3.0} _{-4.4}	-0.01 ^{+0.12} _{-0.13}	63.1 ^{+3.3} _{-3.0}	430 ⁺¹⁵⁰ ₋₁₇₀	0.09 ^{+0.03} _{-0.03}	24.4
GW151012	23.3 ^{+14.0} _{-5.5}	13.6 ^{+4.1} _{-4.8}	0.04 ^{+0.28} _{-0.19}	35.7 ^{+9.9} _{-3.8}	1060 ⁺⁵⁴⁰ ₋₄₈₀	0.21 ^{+0.09} _{-0.09}	10.0
GW151226	13.7 ^{+8.8} _{-3.2}	7.7 ^{+2.2} _{-2.6}	0.18 ^{+0.20} _{-0.12}	20.5 ^{+6.4} _{-1.5}	440 ⁺¹⁸⁰ ₋₁₉₀	0.09 ^{+0.04} _{-0.04}	13.1
GW170104	31.0 ^{+7.2} _{-5.6}	20.1 ^{+4.9} _{-4.5}	-0.04 ^{+0.17} _{-0.20}	49.1 ^{+5.2} _{-3.9}	960 ⁺⁴³⁰ ₋₄₁₀	0.19 ^{+0.07} _{-0.08}	13.0
GW170608	10.9 ^{+5.3} _{-1.7}	7.6 ^{+1.3} _{-2.1}	0.03 ^{+0.19} _{-0.07}	17.8 ^{+3.2} _{-0.7}	320 ⁺¹²⁰ ₋₁₁₀	0.07 ^{+0.02} _{-0.02}	14.9
GW170729	50.6 ^{+16.6} _{-10.2}	34.3 ^{+9.1} _{-10.1}	0.36 ^{+0.21} _{-0.25}	80.3 ^{+14.6} _{-10.2}	2750 ⁺¹³⁵⁰ ₋₁₃₂₀	0.48 ^{+0.19} _{-0.20}	10.8
GW170809	35.2 ^{+8.3} _{-6.0}	23.8 ^{+5.2} _{-5.1}	0.07 ^{+0.16} _{-0.16}	56.4 ^{+5.2} _{-3.7}	990 ⁺³²⁰ ₋₃₈₀	0.20 ^{+0.05} _{-0.07}	12.4
GW170814	30.7 ^{+5.7} _{-3.0}	25.3 ^{+2.9} _{-4.1}	0.07 ^{+0.12} _{-0.11}	53.4 ^{+3.2} _{-2.4}	580 ⁺¹⁶⁰ ₋₂₁₀	0.12 ^{+0.03} _{-0.04}	15.9
GW170817	1.46 ^{+0.12} _{-0.10}	1.27 ^{+0.09} _{-0.09}	0.00 ^{+0.02} _{-0.01}	≤ 2.8	40 ⁺¹⁰ ₋₁₀	0.01 ^{+0.00} _{-0.00}	33.0
GW170818	35.5 ^{+7.5} _{-4.7}	26.8 ^{+4.3} _{-5.2}	-0.09 ^{+0.18} _{-0.21}	59.8 ^{+4.8} _{-3.8}	1020 ⁺⁴³⁰ ₋₃₆₀	0.20 ^{+0.07} _{-0.07}	11.3
GW170823	39.6 ^{+10.0} _{-6.6}	29.4 ^{+6.3} _{-7.1}	0.08 ^{+0.20} _{-0.22}	65.6 ^{+9.4} _{-6.6}	1850 ⁺⁸⁴⁰ ₋₈₄₀	0.34 ^{+0.13} _{-0.14}	11.5

O2 Sensitivity

O1: September 12 2015 - January 19 2016,

O2: November 30 2016 - August 25 2017 [Advanced Virgo joined Aug 1 2017]

O2 data were recalibrated and cleaned to increase sensitivity

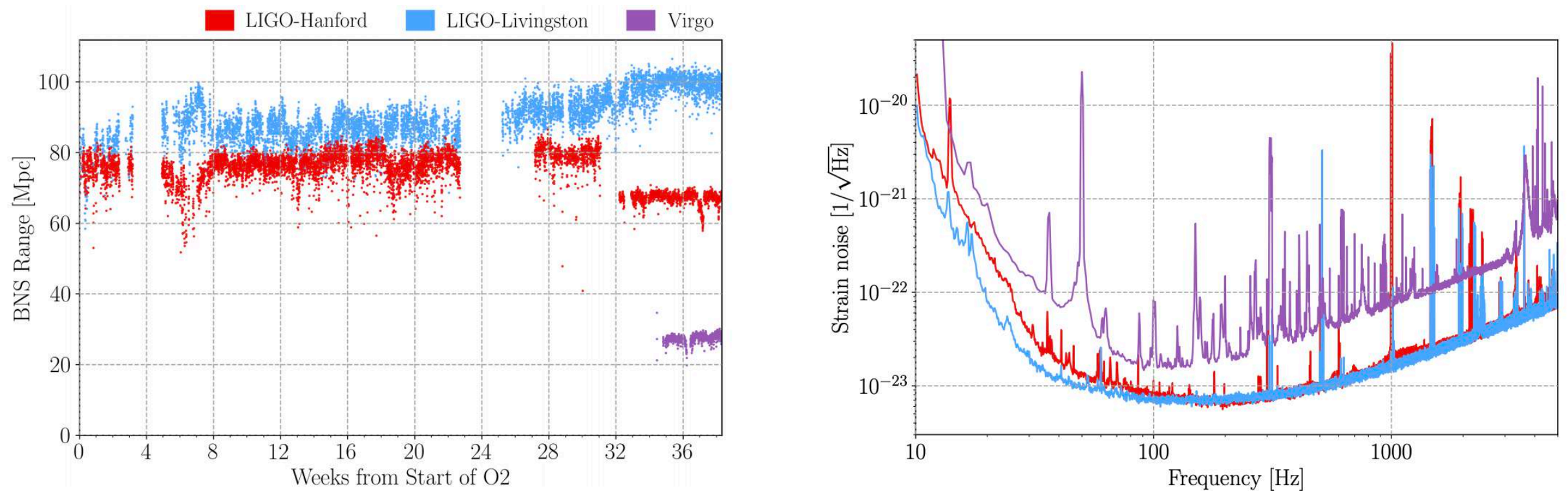
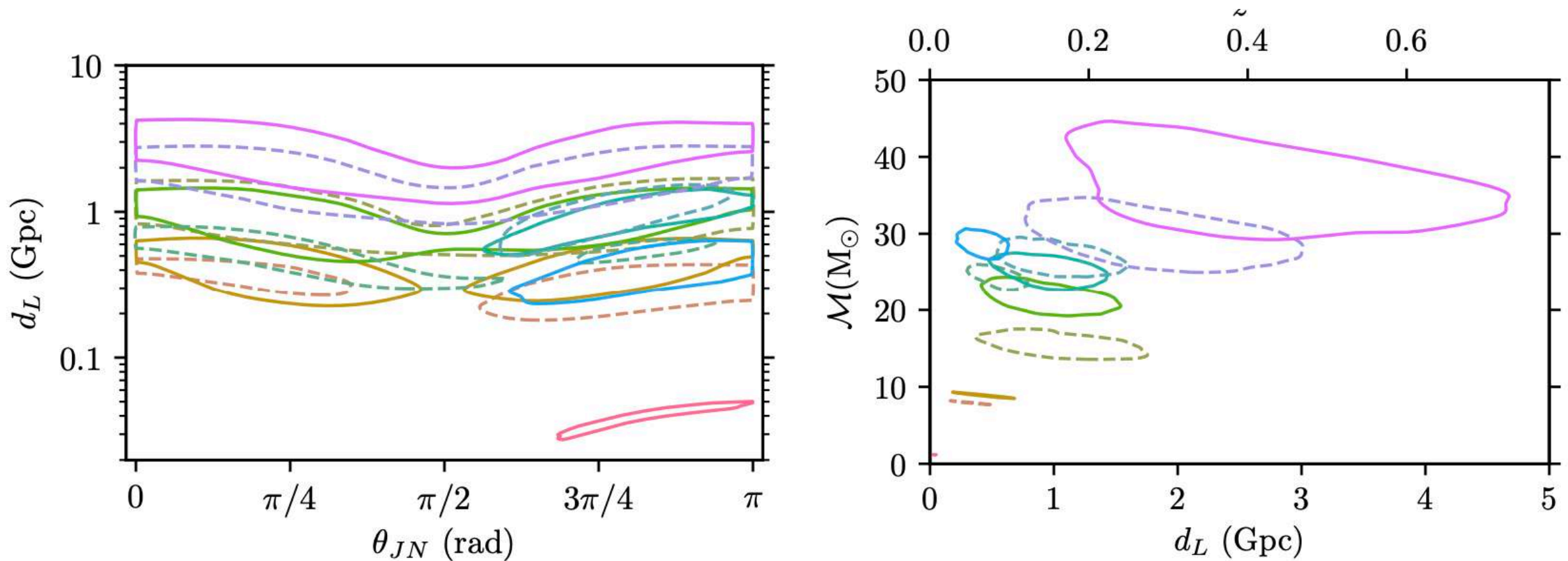


FIG. 1. Left: BNS range for each instrument during O2. The break at week 3 was for the 2016 end-of-year holidays. There was an additional break in the run at week 23 to make improvements to instrument sensitivity. The Montana earthquake's impact on the LHO instrument sensitivity can be seen at week 31. Virgo joined O2 in week 34. Right: Amplitude spectral density of the total strain noise of the Virgo, LHO and LLO detectors. The curves are representative of the best performance of each detector during O2.

Distance + Inclination

Degenerate!

Luminosity distance and chirp mass are positively correlated, as expected for un-lensed BBH observations.



Masses + Final State

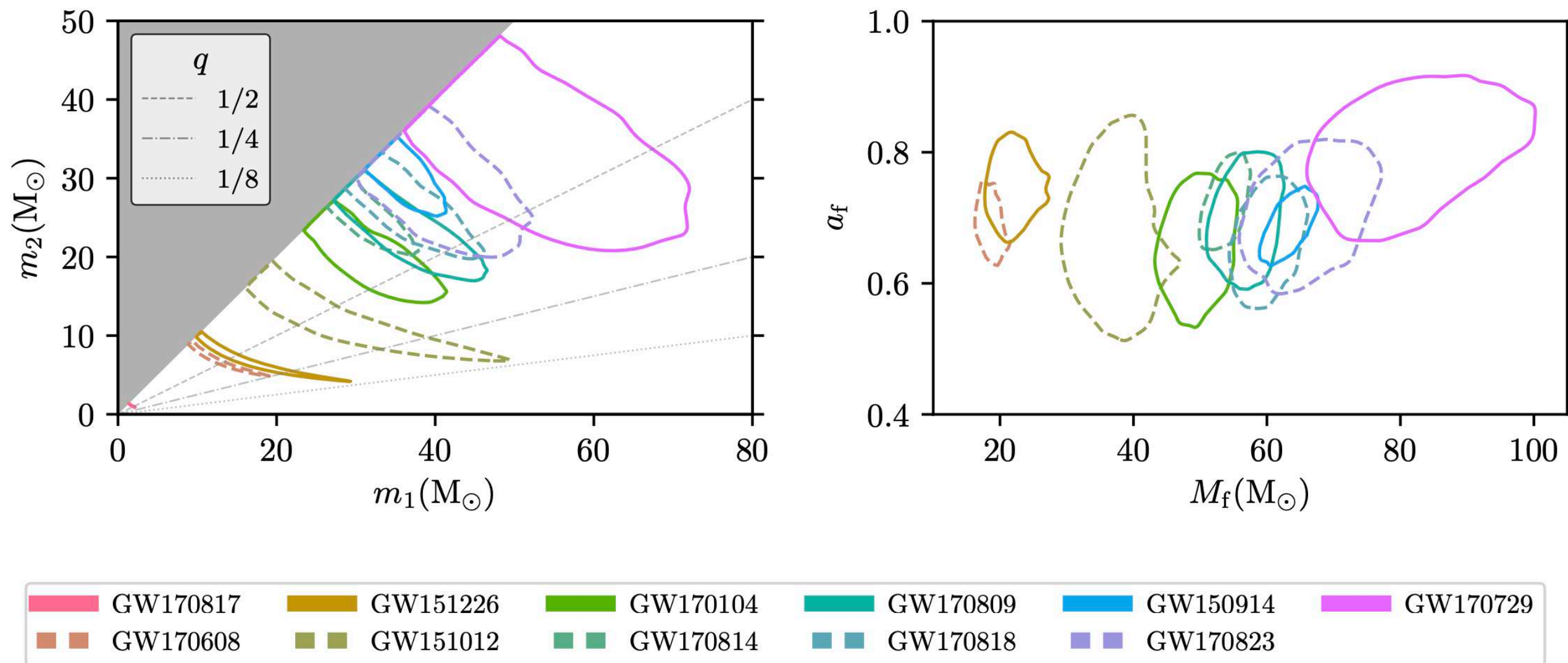
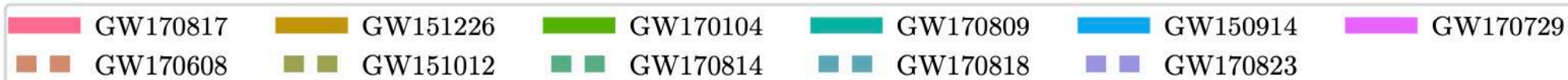
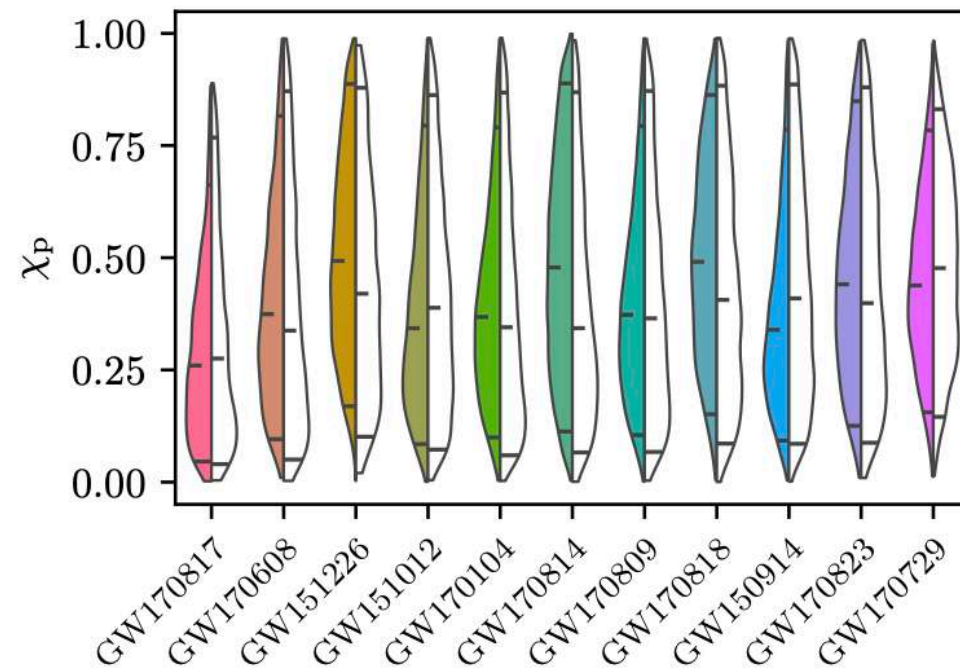
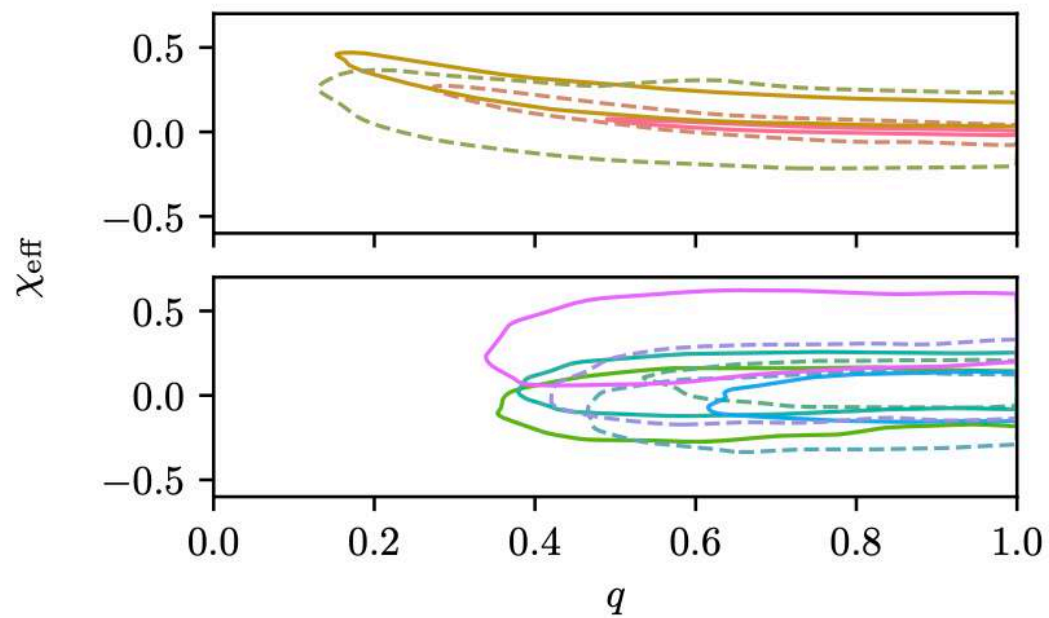
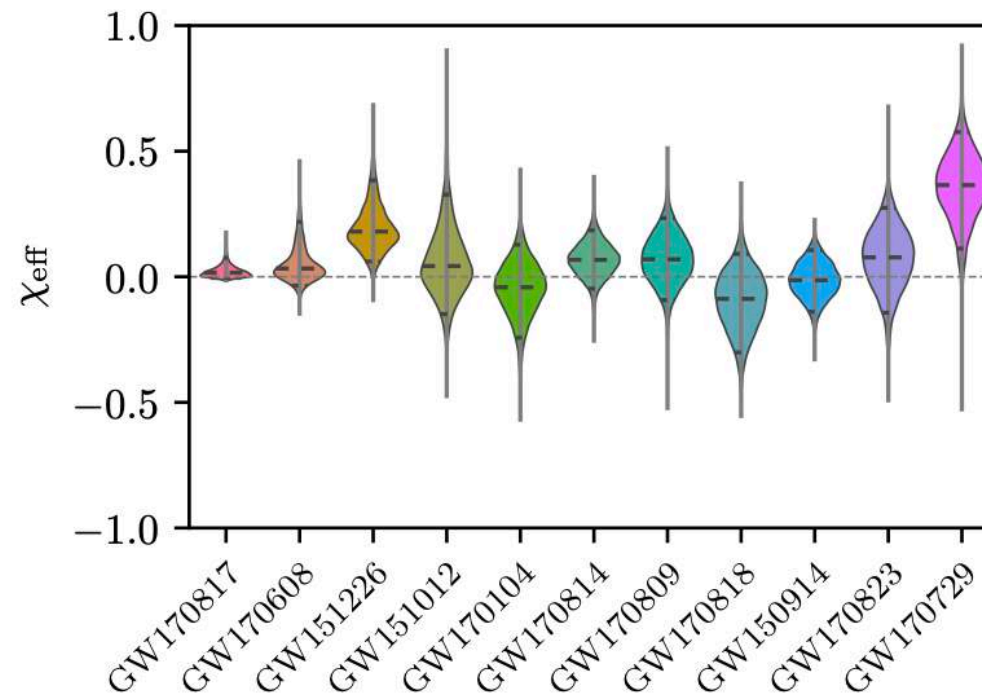
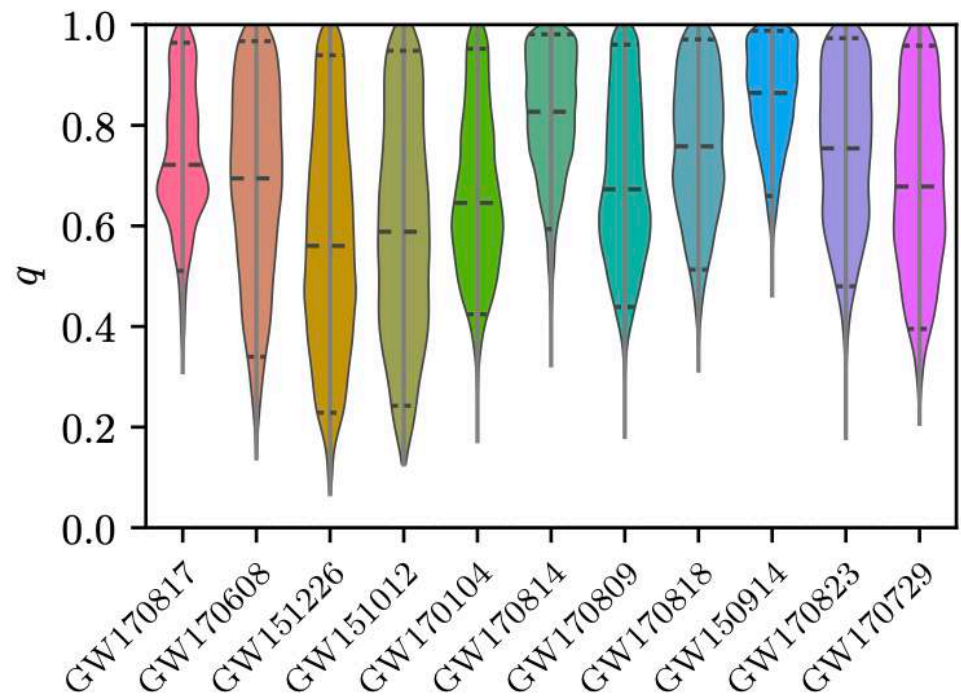


FIG. 4. Parameter estimation summary plots I. Posterior probability densities of the masses, spins, and SNR of the GW events. For the two-dimensional distributions, the contours show 90% credible regions. *Left panel:* Source frame component masses m_1 and m_2 . We use the convention that $m_1 \geq m_2$, which produces the sharp cut in the two-dimensional distribution. Lines of constant mass ratio $q = m_2/m_1$ are shown for $1/q = 2, 4, 8$. For low-mass events, the contours follow lines of constant chirp mass. *Right panel:* The mass M_f and dimensionless spin magnitude a_f of the final black holes. The colored event labels are ordered by source frame chirp mass. The same color code and ordering (where appropriate) apply to Figs. 5 to 8.

Mass Ratio and Spins



Rates

Approximately one GW detection per 15 days of data searched.

O3 run will start in April 2019,
last ~ 1 calendar year - expect to see many more events.

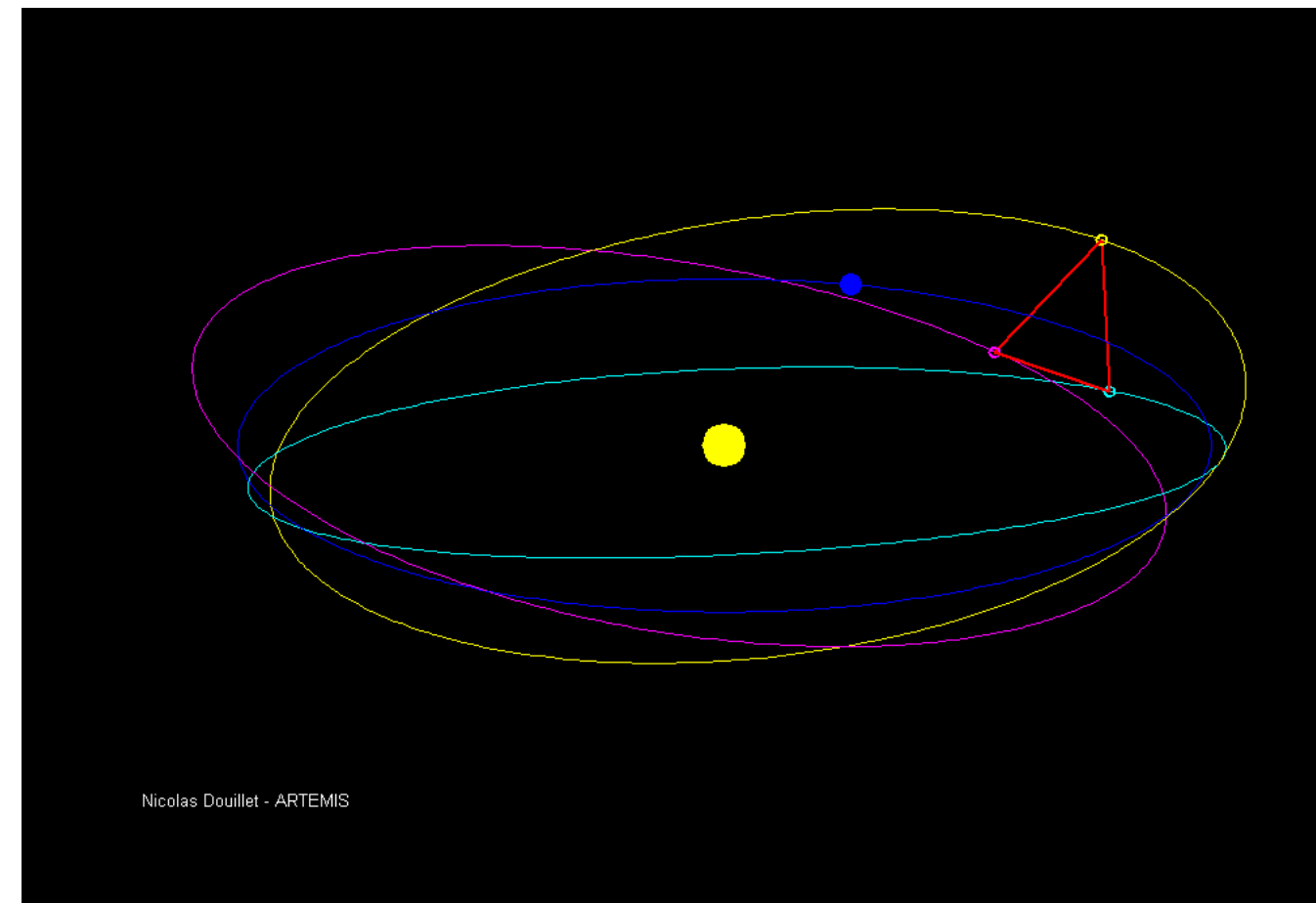
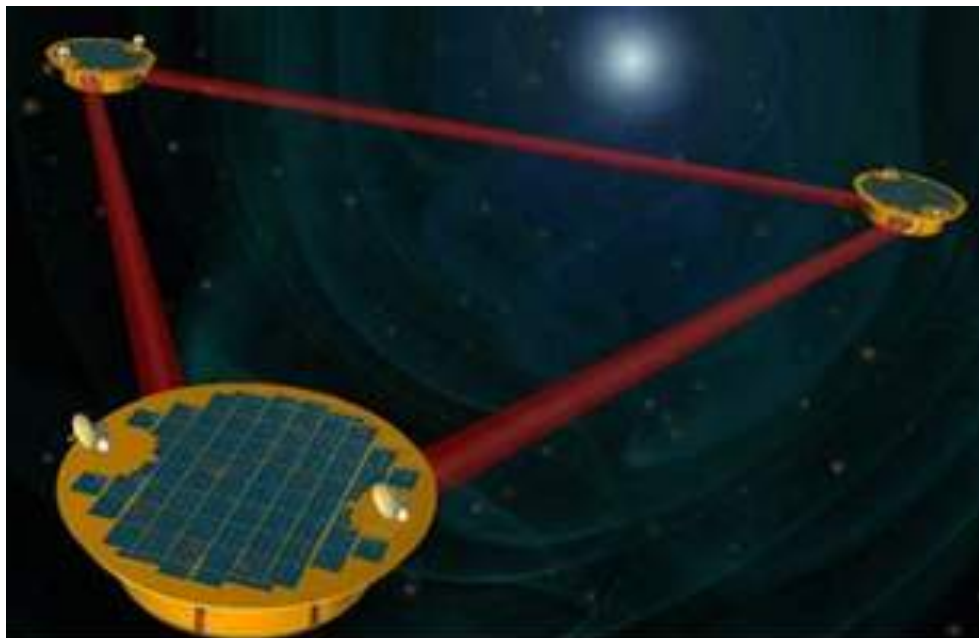
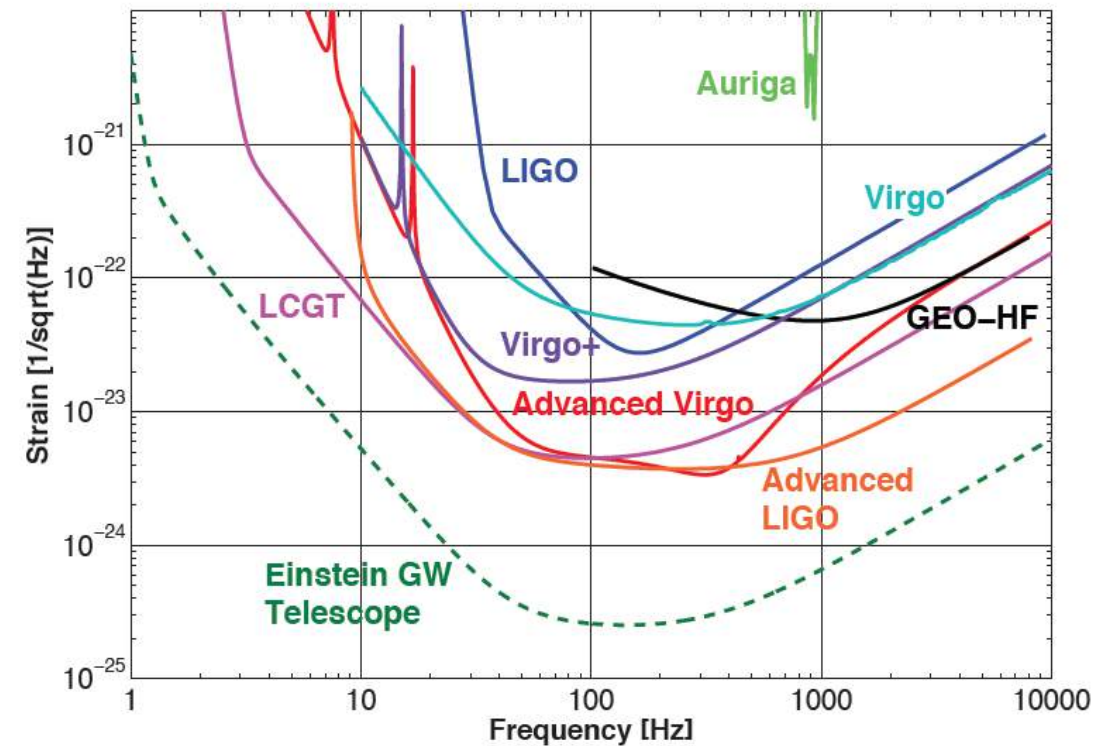
We have determined merger rates of

- BNS: [110, 3840] $\text{Gpc}^{-3} \text{y}^{-1}$
- BBH: [9.7, 101] $\text{Gpc}^{-3} \text{y}^{-1}$
- NSBH merger rate 90% upper limit of 610 (580) $\text{Gpc}^{-3} \text{y}^{-1}$

The Future

- Einstein Telescope:
Third generation detector planned in Europe, similar projects to form international third generation network.
- LISA: ESA space mission ~ 2034
 - 3 spacecraft, low frequency.

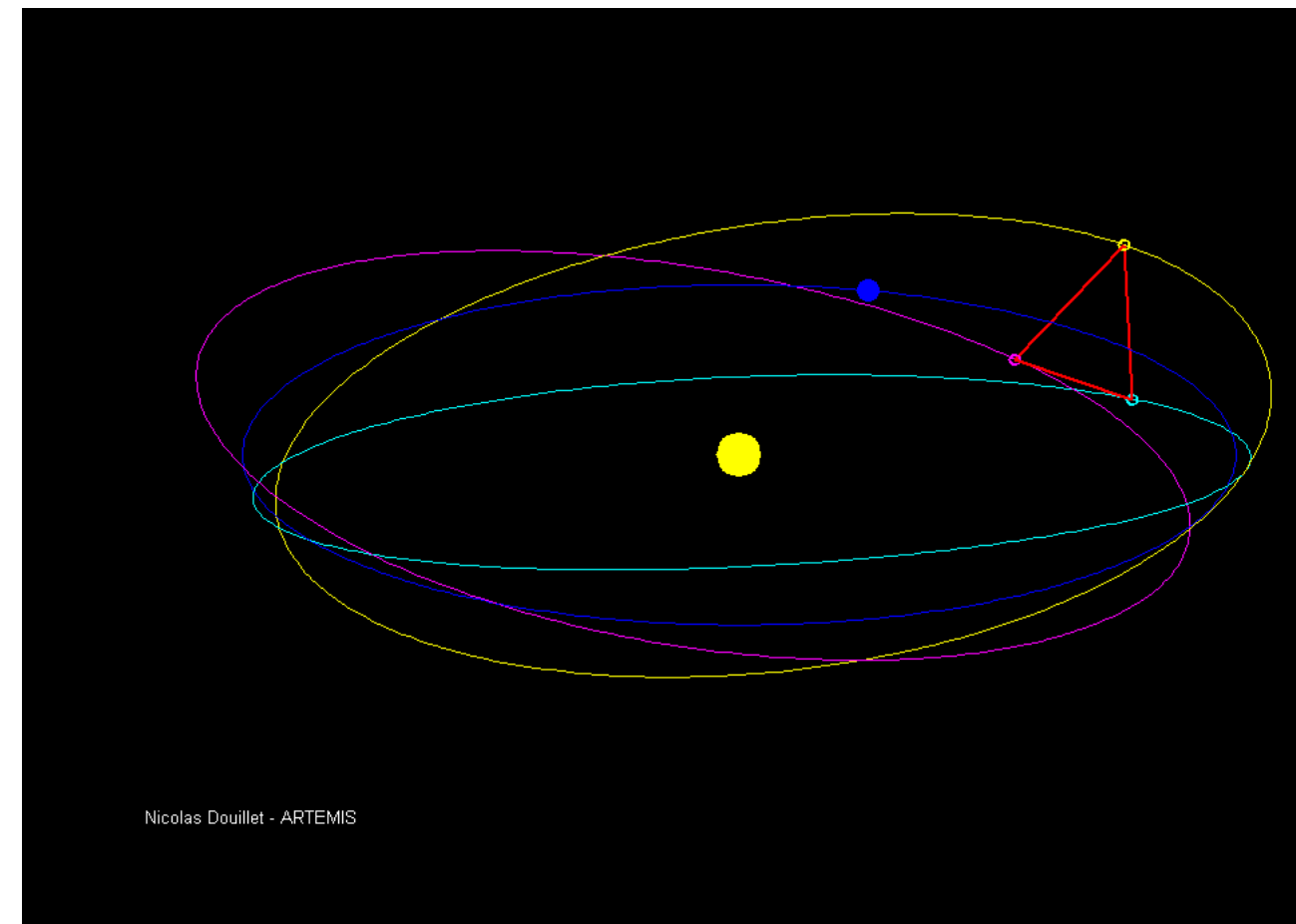
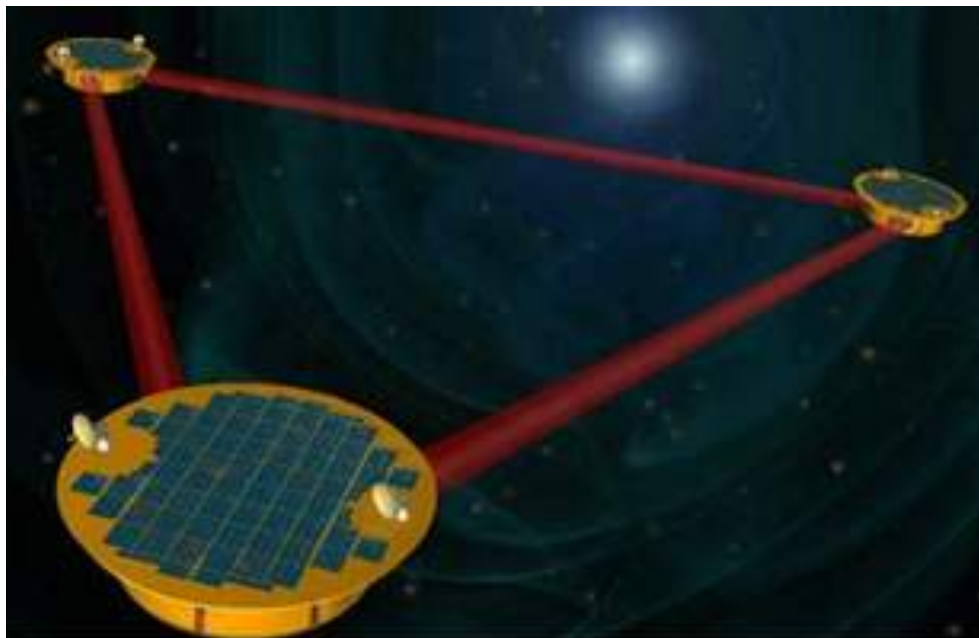
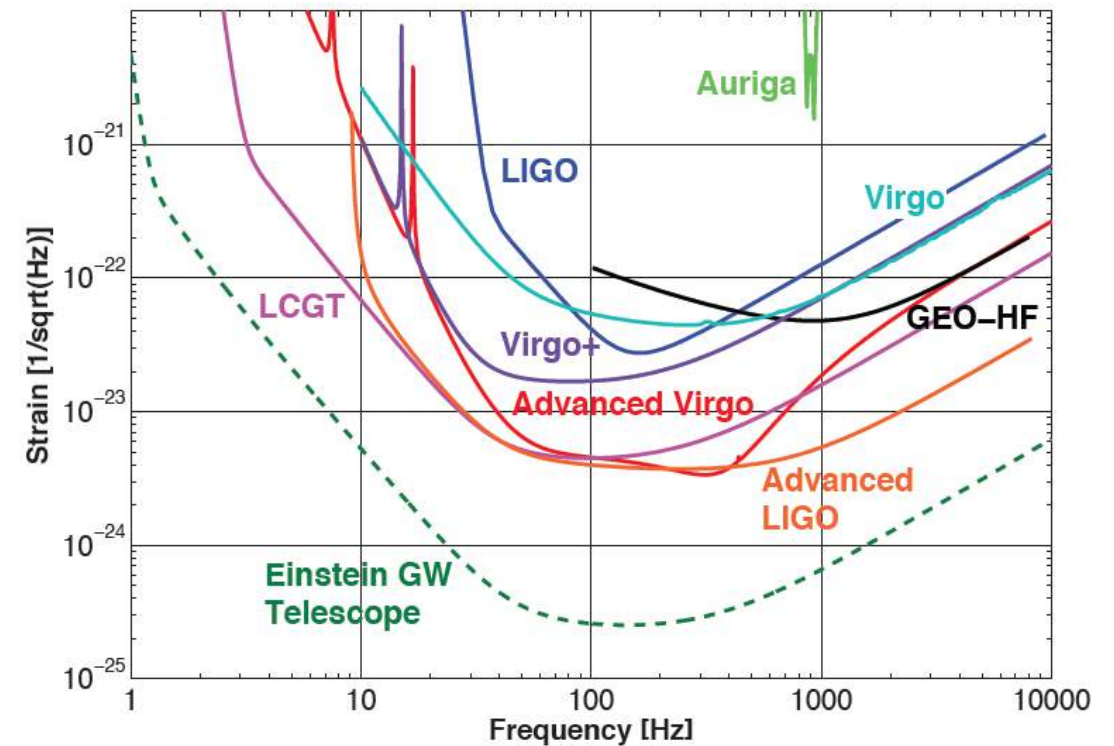
Expected ET Sensitivity



The Future

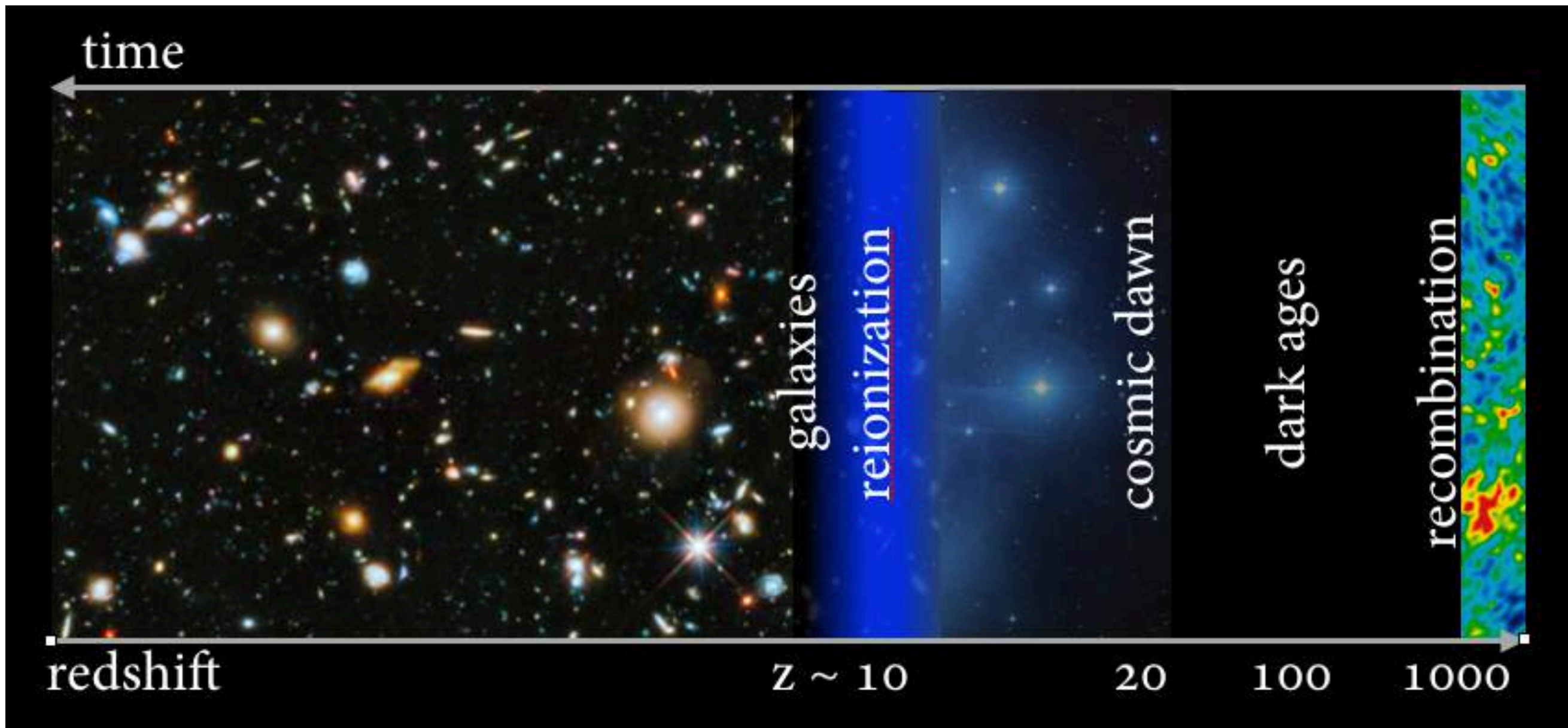
- Einstein Telescope:
Third generation detector planned in Europe, similar projects to form international third generation network.
- LISA: ESA space mission ~ 2034
 - 3 spacecraft, low frequency.

Expected ET Sensitivity



Until now we have seen black hole mergers up to about redshift $z \sim 0.5$.

LISA and ET will allow to see black hole mergers back in the dark ages of the universe, and hopefully gravitational waves created in the first moments of the universe.



Much before: the third observation run O3,
will start in April 2019. Stay tuned for new discoveries

